# BIOCHEMICAL CHARACTERIZATION OF THE SIX-TRANSMEMBRANE EPITHELIAL ANTIGEN OF THE PROSTATE FAMILY OF METALLOREDUCTASES

by

Mark Daniel Kleven

A dissertation submitted in partial fulfillment
of the requirements for the degree

of

Doctor of Philosophy

in

Biochemistry

MONTANA STATE UNIVERSITY
Bozeman, Montana

April 2015

©COPYRIGHT

by

Mark Daniel Kleven

2015

All Rights Reserved

# ACKNOWLEDGEMENTS

My sincere gratitude to my advisor, Dr. Martin Lawrence, who has guided me in my development as a scientist. The following work would not have been possible without his insight and direction. Thanks goes to my graduate committee members, Dr. Valerie Copie, Dr. Brian Bothner, Dr. John Peters, and Dr. Joan Broderick for their advice and assistance. I'm especially thankful for past and present Lawrence group members for their help during my time. This includes Dr. George Gauss, who provided much guidance and support while working on the Steap project. Additionally, Dr. Anoop Sendamarai, Brian Eilers, Dr. Nathanael Lintner, and Cate Burgess for their assistance in and out of the lab. This work would not have been possible without my wife, Amber, who has provided the great love and support that was desperately needed during my studies. Family and friends also make a graduate career so much easier. So, much appreication to my mother, father, Melissa, Michael, Matthew, Max, Mitchell, Jill, Brian, Ashley, Amanda, Henry, and many others for helping me stay sane through this process.

TABLE OF CONTENTS

1. INTRODUCTION ..... 1

Vertebrate Iron Homeostasis ..... 1
Steap3 as the Transferrin Cycle Ferric Reductase ..... 3
The Steap Family and Copper Homeostasis ..... 9
The Crystal Structure of the Steap3 Oxidoreductase Domain ..... 10
Research Goals ..... 13
References ..... 16

2. EXPRESSION AND SOLUBILIZATION OF HUMAN STEAP3 IN HEK-293T CELLS ..... 19

Introduction ..... 19
Materials and Methods ..... 22
Steap3 Expression Construct Cloning ..... 22
Adherent HEK-293 Cell Culture and Transfection ..... 23
Suspension-Adapted HEK-293 Cell Culture and Transfection ..... 23
Adherent HEK-293 Cell Surface Ferric Reductase Assay ..... 24
Suspension-Adapted HEK-293 Cell Surface Ferric Reductase Assay ..... 24
Fluorescence Size Exclusion Chromatography ..... 25
Sample Preparation for Confocal Microscopy ..... 25
Results ..... 26
Steap3 Cell-Surface Ferric Reductase Activity of Tagged Steap3 ..... 26
Optimization of Cell-Surface Ferric Reductase Assay ..... 27
Steap3 Detergent Screen via Fluorescence Size Exclusion Chromatography ..... 29
Detection of Steap Family Dimerization via a Bimolecular Fluorescence Complementation Assay ..... 31
Discussion ..... 34
Steap3 Ferric Reductase Activity is Unaltered by VFP Fusion ..... 34
Steap3 is Most Active at the Cell Surface 24-Hours Post-Transfection ..... 35
Triton X-100 is the Optimal Steap3 Solubilizing Detergent ..... 35
Steap3 is able to Form Dimers with Other Steap Family Members ..... 37
Steap1 and Steap3 Dimerization Induces Perinuclear Localization ..... 38
References ..... 40

3. THE CRYSTAL STRUCTURE OF SIX-TRANSMEMBRANE EPITHELIAL ANTIGEN OF THE PROSTATE 4 (STEAP4), A FERRI/CUPRIREDUCTASE, SUGGESTS A NOVEL INTER-DOMAIN FLAVIN-BINDING SITE ..... 41

TABLE OF CONTENTS – CONTINUED

Contribution of Authors and Co-Authors....41
Manuscript Information Page....43
Abstract....44
Introduction....44
Experimental Procedures....45
Cell Surface Ferric and Cupric Reductase Assays....45
Immunofluorescence Microscopy....46
Expression and Purification of the Steap4 N-Terminal Oxido -Reductase Domain....46
NADPH Oxidase Assay....46
Crystallization, Data Collection, and Model Refinement....47
Results....47
Cell Surface Ferric and Cupric Reductase Activities for Rat Steap4....47
Does Rat Steap4 Exhibit a Preference for $Fe^{3+}$ or $Cu^{2+}$?....47
Potential Steap4 Activity in Acidic Organelles....48
N-Terminal NADPH Oxidase Activity....48
Oligomeric State of the Oxidoreductase Domain in Solution....49
Structure of the Steap4 Oxidoreductase Domain....49
Structural Similarities to Steap3....49
Structural Similarity to the Steap3 Dimer....50
Disordered N-Terminal Residues are Unnecessary for Enzymatic Activity....51
Structural Basis for Steap4 Oxidoreductase Activity....52
Steap4 Variants, L194A, L196A, and W200A....52
Oxidoreductase Domain Variants, L194A, L196A, and W200A....52
Discussion....53
Physiologically Relevant Metalloreductase Activities....53
Oxidoreductase Domain....54
N-Terminal Oxidoreductase Residues....54
An Incomplete Flavin-Binding Site in the Oxidoreductase Domain....54
Acknowledgements....55
References....55

4. EXPRESSION AND PARTIAL PURIFICATION OF HUMAN STEAP3 IN SF9 INSECT CELLS....59

Introduction....59
Materials and Methods....61
Cloning and Baculovirues Bacmid Preparation....61
Sf9 Cell Culture and Baculovirus Generation....61
Expression and Purification of Steap3....62

TABLE OF CONTENTS – CONTINUED

Ferric Reductase Activity Assay ....64
Western Blotting....64
Results ....65
Effect of ALA Addition to Baculovirus-Mediated Expression of Steap3 in Sf9 Cells ....65
Effect of Affinity-Tag Location on Steap3 Expression....67
Time-Course Expression Analysis of Steap-Infected Sf9 Cells....68
Development of Full-Length Steap3 Ferrireductase Assay ....69
Purification of Steap3....70
Liposome Incorporation of Purified Steap3 ....72
Discussion ....74
Expression of Functional Holo-Steap3 Requires ALA Supplementation....74
Steap3 Expression is Unaltered by Affinity Tag Fusion at Either Terminus....75
Steap3 Expression in Sf9 Cells is Optimal at 45 Hours Post-Infection....76
Ferric Reductase Activity of Steap3 Expressed in Sf9 Cells is NADPH-, FAD-, and Temperature-Dependent....76
Steap3 is Unable to be Purified from Sf9 Cells in its Enzymatically-Active Form....77
Reconstitution of Steap3 into Phosphatidylcholine Liposomes is Not Sufficient to Rescue Enzymatic Functionality....78
References ....79

5. CHARACTERIZATION OF FAD, METAL AND B-TYPE HEME BINDING SITES IN THE TRANSMEMBRANE DOMAIN OF SIX-TRANSMEMBRANE EPITHELIAL ANTIGEN OF THE PROSTATE (STEAP) FAMILY OF PROTEINS ....80

Contribution of Authors and Co-Authors....80
Manuscript Information Page....81
Abstract ....82
Introduction ....83
Experimental Procedures....86
Cloning and Mutagenesis of STEAP3 Expression Constructs....86
Expression and Solubilization of STEAP3 ....88
STEAP3 Ferric Reductase Assay....89
Fluorescence Microscopy....89
Heme Absorbance Analysis ....90
Results ....91

TABLE OF CONTENTS – CONTINUED

Ferric Reductase Activity of Detergent-Activity Steap3 .....91
FAD is the Preferred Flavin for Steap .....93
Steap3 is a b-Type Cytochrome .....94
Steap3 Contains a Single b-Type Heme Cofactor .....95
Steap3 Forms an Active Homodimer .....97
Steap3 Electron Transfer Follows an Intra-Subunit Pathway .....99
FAD-Binding Site .....101
$Fe^{3+}$ Binding Site of Steap3 .....106
Discussion .....108
Steap1 Shares the Steap Family FAD and Iron Binding Motfs .....108
Steap3 Homodimer .....109
Steap3 Transmembrane Domain Binds a Single, b-Type Heme .....109
Steap3 Iron Binding Residues Adjacent to the Heme Cofactor .....110
The Transmembrane Domain Contains a High-Affinity FAD Binding Site .....111
The αII/αIII and a αIV/αV Loops Form the FAD Binding Site .....111
The Transmembrane FAD Binding Site Replace the Cytoplasm Proximal Heme .....112
Predicted Structure for the Transmembrane Domain .....112
References .....115

6. CONCLUDING REMARKS .....118

References .....123

APPENDIX A: Supporting information for Chapter 3 .....124

REFERENCES CITED .....133

# LIST OF TABLES


| Table | | Page |
|---|---|---|
| 2.1. | Steap3 fluorescence size-exclusion chromatography detergent screen quantitative and qualitative values | 31 |
| 3.1 | Full-length Steap4 cell surface metalloreductase activity | 48 |
| 3.2 | N-terminal oxidoreductase domain NADPH oxidase activity | 50 |
| 3.3 | X-ray data collection and refinement statistics | 50 |
| 4.1 | Purification table for a representative Streptactin purification of baculovirus-mediated Steap3 expression in Sf9 cells | 72 |
| 5.1 | Primers used in Steap3 cloning | 88 |
| 5.2 | Fractionation of ferric reductase activity in Steap3-VFP transfected cells | 92 |
| 5.3 | FAD kinetic characterization of Steap3 $Fe^{3+}$-reductase activity | 104 |
| 5.4 | $Fe^{3+}$ kinetic characterization of Steap3 $Fe^{3+}$-reductase activity | 107 |

# LIST OF FIGURES

Figure Page

1.1. Overview of the transferrin cycle ....3

1.2. Steap3 knockout mice exhibit hypochromic, microcytic anemia ....4

1.3. Structural organization of Steap3 and its homolog NADPH oxidase ....7

1.4. Human Steap3 oxidoreductase domain crystal structure with NADPH bound....10

1.5. Human Steap3 oxidoreductase domain flavin binding superimposed with FNO crystal structure flavin, $F_{420}$ ....11

1.6. Crystal structure of the human Steap3 oxidoreductase domain dimer with NADPH bound ....12

2.1. Overview of fluorescence size-exclusion chromatography (FSEC) detergent screen ....20

2.2 Cell surface ferric reductase activity of transiently-transfected HEK 293T cells ....28

2.3 Steap3 cell surface ferric reductase assay time course experiment ....29

2.4 Fluorescence signal chromatograms from Steap3 FSEC detergent screen ....30

2.5 Bimolecular fluorescence complementation (BiFC) assay of Steap3 and Steap family members ....33

3.1 Cell surface metalloreductase activity ....47

3.2 Cell surface metalloreductase activity of full-length rat Steap4 (Steap4(1-470)) was measured as a function of pH in the presence of 50 M $Fe^{3+}$-NTA or 50 M $Cu^{2+}$-NTA ....48

3.3 Flavin-dependent NADPH oxidase activity of the purified N-terminal cytoplasmic domain ....49

LIST OF FIGURES – CONTINUED

Figure Page

3.4 Rat Steap4 structure ....51

3.5 Structural differences between Steap3 and Steap4 ....53

3.6 Co-localization of rat Steap4 and transferrin receptor ....54

4.1 Effect of aminolevulinic acid (ALA) supplementation on Steap3 expression....66

4.2 Expression analysis of Steap3 in the BEVS system ....68

4.3 Ferric reductase activity assay development for full-length Steap3 expressed in Sf9 cells ....70

4.4 Sf9-expressed Steap3 observed in elution fractions from Streptactin affinity chromatography ....71

4.5 Liposome incorporation via dialysis does not activity purified Steap3 ....73

5.1 Triton X-100-activated Steap3 is an NADPH- and FAD-dependent ferric reductase ....94

5.2 Steap3 transmembrane domain binds a b-type heme with coordination through H316 and H409 ....96

5.3 Steap3 is able to form homodimers ....98

5.4 Investigating Steap3 electron transfer pathway ....100

5.5 Amino acid conservation of Steap family oxidoreductase and transmembrane domains....103

5.6 Ligand binding site model of the Steap3 transmembrane domain....114

A.1 Sequence alignment of metazoan Steap Proteins....125

# LIST OF ABBREVIATIONS

ALA: δ-aminolevulinic acid
BEVS: baculovirus expression vector system
BiFC: bimolecular fluorescence complementation
Dcytb: duodenal cytochrome b
DMT1: divalent metal trasporter-1
FAD: flavin adenine dinucleotide
FMN: flavin mononucleotide
FNO: $F_{420}H_2$:$NADP^+$ oxidoreductase
FRE1: ferric reductase, family member 1
FSEC: fluorescence size exclusion chromatography
HEK: human embryonic kidney
IUB: iron uptake buffer
NADPH: nicotinamide adenine dinucleotide phosphate
NTA: nitrilotriacetic acid
NTBI: non-transferrin-bound iron
NOX: NADPH oxidase
PEI: polyethyleneimine
RMSD: root-mean square deviation
ROS: reactive oxygen species
Sf9: *Spodoptera frugiperda*, cell line-9
STEAP: six-transmembrane epithelial antigen of the prostate
Tf: transferrin
TfR: transferrin receptor-1
VFP: venus fluorescent protein

# ABSTRACT

Iron and copper are the two most abundant transition metals in humans and are mediators of many essential cellular processes. The entry of these metals into cells require controlled processes, including their reduction prior to uptake. A group of integral membrane enzymes, the six-transmembrane epithelial antigen of the prostate (Steap) family, are able to perform this function. Steap3, in particular, functions as the primary ferric reductase in the transferrin cycle, the dominant mode of erythrocyte iron uptake. How these enzymes perform these functions has remained ill-defined. Here, the biochemical underpinnings of Steap metalloreductase activity have been investigated. To elucidate these mechanisms, expression systems for Steap3 and Steap4 have been developed in bacterial, insect, and human cell lines and purified to varying degrees. By analyzing the truncated cytoplasmic oxidoreductase domain of Steap4, it was found that NADPH is oxidized by transferring a pair of electrons to a flavin. With this truncation, however, flavin only binds weakly and the construct shows no ability to preferentially bind one type of flavin. In contrast, when the full length Steap3 was partially purified, it exhibits high-affinity FAD-binding, indicating that the transmembrane region of the protein contains the major structural features of the FAD binding site. Further, it was found that the cytoplasm-oriented loops between transmembrane helices formed the site. The next cofactor in the electron transport chain is a single b-type heme. Two strictly conserved histidines were identified that coordinate the heme and both are required for heme incorporation. The metal binding site at the extracellular face of the membrane was also characterized. Here, it was found that Steap3 and Steap4 share a conserved high-affinity iron binding site. Additionally, iron and copper both bind with similar affinities to Steap4. Two critical residues of the metal binding site were determined and their predicted proximity to the heme cofactor suggests that the electron is transfer is direct between cofactor and metal. Finally, it was found that Steap's are able to dimerize in the cells, forming homo- and heterodimers Together, the enzymatic mechanism has been characterized in-depth for the first time for these physiologically-significant enzymes.

# CHAPTER ONE

# INTRODUCTION

## Vertebrate Iron Homeostasis

Iron is the most abundant transition metal in the human body. The chemistry of the atom allows for life to access reactions otherwise unworkable. The capacity for electron transfer makes the metal ideal for use by enzymes in catalyzing oxidation-reduction reactions. At the same time, this property makes iron potentially dangerous for the cell, as it is capable of reacting with oxygen compounds, molecular oxygen or peroxides to generate an array of reactive oxygen species (ROS). ROS can then damage cellular proteins, DNA, and lipids. To prevent this harmful chemistry, the body must maintain tight control of its stores of this metal, leading to highly regulated processes for transport as well as use in catalysis. Due to the critical nature of iron transport to human health understanding the underlying mechanisms are of high importance.

Healthy US males typically contain approximately 10 mg of iron per kg of body weight, while healthy females contain around 5 mg of iron per kg of body weight [2]. The majority of iron (~70%) is dedicated to red blood cell hemoglobin and excesses are stored in the liver [4]. The body has no direct mode to excrete iron and iron is only lost through the loss of cells (skin, intestinal, blood, etc.). To maintain iron stores, a diet requires ~2 mg of iron daily. Ingested iron is primarily absorbed in the duodenum and upper jejunum of the intestine [5]. Heme-bound iron and inorganic iron are absorbed through independent pathways. Heme iron is transported into intestinal enterocytes in a poorly-

characterized process. It was originally thought this process was mediated by heme carrier-protein (HCP-1) [6], however, subsequent work showed this protein is actually a folate transporter. Thus the identity of the heme transporter is currently unresolved [7].

However, the situation is somewhat clearer with regard to inorganic iron, where primarily iron primarily in the ferric ($Fe^{3+}$) state, is thought to be reduced at the cell surface by duodenal cytochrome b (Dcytb) [8]. However, mice lacking Dcytb still show normal iron uptake, thus it seems there are additional proteins that serve this function in the absence of Dcytb, leading to redundancy in the system [9]. Dcytb is an integral membrane protein that transfers electrons from cytoplasmic ascorbate across the membrane to reduce intestinal iron. Reduced iron is then transferred across the membrane via divalent metal transporter-1 (DMT1), which only transports ferrous ($Fe^{2+}$) iron.

Upon uptake from diet, ferrous iron is transported out of intestinal enterocytes by ferroportin and subsequently oxidized to $Fe^{3+}$ by hephaestin or ceruloplasmin [10]. $Fe^{3+}$ transport to tissues is mediated by transferrin, which is able to bind two ferric ions with extremely high affinity ($K_D$ of $10^{-23}$ $M^{-1}$ at pH 7.4) [11]. At the plasma membrane of a cell, iron-loaded transferrin binds the transferrin receptor (TfR). TfR forms a homodimer at the cell surface, with each subunit binding a diferric transferrin molecule. Upon Tf binding, clathrin-mediated endocytosis internalizes the complex. As in the import of dietary iron, endosomal iron is transported by DMT1, which is only capable of transporting ferrous iron into the cytoplasm, thus making $Fe^{3+}$ reduction a prerequisite for entry into the cell [12]. To facilitate iron reduction and subsequent transport, the endosome is acidified by a V-type ATPase to a pH around 5-6 [13]. The acidification

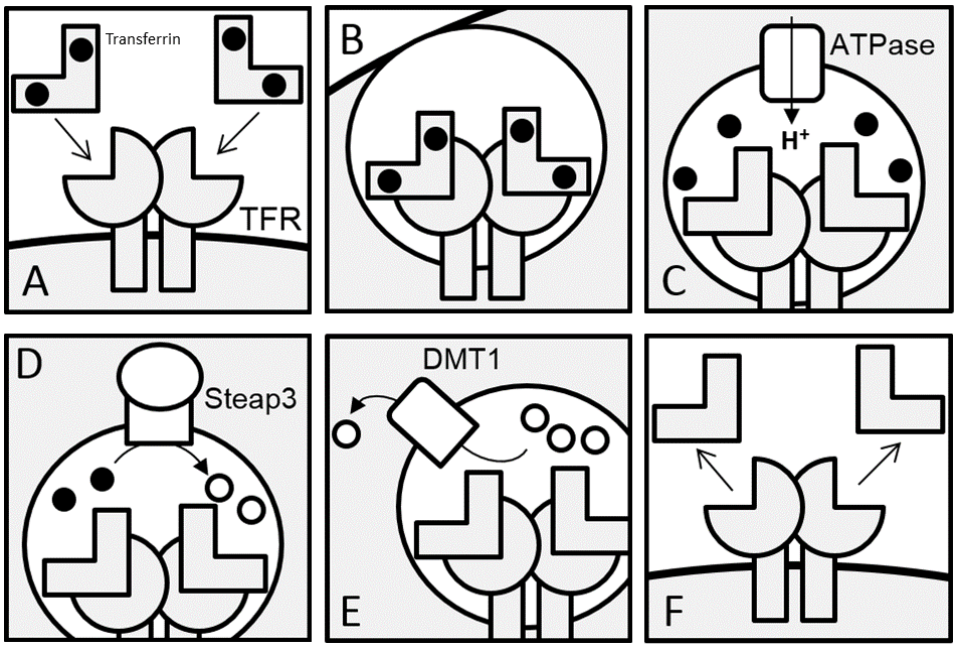


Figure 1.1. Overview of the transferrin cycle. The transferrin cycle is initiated by the binding of two $Fe^{3+}$ (closed circles)-loaded transferrin molecules to the transferrin receptor dimer (A). The transferrin-transferrin receptor complex then undergoes clathrin-mediated endocytosis (B). The endosome is then acidified by an ATPase to a pH of ~5.5 and the $Fe^{3+}$ is released from transferrin (C). The lumenal $Fe^{3+}$ is then reduced by a ferric reductase, Steap3, to $Fe^{2+}$ (open circles; D). The reduced iron is then transported into the cytoplasm by DMT-1 (E). Finally, the endosome is recycled to the cell surface (F) where holo-transferrin displaces apo-transferrin from transferrin receptor.

results in the protonation of a number of histidine residues at the interface of Tf and TfR and a subsequent conformational change that destabilizes the iron binding sites of Tf [14]. The released $Fe^{3+}$ is then reduced by the endosomal ferric reductase to $Fe^{2+}$ and is subsequently transported to the cytoplasm by DMT1.

Steap3 as the Transferrin Cycle Ferric Reductase

The identity of the transferrin cycle ferric reductase was discovered through the

work of Ohgami et al. who identified a mouse line, *nm1054*, that exhibited microcytic, hypochromic anemia that was indicative of a defect in erythrocytic iron uptake [15]. Upon investigating the genetic basis of the phenotype, a six-gene deletion in chromosome 1 was discovered [1]. The gene responsible for the phenotype was revealed to be Steap3, or six-transmembrane epithelial antigen of the prostate family member 3, as *Steap3*$^{-/-}$ mouse line resulted in the same phenotype and, conversely, retrovirally-transduced expression of the Steap3 gene rescued the anemia [1].

Prior to its identification as a ferric reductase, Steap3 was described as a tumor suppressing protein. In rat tumor models, adenovirus-mediated Steap3 expression led to elevated apoptosis and p53 expression [16]. Additionally, it was found that the Steap3

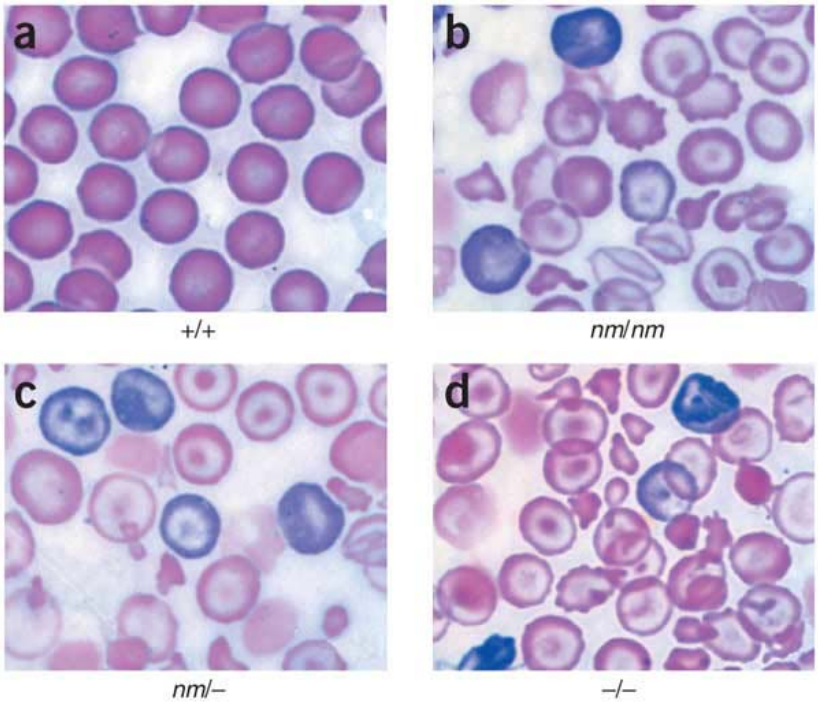


Figure 1.2. Steap3 knockout mice exhibit hypochromic, microcytic anemia. Blood smears from Steap3$^{+/+}$ mice (A), Steap3$^{nm1054/nm1054}$ mice (B), Steap3$^{nm1054/-}$ mice, and Steap3$^{-/-}$ mice. Figure is from [1].

gene promoter contains a p53 response element. In the cell, p53 serves to maintain genomic integrity through control of a wide-range of transcriptional targets [14]. The mechanism of Steap3-mediated apoptosis is believed to occur through its association with Nix, a mitochondrial protein that can increase membrane permeability and induce apoptosis [17]. Subsequent observations included a role in tumor reversion through non-classical secretion of exosomes, notably the secretion of translationally controlled tumor protein (TCTP) [17, 18]. TCTP is a multi-functional protein that has antiapoptotic as well as cell-signaling functions. It remains unclear how, or even if, the enzymatic function of Steap3 is related to its tumor suppressing capabilities.

While a connection between Steap3's p53-associated tumor suppression and transferrin cycle roles is lacking, an analysis of the amino acid sequence by Ohgami et al. strengthened the identification of Steap3 as the ferric reductase in the erythrocyte transferrin cycle [1]. Steap3 was predicted to be a multi-pass integral membrane protein with an N-terminal domain (~200 residues) predicted to lie in the cytoplasm. The transmembrane domain of Steap3 is predicted to contain 6 alpha helices. The sequence is distantly homologous to other integral membrane electron transfer enzymes, such as the yeast ferric reductase, FRE1, and the human NADPH oxidase (NOX) [3]. These proteins transfer electrons originating from NADPH in the cytoplasm across the plasma membrane via a FAD and two bis-histidine-coordinated heme cofactors in the transmembrane region. One pair of heme-coordinating histidine residues is conserved in Steap3, but the other pair corresponding to the cytoplasmic proximal heme are not

present. As a result, Ohgami et al. predicted Steap3 binds a single heme cofactor in the transmembrane domain [3].

However, the cytoplasmic NAPDH-binding domains of these distant transmembrane electron transfer homologs significant sequence similarity to Steap3. Furthermore, the NADPH binding domains of these distant homologs lie at the C-terminus, as opposed to the N-terminal organization in Steap3. Interestingly, Steap3's N-terminal cytoplasmic domain does share sequence similarity with an archaeal and bacterial enzyme, $F_{420}$:$NADP^+$ Oxidoreductase (FNO). FNO is able to catalyze the transfer of electrons from NADPH to the flavin analog $F_{420}$. It contains a characteristic consensus sequence motif (Gly-X-Gly-XX-Gly/Ala) for binding a dinucelotide, such as $NADP^+$. And indeed, the crystal structure for FNO found that the $F_{420}$ bound adjacent to $NADP^+$, with the isoalloxazine ring positioned proximal to the nicotinamide ring of the $NADP^+$ for efficient electron transfer [19].

*E*xperiments by Ohgami et al. demonstrated that Steap3 was capable of reducing not only iron at the cell surface of transiently-transfected cells, but copper as well [1, 20]. Moreover, by mutating residues predicted to interact with either NADPH or a transmembrane heme, they found a complete loss of activity. Together, these findings strongly indicated that Steap3 filled the role as ferric reductase in the transferrin cycle and pointed to an initial model for the Steap3 transmembrane electron transport process. Specifically, they proposed that from NADPH move to a flavin cofactor in the cytoplasmic domain, and then to transmembrane domain-bound heme before reduction of the terminal acceptor, $Fe^{3+}$, on the lumenal side of the membrane.

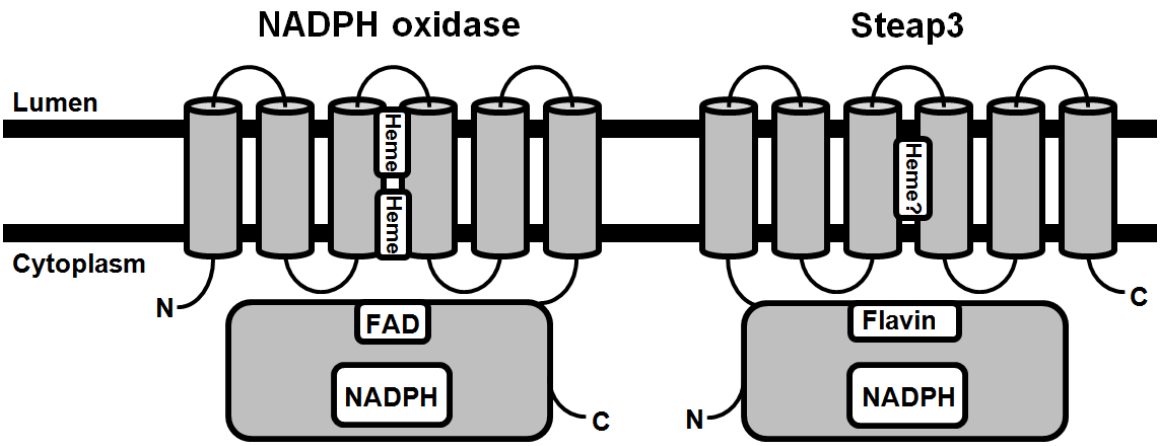


Figure 1.3. Structural organization of Steap3 and its homolog, NADPH oxidase. Transmembrane topology prediction algorithm, TMHMM, predicts a C-terminal transmembrane domain containing 6 transmembrane alpha helices. In contrast to NADPH Oxidase, Steap3 was predicted to contain only a single heme cofactor. Steap3 also differs from NADPH oxidase by having an N-terminal oxidoreductase domain as opposed to a C-terminal domain.

There are three other Steap family members: Steap1, Steap2 and Steap4, and each of these Steap family members are candidates for the redundancy seen in intestinal iron uptake in the absence of Dcytb. They are similar to one another at the amino acid sequence level (>60% similarity) and Steap2 and Steap4 have been shown to exhibit ferric-reductase activities [20], but their involvement in the transferrin cycle remains largely unclear, though it may be tissue-specific as Steap4 has been implicated as the reductase of the transferrin cycle in osteoclasts [21].

Steap1, however, has not been shown to function as a reductase in vitro, perhaps because it is the only family member to lack an N-terminal FNO-like NADPH-binding oxidoreductase domain and thus lacks a source of electrons for reduction. The function of

Steap1 remains unknown, although expression is elevated in prostate cancer cells and is associated with a poor prognosis for the disease [22].

Steap2 also has an ill-defined cellular role and, similar to Steap1, shows significantly increased expression in prostate cancer cells [23]. Its expression is associated with both the proliferative and antiapoptotic pathways in prostate cancer cells [24]. Conversely, an in vitro shRNA knockdown of Steap2 inhibits growth of those prostate cancer cells [24].

Steap4 is also overexpressed in prostate cancer cells, but connections to it mediating inflammatory responses in visceral adipose tissue have also been made. Both obesity and type-II diabetes are related to chronic inflammation in adipose tissue and, indeed, if Steap4 is knocked-out in mice, they exhibit insulin resistance and reportedly develop metabolic syndrome as a result of increased inflammation. However, its role in metabolic syndrome remains controversial (M. Fleming, personal communication, October 2013), [25]. As a result, Steap4 has received significant interest for its putative anti-obesity/diabetes role.

While Steap family members have varied physiological associations, other than Steap3 in the transferrin cycle, it remains unclear what biochemical function they are performing, for example, in prostate cancer cells or adipose cells. with the exception of Steap1, Steap family members are capable of non-transferrin-bound iron (NTBI) reduction [20]. Serum NTBI represents an exceedingly small fraction of the total body iron during normal conditions, but can reach micromolar levels during iron overload. As NTBI is susceptible to Fenton chemistry, Steap3 and the other family members could

function to alleviate this source of oxidative stress. In mouse models both Steap3 and Steap4 are highly expressed in the liver, a site of rapid clearance of NTBI primarily through the transporter Zip14, which is selective for $Fe^{2+}$ [1, 26, 27]. As such an important secondary role for the Steap proteins outside of the transferrin cycle may be in reducing serum NTBI in concert with transport via Zip14.

The Steap Family and Copper Homeostasis

Copper is the third-most abundant transition metal in the body [28]. Physiologically, it is found in the $Cu^{2+}$ as well as the $Cu^{+}$ state. Much like iron, proteins are able to exploit copper's redox chemistry to catalyze electron transfer reactions. Also similar to iron is copper's capacity to form damaging ROS, thus requiring controlled transport and storage processes.

Ohgami et al. discovered that Steap2, Steap3 and Steap4 also function as cupric reductases *in vitro* [20]. However, the role of the Steap family in copper homeostasis is not well-understood. Copper uptake in the cell is similar to iron as copper must be reduced prior to entry, though an endocytotic cycle is not employed for copper entry. The primary plasma membrane copper transporter, Ctr1, only transports the $Cu^{+}$ oxidation state, with plasma copper present in the $Cu^{2+}$ state [29]. As such, a cupric reductase is predicted to work in concert with Ctr1. The Steap family and duodenal cytochrome b (Dcytb) are the only reductases identified to date capable of carrying out this function. *In vitro* experiments have shown that Dcytb exhibits a Michaelis constant, $K_M$, of 23.1 µM for $Cu^{2+}$-histidine [30]. However, plasma levels of non-ceruloplasmin-bound, or "free", copper in healthy individuals are generally below 1.6 µM [31], suggesting Dcytb may not

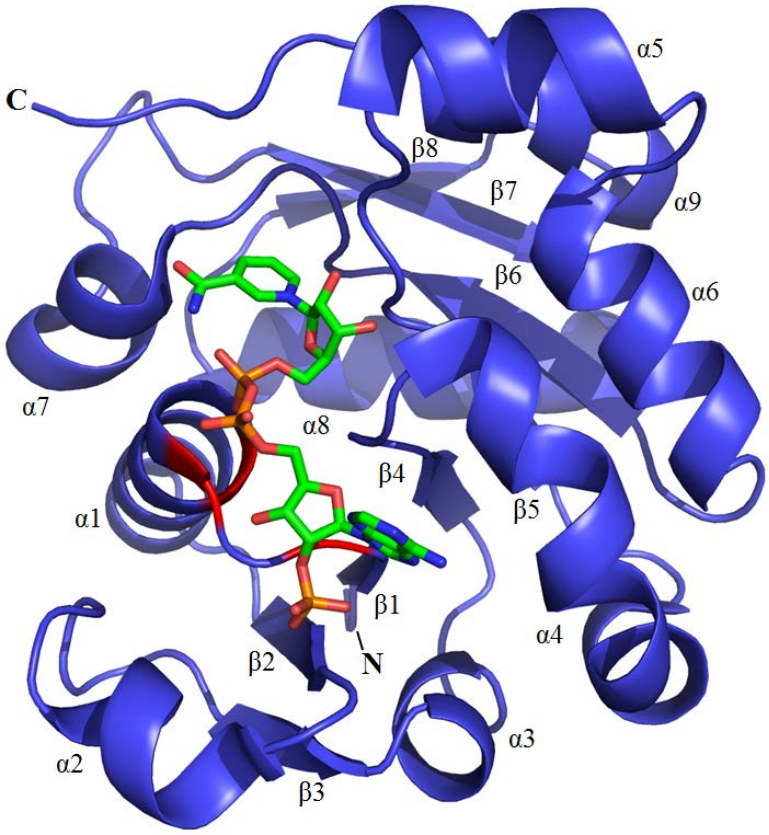


Figure 1.4. Human Steap3 oxidoreductase domain crystal structure with NAPDH bound (PDB ID: 2VQ3). Secondary structural elements are labeled. NADPH shown in green. The dinucleotide binding motif residues ($Gly^{35}$-X-$Gly^{37}$-X-X-$Ala^{40}$) are shown in red.

be the optimal enzyme for this role and instead a Steap family member could be the primary cupric reductase.

The Crystal Structure of the Steap3 Oxidoreductase Domain

In an effort to elucidate the structural basis for Steap3 electron transfer, Sendamarai et al. determined the crystal structure of the N-terminal oxidoreductase domain for Steap3 (residues 1-215) [3]. As expected, the structure was similar to the homolog FNO (backbone RMSD of 1.44Å). Like FNO, Steap3 is able to bind and co-

crystallize with NADPH through a Rossman fold. Steap3, however, was not able to co-crystallize with a flavin, and while inspection of the structure did reveal an open cleft immediately adjacent to the nicotinamide ring of NADPH that might accommodate the isoalloxazine ring of FAD, an obvious biding site for the adenine, ribose, diphosphate and ribitol moieties of FAD were not obvious In addition, flavin docking studies based upon the relative postion of the NADPH molecules, revealed steric clash between the isoalloxazine ring of any flavin, andleucine-206 side chain (Figure 4). It was suggested that truncation leading to expression of the N-terminal domain had allowed Leu-206 to fall into the isoalloxazine binding pocket, preventing recognition of the isoalloxazine

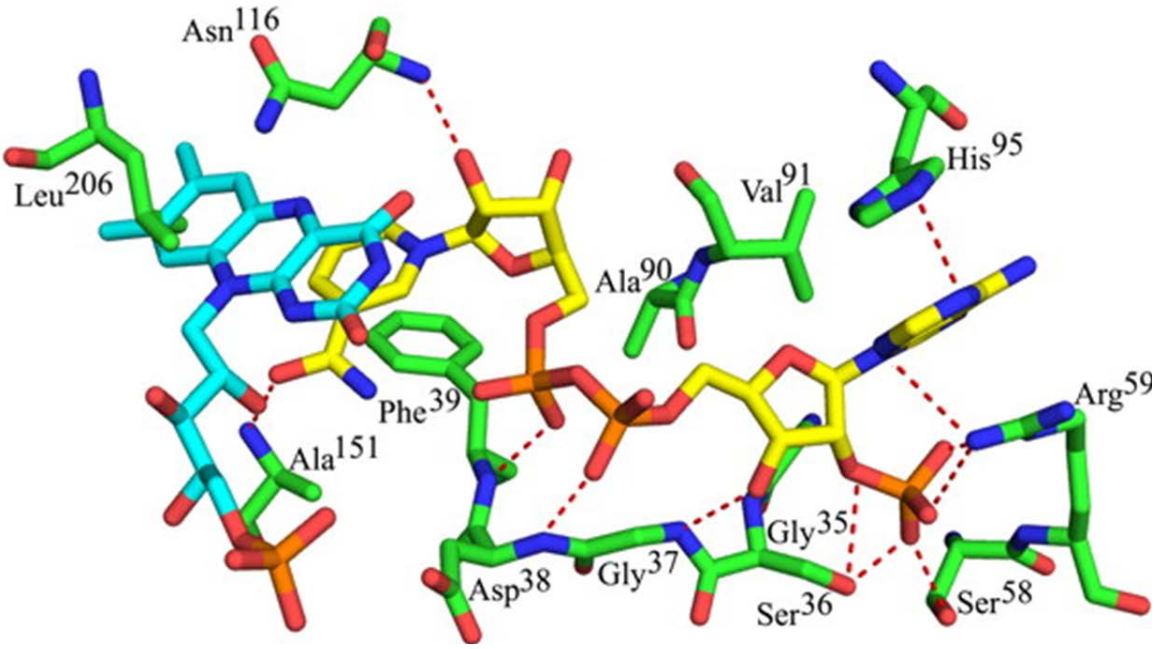


Figure 1.5. Human Steap3 oxidoreductase domain flavin binding site superimposed with FNO crystal structure flavin, $F_{420}$. (PDB ID: 2VQ3; figure featured in [3]. Steap3 sidechains are shown in green, isoalloxazine ring from biliverdin IX reductase shown in teal and NADPH shown in yellow.

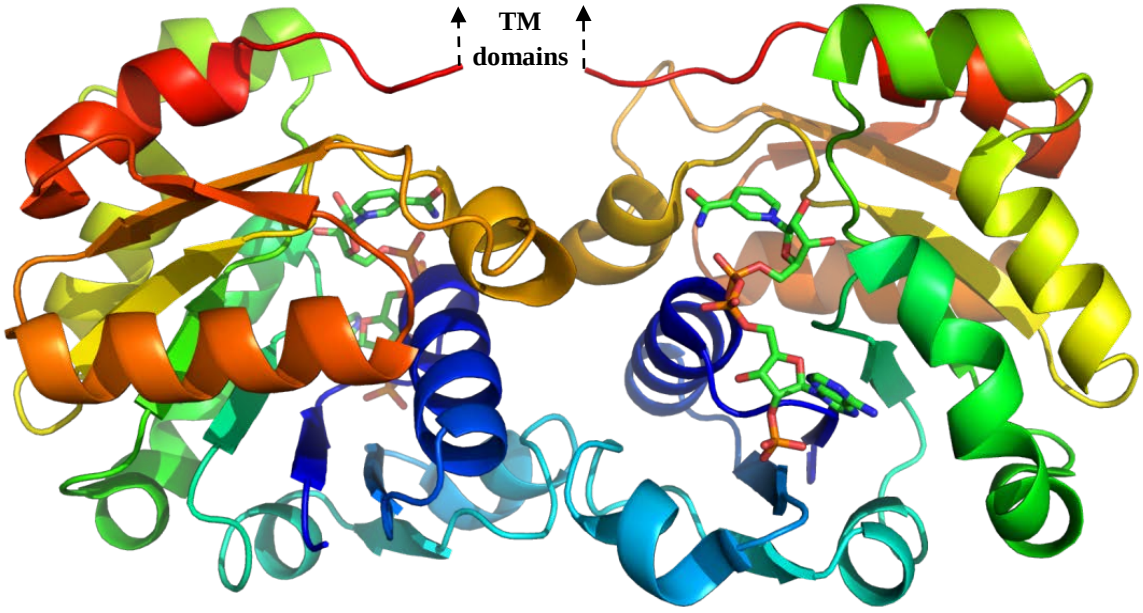


Figure 1.6. Crystal structure of the human Steap3 oxidoreductase domain dimer with NADPH bound (PDB ID: 2VQ3). Structure is colored in "chainbows" convention with N-terminus as dark blue and C-terminus as red. The relative position of the transmembrane (TM) domains are indicated by dashed arrow.

ring. In contrast, in the full-length protein Leu-206 would instead reside in a polypeptide chain that transitioned up into the transmembrane domain. This is in contrast to FNO, which as a soluble protein has an extended C-terminal helix that completes its $F_{420}$ binding pocket. Though flavin binding was not observed, it still seemed necessary for Steap3 to bind a flavin, as the intermediate isoalloxazine ring of flavin is needed to "throttle-down" from a two electron reduction by NADPH to a one electron reduction of copper.

In studying the oxidoreductase domain, Sendamarai et al. also discovered the ability of the protein to form homodimers. When subjected to size exclusion

chromatography, the truncated protein exhibited concentration-dependent dimerization. The crystallized protein also formed also formed two-fold symmetric dimers . The dimer interface was small, composing only 717 $Å^2$ of the solvent-exposed surface area. In the full-length membrane-bound protein, additional interactions along with the 2-dimensional restriction of movement may strengthen the dimerization. Interestingly, the dimer interface was proximal to the NADPH-binding site. The location of the interface suggests that dimerization of the full-length protein may be important to NADPH binding and, as a result, ferric reductase activity.

In the context of the transferrin cycle, the stoichiometry of a Steap3 dimer has an interesting parallel with the holo-transferrin:TfR complex. The Tf:TfR complex contains four $Fe^{3+}$ atoms that must be reduced prior to cell entry and the Steap3 dimer carries a total of four reducing equivalents from the NADPH molecule bound to each protomer. Thus dimerization may serve as a regulatory mechanism, whereby electrons are transferred across the membrane only in the presence of endosomal iron from transferrin.

## Research Goals

The importance ofSteap family proteins to human health has been firmly established. However many fundamental structure-function relationships remain unknown. For example; what is the enzymatic mechanism of Steap3-mediated $Fe^{3+}$ reduction? What is the path of electrons that originate on NADPH and end on a reduced iron atom? To this end, a flavin is strongly implicated in electron transfer, but does not co-crystallize with the truncated oxidoreductase domain of Steap3. Does the protein

really bind a flavin, and if so, which flavin does it prefer? If it binds a flavin, what part of the protein composes the binding site since the oxidoreductase domain alone appears to be inadequate? With regard to the transmembrane domain, most homologs contain two heme cofactors, while Steap3 is only predicted to contain one. Does Steap3 only bind a single heme? What type of heme does Steap3 bind? How does Steap3 reduce iron/copper at the extracellular or lumenal face of the membrane? Does it prefer one metal over another? Does the metal drop into a binding pocket near the porphyrin ring of the heme for direct electron transfer or is there a distant metal binding site and electron-tunneling residues in the intervening space? The truncated Steap3 oxidoreductase domain can dimerize, but is the full-length protein able to form dimers and if so, is that dimer active? Furthermore, if homodimers exist, can Steap family heterodimers also form?

Prior work on Steap family members has relied mainly on mouse knockouts, small-scale cell-surface expression, or recombinant *E. coli*-expressed truncated protein. To answer many of the above questions, a biochemical study of the protein is required, ideally, on purified full-length protein. To our knowledge, a purification of any active Steap family member has not been reported. As such, expression platforms must be tested and purification conditions need to be empirically-determined, including lysis conditions, solubilizing detergent, and affinity fusion tag identity. Development of a ferric reductase activity assay for the full-length protein is also a necessary prerequisite before answering the above questions. The work by Ohgami et al. utilized a cell surface ferric and cupric reductase assay. Using this assay as a starting point, it will need to be modified for kinetic studies of solubilized or purified Steap3, which would require addition of NADPH and/or

a flavin. This assay would allow for structure-function studies of the full-length Steap family of protein in an effort to answer the fundamental questions outlined above.

References


1. Ohgami, R.S., et al., *Identification of a ferrireductase required for efficient transferrin-dependent iron uptake in erythroid cells.* Nat. Genet., 2005. **37**(11): p. 1264-9.

2. Cook, J.D., C.H. Flowers, and B.S. Skikne, *The quantitative assessment of body iron.* Blood, 2003. **101**(9): p. 3359-64.

3. Sendamarai, A.K., et al., *Structure of the membrane proximal oxidoreductase domain of human Steap3, the dominant ferrireductase of the erythroid transferrin cycle.* Proc. Natl. Acad. Sci. U. S .A., 2008. **105**(21): p. 7410-5.

4. Andrews, N.C., *Iron homeostasis: insights from genetics and animal models.* Nat Rev Genet, 2000. **1**(3): p. 208-17.

5. Muir, A. and U. Hopfer, *Regional specificity of iron uptake by small intestinal brush-border membranes from normal and iron-deficient mice.* Am J Physiol, 1985. **248**(3 Pt 1): p. G376-9.

6. Shayeghi, M., et al., *Identification of an intestinal heme transporter.* Cell, 2005. **122**(5): p. 789-801.

7. Nakai, Y., et al., *Functional characterization of human proton-coupled folate transporter/heme carrier protein 1 heterologously expressed in mammalian cells as a folate transporter.* J Pharmacol Exp Ther, 2007. **322**(2): p. 469-76.

8. Latunde-Dada, G.O., R.J. Simpson, and A.T. McKie, *Duodenal cytochrome B expression stimulates iron uptake by human intestinal epithelial cells.* J Nutr, 2008. **138**(6): p. 991-5.

9. Gunshin, H., et al., *Cybrd1 (duodenal cytochrome b) is not necessary for dietary iron absorption in mice.* Blood, 2005. **106**(8): p. 2879-83.

10. Vulpe, C.D., et al., *Hephaestin, a ceruloplasmin homologue implicated in intestinal iron transport, is defective in the sla mouse.* Nat Genet, 1999. **21**(2): p. 195-9.

11. Aisen, P. and I. Listowsky, *Iron transport and storage proteins.* Annu Rev Biochem, 1980. **49**: p. 357-93.

12. Fleming, M.D., et al., *Microcytic anaemia mice have a mutation in Nramp2, a candidate iron transporter gene.* Nat Genet, 1997. **16**(4): p. 383-6.

13. Cain, C.C., D.M. Sipe, and R.F. Murphy, *Regulation of endocytic pH by the Na+,K+-ATPase in living cells.* Proc Natl Acad Sci U S A, 1989. **86**(2): p. 544-8.

14. Eckenroth, B.E., et al., *How the binding of human transferrin primes the transferrin receptor potentiating iron release at endosomal pH.* Proceedings of the National Academy of Sciences of the United States of America, 2011. **108**(32): p. 13089-13094.

15. Ohgami, R.S., et al., *nm1054: a spontaneous, recessive, hypochromic, microcytic anemia mutation in the mouse.* Blood, 2005. **106**(10): p. 3625-3631.

16. Steiner, M.S., et al., *Growth inhibition of prostate cancer by an adenovirus expressing a novel tumor suppressor gene, pHyde.* Cancer Research, 2000. **60**(16): p. 4419-4425.

17. Passer, B.J., et al., *The p53-inducible TSAP6 gene product regulates apoptosis and the cell cycle and interacts with Nix and the Myt1 kinase.* Proc. Natl. Acad. Sci. U. S .A., 2003. **100**(5): p. 2284-9.

18. Amzallag, N., et al., *TSAP6 facilitates the secretion of translationally controlled tumor protein/histamine-releasing factor via a nonclassical pathway.* J. Biol. Chem., 2004. **279**(44): p. 46104-12.

19. Warkentin, E., et al., *The structure of F420-dependent methylenetetrahydromethanopterin dehydrogenase: a crystallographic 'superstructure' of the selenomethionine-labelled protein crystal structure.* Acta Crystallogr. D Biol. Crystallogr., 2005. **61**(Pt 2): p. 198-202.

20. Ohgami, R.S., et al., *The Steap proteins are metalloreductases.* Blood, 2006. **108**(4): p. 1388-94.

21. Zhou, J., et al., *Steap4 Plays a Critical Role in Osteoclastogenesis in Vitro by Regulating Cellular Iron/Reactive Oxygen Species (ROS) Levels and cAMP Response Element-binding Protein (CREB) Activation.* Journal of Biological Chemistry, 2013. **288**(42): p. 30064-30074.

22. Hubert, R.S., et al., *STEAP: a prostate-specific cell-surface antigen highly expressed in human prostate tumors.* Proc. Natl. Acad. Sci. U. S. A., 1999. **96**(25): p. 14523-8.

23. Korkmaz, K.S., et al., *Molecular cloning and characterization of STAMP1, a highly prostate-specific six transmembrane protein that is overexpressed in prostate cancer.* J. Biol. Chem., 2002. **277**(39): p. 36689-96.

24. Wang, L., et al., *STAMP1 is both a proliferative and an antiapoptotic factor in prostate cancer.* Cancer Res, 2010. **70**(14): p. 5818-28.

25. Wellen, K.E., et al., *Coordinated regulation of nutrient and inflammatory responses by STAMP2 is essential for metabolic homeostasis.* Cell, 2007. **129**(3): p. 537-48.

26. Ramadoss, P., et al., *Regulation of hepatic six transmembrane epithelial antigen of prostate 4 (STEAP4) expression by STAT3 and CCAAT/enhancer-binding protein alpha.* J. Biol. Chem., 2010. **285**(22): p. 16453-66.

27. Zhao, N., et al., *ZRT/IRT-like protein 14 (ZIP14) promotes the cellular assimilation of iron from transferrin.* J. Biol. Chem., 2010. **285**(42): p. 32141-50.

28. Taki, M., et al., *Development of highly sensitive fluorescent probes for detection of intracellular copper(I) in living systems.* J Am Chem Soc, 2010. **132**(17): p. 5938-9.

29. Lee, J., et al., *Biochemical characterization of the human copper transporter Ctr1.* J Biol Chem, 2002. **277**(6): p. 4380-7.

30. Wyman, S., et al., *Dcytb (Cybrd1) functions as both a ferric and a cupric reductase in vitro.* FEBS Lett., 2008. **582**(13): p. 1901-6.

31. McMillin, G.A., J.J. Travis, and J.W. Hunt, *Direct Measurement of Free Copper in Serum or Plasma Ultrafiltrate.* American Journal of Clinical Pathology, 2009. **131**(2): p. 160-165.

# CHAPTER TWO

# EXPRESSION AND SOLUBILIZATION OF HUMAN STEAP3 IN HEK-293T CELLS

## Introduction

Performing functional studies of an integral membrane protein involves optimization unique from soluble proteins. The expression system must be chosen carefully as those commonly employed have unique properties that may or may not impact the expression and folding of the protein of interest. Human embryonic kidney cells have been a popular choice in the expression of recombinant mammalian proteins since the cell line was generated in 1977 [1]. The cell line is easily maintained and robustly transfectable. The higher-order eukaryotic post-translational processing is especially important in the expression of integral membranes. In Escherichia coli cells, an overexpressed human integral membrane protein will commonly misfold, creating toxic inclusion bodies to the host cell. Additionally, prokaryotic and lower-order eukaryotic systems will either not include post-translational modifications or have altered modifications from their in vivo state. Furthermore, the lipid environment is an important factor to the stability to an integral membrane and non-mammalian systems will have different lipid compositions. These factors can play significant roles in the recombinant expression of mammalian proteins, making a human cell line like HEK 293 an attractive option. Functional assays must be designed with the topology of the protein in the membrane and resulting accessibility of a site of interest for that assay.

As it is exceptionally useful to assay a protein of interest away from others, the methods for purification of an integral membrane protein must be carefully and, in most cases, empirically determined. Detergents are a primary concern in the purification of a membrane protein. For effective membrane extraction and purification, a range of detergents need to be assessed to identify the optimal one. A detergent may seemingly perform well as assessed by a method such as SDS-PAGE, but if the protein forms high-order aggregates that are non-physiological, then subsequent analysis will be negatively affected. A means to screen detergents quickly and effectively is through the use of size-exclusion chromatography in which a fluorescent protein-tagged protein of interest is used, a process called fluorescence size exclusion chromatography (FSEC; [2]).

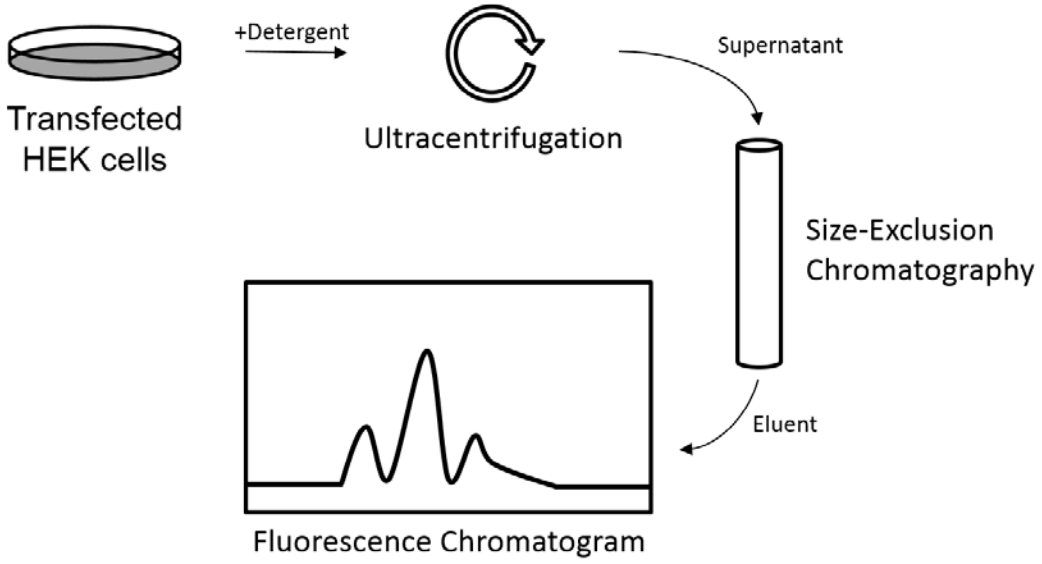


Figure 2.1. Overview of fluorescence size-exclusion chromatography (FSEC) detergent screen.

Homogeneity of the protein species can be easily assessed by surveying the fluorescence of the eluted material. Coupled with the measuring of fluorescence recovery after ultracentrifugation of the detergent-added material, an optimal detergent can be chosen.

To examine the viability of transiently expressing recombinant Steap3 in the HEK cell line, HEK 293T (a variant containing the large T antigen from the SV-40 virus). An expression analysis with various constructs. As the activity of the enzyme is a focal point of analysis, expression constructs were assessed on the basis of cell surface ferric reductase activity. With active construct, the ability of detergents to solubilize them from the lipid bilayer was assessed with a fluorescence size exclusion chromatography screen.

Solving the Steap3 cytoplasmic oxidoreductase domain crystal structure brought many interesting observations. One notable one was that the domain crystallized as a two-fold symmetrical dimer. Additionally, it was observed to migrate in size exclusion chromatography as a dimer. The dimer interface was small, composing only 8% of the solvent-exposed surface area, but was well-conserved. The oligomeric state of the full-length has remained unknown, however. Dimerization may functionally critical as the interface in the oxidoreductase domain is adjacent to the NADPH binding site. Additionally, in the context of the transferrin cycle, a dimerized complex would be able to reduce four iron atoms from the two bound NADPH molecules and the Tf:Tfr complex binds four iron atoms. The stoichiometric symmetry not only produces the hypothesis of a Steap3 dimer, but a Steap3-Tf:TfR supercomplex as well.

As no Steap family member has been purified, partially or otherwise, to date, the work described here seeks to provide important foundational details for Steap3

recombinant expression, activity, and purification. Can we measure the ferric reductase activity of Steap3 using the established assay and then adapt that assay to fit our larger-scale needs? To seek to purify Steap3, the extraction from the lipid membrane is one of the most crucial steps. Can we solubilize Steap3 from the membrane with a detergent? If so, which detergent optimally solubilizes Steap3? Finally, with an established expression system for Steap3, can we use it to investigate an important attribute of Steap3? The oxidoreductase domain dimerizes, but is this an artefact of truncation or does the full-length protein dimerize as well? These findings will serve as an important foundation for future studies of Steap3 or other Steap family members.

## Materials and Methods

### Steap3 Expression Construct Cloning

*Mus musculus* Steap3 cloned in to the pCMV.tag4a expression plasmid was provided by Dr. Mark Fleming. To generate venus fluorescent protein (VFP)-tagged Steap3 fusions, the Steap3 gene was PCR-amplified to include attB transposition sites and subcloned into the pDONR201 donor vector using the BP clonase II enzyme of the Gateway system (Invitrogen) to create the entry vector pENTR.Steap3. A gateway destination vector encoding for a C-terminal VFP fusion tag (pDEST.Venus) was generously provided by Mensur Dlakic (Montana State University). The LR clonase II enzyme kit (Invitrogen) was used to transpose the Steap3 gene in pENTR.Steap3 to the pDEST.Venus destination vector to create the Steap3.Venus expression vector.

Adherent HEK-293 Cell
Culture and Transfection

For adherent cell experiments, HEK-293T cells from ATCC were cultured in Dulbecco's modified Eagle's medium (DMEM) supplemented with 10% fetal bovine serum (FBS), 100 U/ml Penicillin and 100 µg/mL Streptomycin at 37 °C in a humidified incubator with 5% CO2. On the day of transfection, cells were at ~70% confluence. Cells were transected with GenePorter2 (Genlantis) and 2 µg of plasmid DNA according to manufacturer's instructions. The lipid-DNA solution was added to cells in DMEM media that did not contain FBS or antibiotics. Four hours post-transfection, the transfection media was replaced with fresh FBS- and antibiotic-containing media.

Suspension-Adapted HEK-293
Cell Culture and Transfection

HEK 293F cells (Invitrogen) were cultured in Freestyle 293 expression medium in spinner flasks rotating at 100 R.P.M. on a magnetic spinner plate in a 37 °C humidified incubator with 5% $CO_2$ atmosphere. Cells were grown to log phase on the day of transfection and centrifuged at 1000 xG for 5 minutes. Conditioned media was removed and cells were resuspended in fresh media to $1x10^6$ cells/ml. In 2 mL of PBS, pH 7.4, 20 µg of plasmid DNA and 40 µg of linear polyethyleneimine (PEI; Polysciences) were added and the mixture was incubated at room temperature for 15 minutes. The DNA-PEI mixture was then added to 20 mL of cells in a spinner flask in a humidified 37 °C incubator with 5% $CO_2$. The cells were then grown for 16-72 hours before harvesting.

Adherent HEK-293 Cell
Surface Ferric Reductase Assay

Steap3 Forty-eight hours after transfection, the cells were washed three times with phosphate-buffered, pH 7.4, and incubated in iron uptake buffer (IUB; 25 mM MES, 25 mM MOPS, 140 mM NaCl, 5 mM glucose, 5.4 mM KCl, 1.8 mM $CaCl_2$, 800 μM $MgCl_2$) with 50 μM $Fe^{3+}$-NTA and 200 μM ferrozine. After a one hour incubation at 37 °C, the supernatant was removed and the formation of $Fe^{2+}$-ferrozine complexes was analyzed by a spectrophotometer at 562 nm ($\varepsilon$ = 27,900 $M^{-1}cm^{-1}$). Cell number was determined by detaching cells from the well surface with trypsin-EDTA solution and addition of 10 μL of suspended cells to a hemacytometer with subsequent analysis with an inverted light microscope.

Suspension-Adapted HEK-293
Cell Surface Ferric Reductase Assay

The ferric reductase assay was performed essentially as described above with the following changes. 16-72 hours after transfection, cells were centrifuged 1000 xG for 5 minutes and the cell pellet was washed two times with PBS, pH 7.4. The cell pellet was then resuspended in IUB with Fe-NTA and ferrozine and transferred to a 6- or 24-well plate. After a one hour incubation at 37 °C, the reduction of $Fe^{3+}$ was determined through the detection of $Fe^{2+}$-ferrozine complexes by monitoring absorbance at 562 nm ($\varepsilon$ = 27,900 $M^{-1}cm^{-1}$). Data was analyzed by GraphPad Prism 5.0 (GraphPad Software).

Fluorescence Size Exclusion Chromatography

Forty-eight hours after transfection, cells in 6-well plates were washed three times with PBS, pH 7.4. Cells were then detached by gentle pipetting and suspended in 5 mL of PBS, pH 7.4, detergent [20 mM n-dodecyl-β-D-maltopyranoside (Anatrace), 20 mM Triton X-100 (Alfa Aesar), 250 mM octyl-β-D-glucopyranoside (Calbiochem), 125 mM CHAPS (MP Biomedicals), 100 mM sodium dodecyl sulfate (SDS; Fisher), 0.6 mM Tween 80 (Sigma), 1 mM Brij-35 (Fisher], and 1X protease inhibitor cocktail III (Calbiochem). The suspended cells were rotated for one hour at 4 °C. After rotation, insoluble material was pelleted in a Beckman-Coulter Optima Max ultracentrifuge at 66,000 xG for 40 minutes. The supernatant was then injected into a Superdex 200 (S-200) size-exclusion column equilibrated in 20 mM Tris-HCl, pH 8.0, 150 mM NaCl, 1 mM EDTA, 1 mM n-dodecyl-β-D-maltopyranoside (Anatrace) at 4 °C with a flow rate of 0.4 mL/min. Fluorescence chromatograms were recorded with an in-line Waters 470 scanning fluorescence detector (515 nm excitation, 530 nm emission). Additionally, solubilized material before and after ultracentrifugation was analyzed fluorometrically with a Tecan Safire microplate fluorometer (515 nm excitation, 530 nm emission). Qualitative assessment of a detergent was through the magnitude of solubilized fluorescence after ultra-centrifugation alongside the peak mono-dispersity in the fluorescence chromatogram.

Sample Preparation for Confocal Microscopy

HEK-293T cells were grown and transfected as described above, with the exception that cells were grown on glass cover slips in a 6-well plate well. 24-hours post-

transfection, cells were washed three times with PBS. Plasma membranes were labeled with wheat germ agglutinin conjugated to AlexaFluor-633 (Invitrogen) at 5 µg/mL in PBS was applied to the cells for 10 minutes at 37 °C. Cells were then washed three times with PBS. Cells were then fixed with 4% formaldehyde in PBS for 15 minutes at 37 °C, after which they were washed three times with PBS. Nuclei were then stained by incubation with 1 µg/mL DAPI in PBS for 5 minutes at room temperature protected from light, followed by three washes of PBS. Finally, the cell-containing coverslips were removed from the wells and placed on a cover slide, immersed in a single drop of Vectashield mounting medium, and sides were sealed with nail polish. The mounted cells were viewed on a Leica TCS-SP2 AOBS confocal scanning laser microscope with a UV laser for DAPI imaging, ArKr laser for venus fluorescent protein imaging, and He/Ne laser for wheat germ agglutinin imaging. Image analysis was performed with Imaris (Bitplane) and ImageJ (rsb.info.nih.gov/ij).

## Results

### Steap3 Cell-Surface Ferric Reductase Activity of Tagged Steap3

In identifying Steap3 as the ferric reductase in the transferrin cycle, an in vitro transient-expression activity analysis was used to confirm its enzymatic activity [3]. This analysis utilized an $Fe^{3+}$-NTA:ferrozine colorimetric assay to determine activity of protein at the surface of live HEK 293T cells. To assess the quality of our system, the experiment was partially repeated, but with the addition of a new Steap3 expression vector. The Steap3.Venus expression vector contains a venus fluorescent protein fusion at

the C-terminus. Fluorescent protein fusions have become popular for use in biochemical applications as a means of tracking the presence of a protein of interest. For use in further applications it was important to ensure Steap3 activity was not disrupted by the presence of a large fusion to the C-terminus. Similar to that found by Ohgami et al, mouse Steap3-transfected HEK cells exhibit ferric reductase activity significantly above empty vector-transfected cells (Figure 2.2) [3]. Furthermore, the cell-surface ferric reductase activity for the venus-fluorescent protein-tagged Steap3 was not significantly altered (Figure 2.2).

## Optimization of Cell-Surface Ferric Reductase Assay

To use the cell surface ferric reductase assay for Michaelis-Menten kinetic studies, the assay required a larger scale format than that previously described. A spinner-flask culture format was tested. In this format, a single transfected culture would be split into individual wells of a multi-well culture plate at the time of assaying and be subjected to a particular iron concentration. To examine the optimal time to assay post-transfection a time-scale activity experiment was performed. At specific time points, a portion of cells from the transfected culture were taken and examined for cell-surface ferric reductase activity (Figure 2.3). The resulting highest activity-per-cell occurred at 24 hours post-transfection with the activity declining with time.

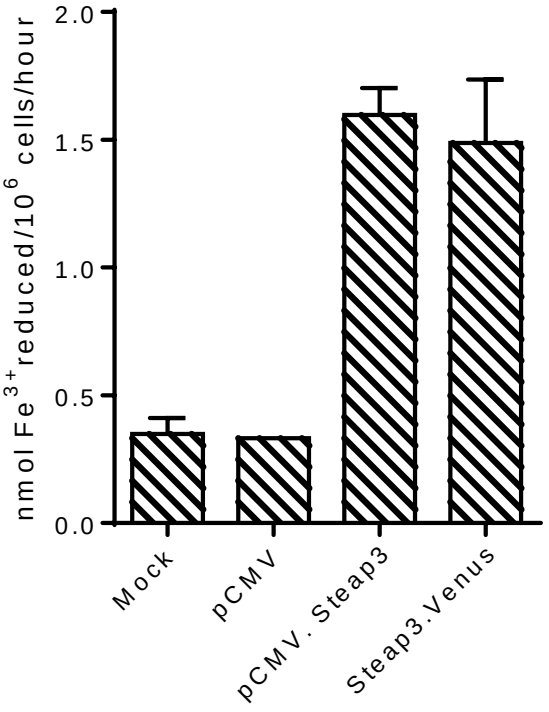


Figure 2.2. Cell surface ferric reductase activity of transiently-transfected HEK 293T cells. Cells were assayed for ferric reductase activity 24 hours-post transfection. Data shown is mean with error bars representing standard deviation from three independent transfections.

This is likely due to the lack of selective pressure for cells carrying the expression plasmid. Future large-scale cell-surface reductase assays with performed with transfected cells 24 hours-post-transfection.

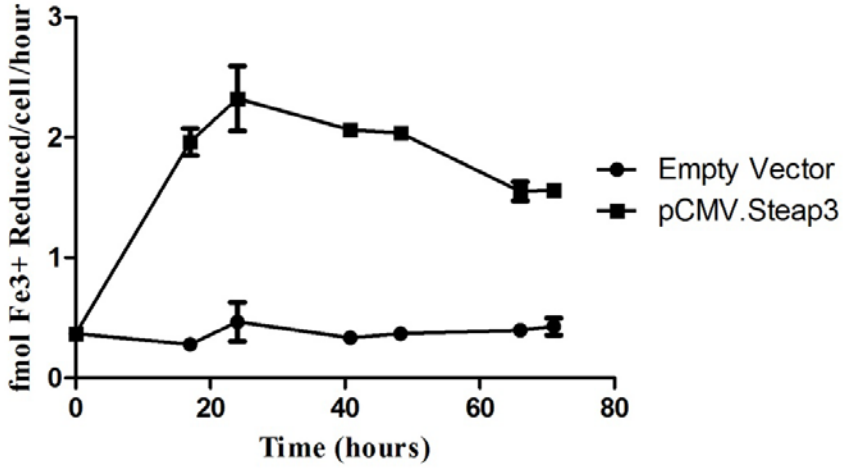


Figure 2.3. Steap3 cell surface ferric reductase assay time course experiment. HEK 293F cell surface ferric reductase assays were performed at time points from 0-72 hours. All assays were performed in triplicate.

## Steap3 Detergent Screen via Fluorescence Size Exclusion Chromatography

Solubilizing an integral membrane protein from the lipid bilayer requires the use of a detergent to form a micelle about the membrane-embedded portion of the protein. While there are many commercially-available detergents for this purpose, a particular integral membrane protein will likely only adequately solubilize in a small number of them. To determine an optimal solubilizing detergent for Steap3 from HEK-293T membranes, a detergent screen utilizing fluorescence size exclusion chromatography (FSEC) was performed with several detergents. FSEC relies on a fluorescent analyte to record its elution from the column. To this end, *Mus musculus* Steap3 was cloned into the pDEST.Venus vector. The gene product from this vector includes an N-terminal FLAG fusion and C-terminal venus fluorescent protein fusion. Transfected HEK-293T cells solubilized in a detergent were ultracentrifuged and the resulting supernatant was

subjected to FSEC using a Superdex S-200 column. Detergents were assessed on their ability to solubilize fluorescent-tagged Steap3 and the dispersity from chromatography.

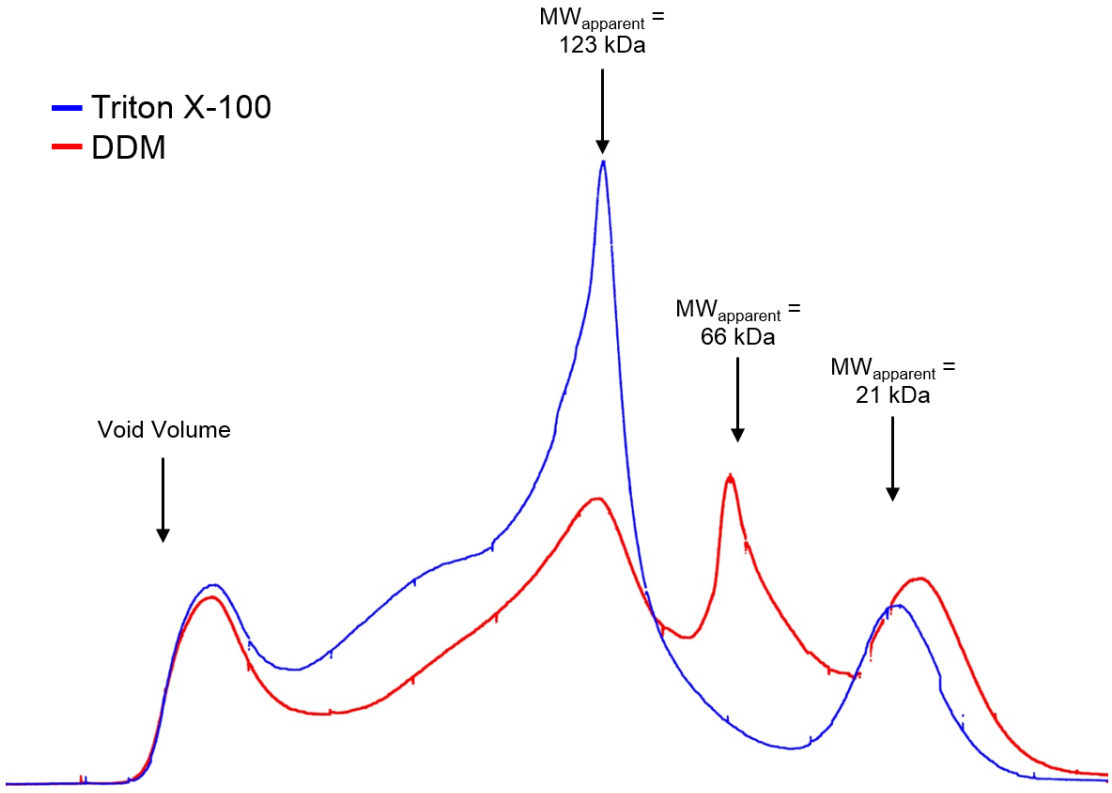


Figure 2.4. Fluorescence signal chromatograms from Steap3 FSEC detergent screen. Two representative chromatograms for detergent-solubilized protein from Steap3.Venus-transfected HEK 293T cells. Labeled molecular weight values are from a standard curve created with protein standard run in the respective detergent-containing running buffer.

Among the detergents tested, Triton X-100 and sodium dodecyl sulfate (SDS) exhibited the highest degree of both fluorescence recovery post-ultracentrifugation and monodispersity (Table 1). Triton X-100-solubilized Steap3 appeared to migrate primarily as a monomer on an S-200 column with an apparent molecular weight of 123 kDa

(Figure 2.4). A VFP-fused Steap3 molecule has a molecular weight of 74 kDa and the remainder of the species weight is expected to be due to the detergent micelle. Triton X-100 was chosen for use in future studies due to the incompatibility of SDS with various affinity purification media.

Table 2.1. Steap3 fluorescence size-exclusion chromatography detergent screen quantitative and qualitative values. "Solubilized" represents supernatant from lysate ultracentrifugation.

| | **Fluorescence units** | | **Percent** | **Chromatogram** |
|---|---|---|---|---|
| **Detergent** | **Lysate** | **Solubilized** | **Recovery** | **Quality** |
| Brij-35 | 48450 | 15414 | 32 | Polydisperse |
| CHAPS | 24753 | 16995 | 69 | Polydisperse |
| DDM | 16850 | 19687 | 117 | Polydisperse |
| Octylglucopyranoside | 43303 | 17195 | 40 | Polydisperse |
| SDS | 16969 | 27207 | 160 | Monodisperse |
| Triton X-100 | 15209 | 21245 | 140 | Monodisperse |
| Tween-80 | 29906 | 2385 | 8 | Low Fluorescence |

## Detection of Steap3 Dimerization via a Bimolecular Fluorescence Complementation Assay

The structural studies of the oxidoreductase domains of Steap3 and Steap4 revealed the ability of the domain to form two-fold symmetrical dimers. Thus, we hypothesized that the full-length Steap3 protein is able to form dimers in the cell. Furthermore, the structures of Steap3 and Steap4 are very similar, with a backbone RMSD of 1Å [4, 5]. This, coupled with the significant sequence similarity of the four family members (>60%) led us to hypothesize that Steap family heterodimers are also able to form. To test these hypotheses, a bimolecular fluorescence complementation assay was performed, wherein interacting proteins of interest are each fused to the N- or C-terminal half of a fluorescent protein. Dimerization is then identified as a result in

recombination of the fluorescent protein into a functional fluorophore. Steap3 fused to the C-terminal venus fluorescent protein (VFP) fragment was co-transfected in HEK-293T cells along with other Steap family members fused to the N-terminal VFP fragment (Figure 2.5). Steap3 paired with each Steap family member, including Steap3, resulted in fluorescence as analyzed by confocal microscopy.

In comparison to Steap3 fused to the full-length VFP, the BiFC pairings of Steap3 with Steap2, Steap3 and Steap4 resulted in similar fluorescence distribution in the cells. Steap1 and Steap3, however, resulted in a unique perinuclear fluorescent pattern. Steap3 was also co-transfected with CCR5 (row 2 in Figure 2.5), an unrelated integral membrane protein, to serve as a negative control. Fluorescence is present in these cells, but is in a unique localization with the majority of the fluorescence appearing in a large intracellular structure. This structure is similar to those found in negative controls in other membrane protein BiFC studies and is perhaps a cellular sequestration of an unnatural association of proteins [6].

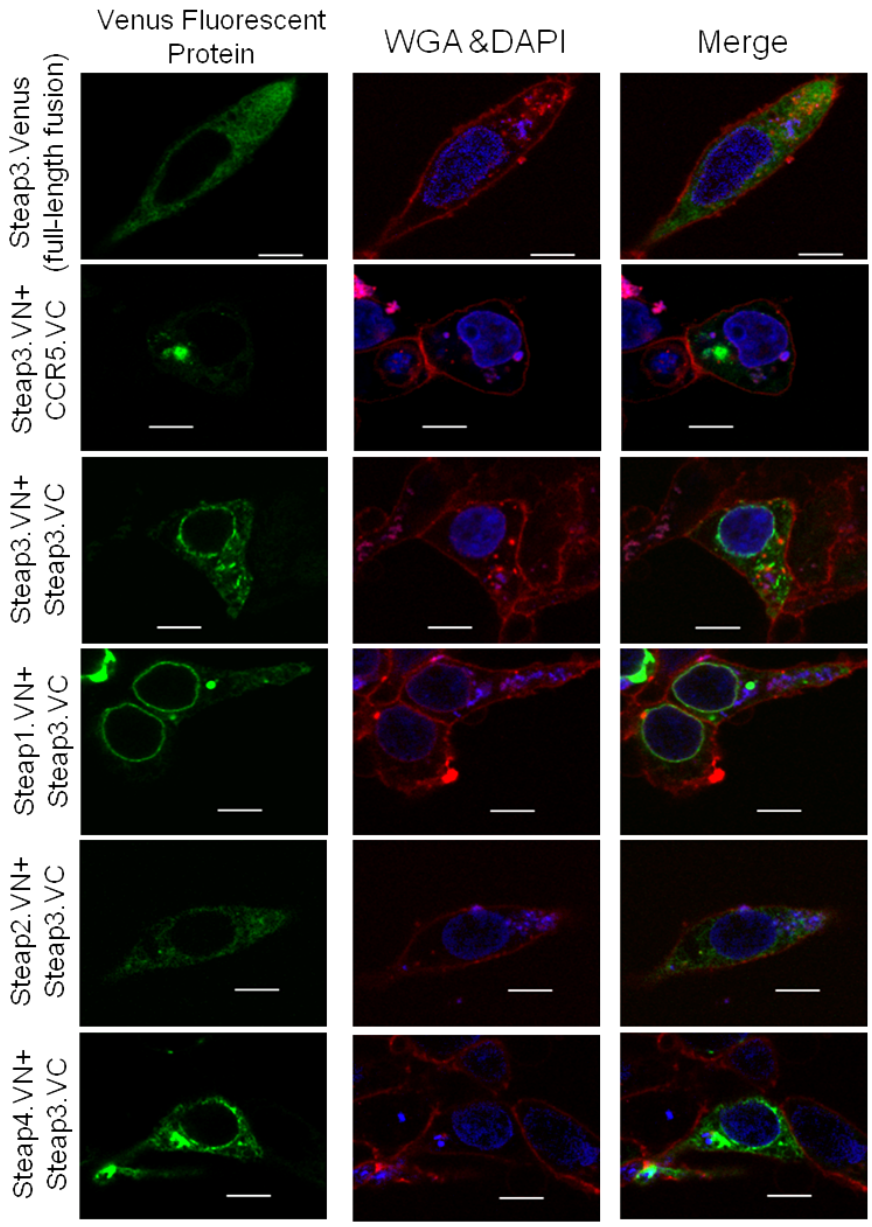


Figure 2.5. Bimolecular fluorescence complementation (BiFC) assay of Steap3 and Steap family members. HEK-293T cells co-transfected with expression plasmids were analyzed with laser-scanning confocal microscopy. Expression plasmids used in the respective transfections are indicated on the left-side of the rows. “Venus” represents a fusion of the full-length venus fluorescent protein (VFP), “VN” represents a fusion of residues 1-173 of VFP and “VC” represents a fusion of residues 155-238 of the VFP. The fluorescent signals for the respective fluorophores are indicated above the columns, with the merged signals in the right column. “WGA” is wheat germ agglutinin-AlexaFluor 633, a plasma membrane-binding fluorophore.

# Discussion

Though membrane protein expression and purification has developed greatly recently, there remains a dearth of structural and biochemical information in comparison to soluble proteins. Only recently was a structure determined for another membrane protein ferric reductase, duodenal cytochrome b [7]. Even still, methods utilized for one membrane protein likely will not directly apply to another. As a result, to perform detailed biochemical analyses of Steap3, methods had to be developed.

## Steap3 Ferric Reductase Activity is Unaltered by VFP Fusion

The enzymatic activity of Steap3 is an important parameter to establish. Not only are the ferric and cupric reductase kinetics unexplored and of high interest, being able to monitor activity as a purification progresses is highly valuable. A ferric reduction assay for Steap3 at the surface of transfected cells was utilized in the seminal Steap3 work to identify it as a reductase and a similar one was used to identify it as a cupric reductase. For our purposes in subsequent studies, it was necessary to employ this assay and, furthermore, to ensure that Steap3 carrying a venus fluorescent protein (VFP) fusion at the C-terminus did not impair activity. In our hands, untagged Steap3 displayed significant above background ferric reductase activity (Figure 2.2). This represents an important initial benchmark, indicating successful culture and transfection of HEK-293T cells as well as Steap3 expression. Additionally, no change in ferric reductase activity from un-tagged Steap3 was observed for the Steap3-VFP fusion. Thus for FSEC work, it was assumed that Steap3-VFP was a viable enzyme valid for solubilization studies.

## Steap3 is Most Active at Cell-Surface 24-Hours Post-Transfection

In lieu of purified protein, the cell-surface ferric reductase assay can also be utilized for characterizing the activity in additional ways, such as kinetic analysis, mutational analysis or inhibitor studies. To perform such studies, the single well of a 6-well plate employed above would not be sufficient. To increase the scale of the ferric reductase assay system, a suspension-adapted culture was utilized. In transfection of a single culture of cells and aliquoting into wells of a tray at a later time point, it could be ensured that each well had roughly identical conditions except for the variable being tested. To this end, HEK 293F cells were selected for culturing. The commercially available cell line is suspension-adapted and has been used previously for recombinant protein expression studies [8]. To determine the optimal time-point to partition the cells from the master transfection culture, a time-point study was performed (Figure 2.3). At select times, a portion of the culture was plated and assayed for ferric reductase activity. There, it was observed that the activity-per-cell increased until 24hours post-transfection and then gradually-decreased thereafter. This is likely due to the lack of selective pressure on the transiently-transfected cells, where untransfected cells likely grow faster, reducing the per-cell activity of the culture. In any case, for future activity work with Steap3 a 24-hour time point post-transfection was utilized to assay the cells.

## Triton X-100 is the Optimal Steap3 Solubilizing Detergent

The extraction of Steap3 from the lipid bilayer in a functional state is a crucial step towards purifying the enzyme. Many commercially-available detergents have been

used successfully for this purpose [9], but is protein-dependent. To identify the optimal detergent for Steap3 solubilization, a fluorescence size exclusion chromatography (FSEC) screen was performed. Seven detergents were screened, with each of the three major classes of polar head groups represented: ionic, nonionic, and zwitterionic. The dispersity displayed on the fluorescence chromatogram paired with the amount of solubilized fluorescence provided the basis of assessment. An optimal detergent should solubilize a high percentage of initial fluorescence and that solubilized protein should be monodisperse on the chromatogram, the peak elution volume depending of the oligomeric state. Triton X-100, sodium dodecyl sulfate (SDS), and DDM all exhibited greater than 100% fluorescence recoveries post-ultracentrifugation (Table 1). This is likely an effect of heterogeneity of the sample prior to clearing from ultra-centrifugation. The fluorescent chromatograms from Triton X-100 and SDS were both primarily monodisperse (Figure 2.4 and Table 1). SDS, while well-performing under these parameters, is considered a harsh detergent that is not often used in biochemical studies and is incompatible with many affinity purification techniques and functional assays. As a result, Triton X-100 was chosen as the optimal detergent for future work from the screen. Triton X-100 is a non-ionic detergent that is commonly used for solubilization of membrane proteins. As a target of purification of Steap3 would be solving its crystal structure, there are important considerations to be made concerning Triton X-100. It is not ideal for crystallography because it has a large alkyl tail that results in a large micelle. Typically, small, compact micelles are preferred in crystallography. Another property that makes Triton X-100 less desirable for crystallography is its chemical heterogeneity

resulting in irregular micelles. As a result, crystallographic studies would require purification and subsequent replacement of Triton X-100 with a small-chain detergent, such as octylglucoside.

## Steap3 is Able to Form Dimers with Other Steap Family Members

After establishing an HEK-293T expression system for Steap3 we sought to answer an important functional question formed from the previous crystallographic study of the truncated oxidoreductase domain. The oxidoreductase domain was migrated on a size-exclusion column as a dimer in a concentration-dependent fashion [4]. Furthermore, when crystallized, the protein forms a two-fold symmetrical dimer. The dimer interface is fairly small, composing only 8% of the solvent-exposed surface area. Thus, the study presented the question of whether the full-length integral membrane protein forms dimers. Additionally, the high degree of sequence similarity (>60%, [10]) between family members raises the possibility that two family members can form a heterodimer. To investigate this question, the bimolecular fluorescence complementation (BiFC) assay was employed. In the BiFC assay, fragments of the green fluorescent protein are fused to putative interacting partners. If the proteins do indeed interact, bringing the fusions together, they are able to recombine into a GFP beta barrel and subsequent fluorophore maturation. Thus, observed fluorescence (commonly with fluorescence microscopy) is as only as a result of two proteins of interest interacting. Confocal microscopy was utilized to analyze HEK-293T cells co-transfected with Steap3 and other family members (Figure 2.5). Thus, not only could the presence of fluorescence be determined, but the cellular

distribution of that fluorescence as well. Steap3 paired with each Steap family member, including Steap3, produced BiFC-positive cells. Using cells transfected with Steap3 fused to the complete VFP for comparison, Steap3 paired with Steap2, Steap3, and Steap4 produced a comparable subcellular distribution. This distribution is similar to that previously observed for Steap3 [3], where the enzyme is primarily localized to intracellular membranes.

### Steap1 and Steap3 Dimerization Induces Perinuclear Localization

Interestingly, Steap3 paired with Steap1 produced a unique, primarily perinuclear fluorescence pattern. This may be as a result of a dimer pair that is incompatible with necessary trafficking mechanisms, but the pattern is unique from the negative control, Steap3 co-transfected with CCR5, an unrelated chemokine receptor. It is important to note the fact that Steap1 is the only family member that lacks the oxidoreductase domain. Dimerization of Steap3 with other Steap family members could modify or tune function. The proximity of the NADPH binding site to the dimer interface in the oxidoreductase domain crystal structure raises the hypothesis that dimerization is a prerequisite for reductase activity. If that is the case, dimerization with Steap1 would be a mode to sequester Steap3 from other active Steap dimer partners, preventing reductase activity.

Together, this data provides an important establishment of the Steap3 expression system. An established enzymatic assay makes characterization of that activity possible and gives a signal to monitor during purification. Towards purification, identifying Triton X-100 as the optimal solubilization detergent is a key step. Finally, the utilization of the

expression system to identify the dimerization of Steap3 and its family members is an important confirmation of a previous hypothesis for Steap family function, but also an illustration of the utilization of this system.

References


1. Graham, F.L., et al., *Characteristics of a human cell line transformed by DNA from human adenovirus type 5.* J Gen Virol, 1977. **36**(1): p. 59-74.

2. Kawate, T. and E. Gouaux, *Fluorescence-detection size-exclusion chromatography for precrystallization screening of integral membrane proteins.* Structure, 2006. **14**(4): p. 673-81.

3. Ohgami, R.S., et al., *Identification of a ferrireductase required for efficient transferrin-dependent iron uptake in erythroid cells.* Nat. Genet., 2005. **37**(11): p. 1264-9.

4. Sendamarai, A.K., et al., *Structure of the membrane proximal oxidoreductase domain of human Steap3, the dominant ferrireductase of the erythroid transferrin cycle.* Proc. Natl. Acad. Sci. U. S .A., 2008. **105**(21): p. 7410-5.

5. Gauss, G.H., et al., *The Crystal Structure of Six-transmembrane Epithelial Antigen of the Prostate 4 (Steap4), a Ferri/Cuprireductase, Suggests a Novel Interdomain Flavin-binding Site.* Journal of Biological Chemistry, 2013. **288**(28): p. 20668-20682.

6. Haider, A.J., et al., *Dimerization of ABCG2 analysed by bimolecular fluorescence complementation.* PLoS One, 2011. **6**(10): p. e25818.

7. Lu, P., et al., *Structure and mechanism of a eukaryotic transmembrane ascorbate-dependent oxidoreductase.* Proc Natl Acad Sci U S A, 2014. **111**(5): p. 1813-8.

8. Hasebe, A., et al., *Efficient production and characterization of recombinant human NELL1 protein in human embryonic kidney 293-F cells.* Mol Biotechnol, 2012. **51**(1): p. 58-66.

9. Seddon, A.M., P. Curnow, and P.J. Booth, *Membrane proteins, lipids and detergents: not just a soap opera.* Biochim Biophys Acta, 2004. **1666**(1-2): p. 105-17.

10. Ohgami, R.S., et al., *The Steap proteins are metalloreductases.* Blood, 2006. **108**(4): p. 1388-94.

# CHAPTER THREE

## THE CRYSTAL STRUCTURE OF SIX-TRANSMEMBRANE EPITHELIAL ANTIGEN OF THE PROSTATE 4 (STEAP4), A FERRI/CUPRIREDUCTASE, SUGGESTS A NOVEL INTERDOMAIN FLAVIN-BINDING SITE.

### Contribution of Authors and Co-Authors

Manuscript in Chapter 3

Author: George H. Gauss

Contributions: Performed cloning and screening of Steap4 oxidoreductase domain constructs. Developed purification protocol for the purification of Steap4 oxidoreductase domain. Developed NADPH oxidase activity assay. Performed x-ray crystallography of Steap4 oxidoreductase domain. Assisted in purification of Steap4 constructs for activity analysis. Assisted in performing kinetic analysis of both oxidoreductase domain and full-length Steap4. Generated figures and wrote the manuscript in preparation for submission.

Co-author: Mark Kleven

Contributions: Performed cloning of full-length Steap4 constructs. Developed cell-surface ferric and cupric reductase activity assays. Assisted in purification of Steap4 constructs for activity analysis. Assisted in performing kinetic analysis of both oxidoreductase domain and full-length Steap4. Performed immunofluorescence microscopy of Steap4 constructs. Generated multiple sequence alignment of Steap family amino acid sequences. Assisted with generating figures and preparation of manuscript.

Co-author: Anoop K. Sendamarai

Contributions: Generated Steap3 oxidoreductase domain construct for activity studies. Solved Steap3 oxidoreductase domain crystal structure that was utilized in Steap4 structure determination.

Contribution of Authors and Co-Authors (Continued)

Co-author: Mark D. Fleming

Contributions: Provided Steap family cDNA constructs. Assisted in preparation of manuscript.

Co-author: C. Martin Lawrence

Contributions: Assisted in determination of Steap4 crystal structure. Researched literature and contributed to interpretation of data. Co-wrote manuscript in preparation for submission.

Manuscript Information Page

George H. Gauss, Mark D. Kleven, Anoop K. Sendamarai, Mark D. Fleming, C. Martin Lawrence
Journal of Biological Chemistry
Status of Manuscript:
____ Prepared for submission to a peer-reviewed journal
____ Officially submitted to a peer-review journal
____ Accepted by a peer-reviewed journal
_X__ Published in a peer-reviewed journal

This research was originally published in Journal of Biological Chemistry. George H. Gauss, Mark D. Kleven, Anoop K. Sendamarai, Mark D. Fleming, C. Martin Lawrence. The crystal structure of six-transmembrane epithelial antigen of the prostate 4 (Steap4), a ferri/cuprireductase, suggests a novel interdomain flavin-binding site. *Journal of Biological Chemistry*. 2013; 288: 20668-20682. © the American Society for Biochemistry and Molecular Biology.

THE JOURNAL OF BIOLOGICAL CHEMISTRY VOL. 288, NO. 28, pp. 20668–20682, July 12, 2013
© 2013 by The American Society for Biochemistry and Molecular Biology, Inc. Published in the U.S.A.

# The Crystal Structure of Six-transmembrane Epithelial Antigen of the Prostate 4 (Steap4), a Ferri/Cuprireductase, Suggests a Novel Interdomain Flavin-binding Site*[S]

Received for publication, April 24, 2013, and in revised form, May 30, 2013 Published, JBC Papers in Press, June 3, 2013, DOI 10.1074/jbc.M113.479154

**George H. Gauss[‡], Mark D. Kleven[‡], Anoop K. Sendamarai[‡1], Mark D. Fleming[§], and C. Martin Lawrence[‡2]**

*From the [‡]Department of Chemistry and Biochemistry, Montana State University, Bozeman, Montana 59717 and the [§]Department of Pathology, Children's Hospital and Harvard Medical School, Boston, Massachusetts 02115*

**Background:** In-depth biochemical and structural analyses of Steap4 are lacking.
**Results:** Crystallographic and kinetic characterization of Steap4 metalloreductase and flavin-dependent NADPH oxidase activities are reported.
**Conclusion:** Physiologically relevant ferric/cupric reductase and flavin-dependent NADPH oxidase activities are observed at neutral and endosomal pH; the N-terminal tail is dispensable for these activities.
**Significance:** Metalloreductase activity should be considered in Steap4-associated insulin resistance.

**Steap4 is a cell surface metalloreductase linked to obesity-associated insulin resistance. Initial characterization of its cell surface metalloreductase activity has been reported, but thorough biochemical characterization of this activity is lacking. Here, we report detailed kinetic analysis of the Steap4 cell surface metalloreductase activities. Steap4 shows physiologically relevant $K_m$ values for both $Fe^{3+}$ and $Cu^{2+}$ and retains activity at acidic pH, suggesting it may also function within intracellular organelles to reduce these metals. Flavin-dependent NADPH oxidase activity that was much greater than the equivalent Steap3 construct was observed for the isolated N-terminal oxidoreductase domain. The crystal structure of the Steap4 oxidoreductase domain was determined, providing a structural explanation for these differing activities. Structure-function work also suggested Steap4 utilizes an interdomain flavin-binding site to shuttle electrons between the oxidoreductase and transmembrane domains, and it showed that the disordered N-terminal residues do not contribute to enzymatic activity.**

The first member of the six-transmembrane epithelial antigen of the prostate (Steap)[3] family of proteins was identified as a prostate-specific gene highly expressed in advanced prostate cancer (1). Three additional members of the family were subsequently identified and designated Steap2, Steap3, and Steap4 (Steap2–4). Steap2–4 differ significantly from Steap1 by the addition of a cytosolic N-terminal oxidoreductase domain. This N-terminal domain works in conjunction with the C-terminal transmembrane domain to confer cell surface ferric and cupric reductase activity to these larger Steap2–4 family members (2, 3).

Steap1 and Steap2 are highly overexpressed in a number of different human cancers (prostate, bladder, colon, pancreas, ovary, testis, breast, cervix, and Ewing sarcoma) (4–6); however, their roles in both normal and cancer cells are not well understood (7). In contrast, Steap3 is the only family member for which a clear physiological role has been demonstrated. It serves as the major ferric reductase of the transferrin cycle, where it reduces endosomal $Fe^{3+}$ to $Fe^{2+}$, which is then transported across the endosomal membrane by DMT-1 (divalent metal transporter-1) (2, 8–10). Accordingly, the Steap3$^{-/-}$ mouse exhibits microcytic, hypochromic anemia (2), and a similar phenotype has been linked to low STEAP3 expression in humans (11).

Like Steap1 and Steap2, functions for Steap4 (also known as Stamp2 and TIARP) are also less clearly defined. In addition to its cell surface metalloreductase activity, it has also been suggested to facilitate trafficking in endocytic and exocytic pathways and to play a role in macrophage inflammation, where it protects against atherosclerosis (6, 12). In addition, the literature also frequently identifies Steap4 as an obesity-related protein associated with insulin sensitivity, with knockdown or loss of Steap4 leading to insulin resistance (6, 13–17). Obesity-associated insulin resistance is a complex metabolic disorder that currently defies explanation by a single etiological pathway, but three recurring themes are found (18). These are as follows: (i) accumulation of ectopic lipid metabolites; (ii) activation of the unfolded protein response pathway; and (iii) activity of innate immune pathways.

With regard to theme iii, Steap4 expression in adipocytes is normally induced by nutritional stress, leptin, and proinflammatory cytokines, including tumor necrosis factor α (TNFα),

* This work was supported, in whole or in part, by National Institutes of Health Grant RO1 GM084326 (to C. M. L. and M. D. F.). Portions of this work were carried out at the Stanford Synchrotron Radiation Laboratory, a national user facility operated by Stanford University on behalf of the United States Department of Energy, Office of Basic Energy Sciences.
[S] This article contains supplemental Fig. 1 and additional references.
*The atomic coordinates and structure factors (code 2YJZ) have been deposited in the Protein Data Bank (http://wwpdb.org/).*
[1] Present address: Dept. of Pathology, Children's Hospital and Harvard Medical School, 300 Longwood Ave., Boston, MA 02115.
[2] To whom correspondence should be addressed. Tel.: 406-994-5382; Fax: 406-994-5407; E-mail: lawrence@chemistry.montana.edu.
[3] The abbreviations used are: Steap, six-transmembrane antigen of the prostate; Dcytb, duodenal cytochrome *b*; $F_{420}$, 8-hydroxy-5-deazaflavin; FNO, $F_{420}H_2$/$NADP^+$ oxidoreductase; Fre, ferric reductase; Nox, NADPH oxidase; NTA, nitrilotriacetic acid; STAT3, signal transducer and activator of transcription 3; TCEP, tris(2-carboxyethyl)phosphine; NTBI, nontransferrin-bound iron; Tricine, *N*-[2-hydroxy-1,1-bis(hydroxymethyl)ethyl]glycine; BisTris, 2-[bis(2-hydroxyethyl)amino]-2-(hydroxymethyl)propane-1,3-diol.

interleukin-1$\beta$, and interleukin-6, where it promotes insulin sensitivity (13, 15, 17, 19–27). Similarly, in hepatocytes and HeLa cells, CCAAT/enhancer-binding protein $\alpha$ directly induces transcription of Steap4 in response to feeding, and both CCAAT/enhancer-binding protein $\alpha$ and the proinflammatory transcription factor STAT3 positively regulate Steap4 in response to IL-6 (17, 23).

Conversely, knockdown or loss of Steap4 expression in adipocytes inhibits translocation of GLUT4 to the plasma membrane, inhibiting insulin-stimulated glucose transport, rendering the cells insulin-insensitive (13, 28). Lack of Steap4 also leads to increased production of IL-6 in these cells. Consistent with these observations, Steap4$^{-/-}$ mice are reported to exhibit aberrant inflammatory responses to nutrients and acute inflammatory stimuli, and their adipose tissue exhibits overt inflammation. Furthermore, the mice are also reported to develop insulin resistance (17). Finally, recent studies have also found correlations between STEAP4 and insulin resistance in humans (19, 29–33).

A central question, then, is whether the metalloreductase activity of Steap4 in adipocytes and hepatocytes is related to its association with insulin resistance. In this regard, connections between iron metabolism and the unfolded protein response (see theme ii, above) are well established (34). So too are connections between iron metabolism and innate immunity (34), including the Steap4-specific connections to IL-6, TNF$\alpha$, and STAT3 discussed above (theme iii). From this perspective then, a role in iron homeostasis seems consistent with its role in insulin sensitivity, and for this reason, biochemical understanding of the Steap4 metalloreductase activity is of significant interest.

Our current understanding of the structural, functional, and mechanistic aspects of Steap4 metalloreductase activity are largely inferred from Steap3, where the N-terminal oxidoreductase domain is believed to utilize NADPH to reduce a currently undefined flavin (2, 35). The electrons in the reduced flavin are thought to flow, one at time, into a single heme group housed within the C-terminal transmembrane domain. The heme then facilitates translocation of the electrons across the lipid bilayer to the lumen of the endosome, where $Fe^{3+}$ is reduced to $Fe^{2+}$ (2, 35). This heme-containing C-terminal domain shows distant homology to the transmembrane domains of the eukaryotic Fre and Nox family proteins and to YedZ in bacteria (2, 36), each of which are involved in transmembrane electron transfer.

Outside the Steap family, the closest structural homologs for the N-terminal oxidoreductase domain is the prokaryotic $\underline{F}_{420}H_2$:$\underline{N}ADP^+$ $\underline{o}$xidoreductase, or FNO family of proteins. These enzymes utilize a unique deazaflavin (8-hydroxy-5-deazaflavin or $F_{420}$) that is not found in mammals (2, 35, 37). Accordingly, as in FNO, the structure of the Steap3 oxidoreductase domain revealed a dinucleotide binding fold that recognizes NADPH, followed by a smaller ~60-residue subdomain presumably involved in flavin recognition, either FAD or FMN (35). The biochemical and structural analysis of Steap3 also suggested that the full-length protein may function as a dimer *in vivo* (35).

Based on sequence homology and mutagenesis studies (2), Steap2 and Steap4 are also hypothesized to utilize NADPH. However, to date, NADPH oxidase activity has not been demonstrated for any member of the Steap protein family, and there is precedence for the use of other electron donors in cell surface metalloreductases. For example duodenal cytochrome *b* (Dcytb) utilizes ascorbate (39, 40). Similarly, although Steap proteins are thought to utilize a flavin as cosubstrate or cofactor (2, 35), direct experimental evidence for a reduced flavin intermediate is also lacking. Indeed, other than an initial demonstration of cell surface metalloreductase activity in whole cells, an in-depth kinetic analysis of these activities for any member of the Steap family is lacking.

Here, we report the first detailed kinetic analysis of cell surface metalloreductase activity for the full-length Steap4 protein, including pH profiles and metal specificities. We also report the crystal structure of the Steap4 N-terminal oxidoreductase domain and kinetic characterization of its NADPH oxidase and flavin reductase activities. This represents the first structural study of Steap4 and the first detailed kinetic analysis of the NADPH oxidase, flavin reductase, and metalloreductase activities for any Steap protein.

## EXPERIMENTAL PROCEDURES

*Cell Surface Ferric and Cupric Reductase Assays*—A *Rattus norvegicus* Steap4 full-length cDNA clone (Open Biosystems) was PCR-amplified and ligated into pCDNA3.1 (Invitrogen) with an N-terminal Strep-II tag using HindIII and XbaI restriction sites. Steap4 mutants were made by PCR with appropriate primers and were cloned into the same sites or were made from the wild-type Steap4 vector using a QuikChange mutagenesis kit (Stratagene). All constructs were sequence-verified. HEK-293F cells (Invitrogen) were maintained in Freestyle 293 Expression Medium (Invitrogen) in spinner flasks at 37 °C and 5% v/v $CO_2$. Transfections utilized linear 25-kDa polyethyleneimine (PEI; Polysciences) as described previously (41). Briefly, plasmid and PEI (26 and 52 $\mu$g, respectively) were added to 2.6 ml of phosphate-buffered saline (PBS), pH 7.2. The solution was incubated at room temperature for 15 min before adding to a spinner flask containing 23.4 ml of cells resuspended in fresh medium at $1.11 \times 10^6$ cells/ml (1 $\mu$g of DNA per $10^6$ cells).

Twenty four hours post-transfection, cells were assayed for metalloreductase activity as with a colorimetric end point assay. Cells were pelleted (1,000 × *g*, 5 min), washed three times with PBS, pH 7.2, and resuspended in 25 mM MES, 25 mM MOPS, 140 mM NaCl, 5.4 mM KCl, 5 mM glucose, 1.8 mM $CaCl_2$, 800 $\mu$M $MgCl_2$, pH 7.2, and aliquoted into 24-well plates ($2.5 \times 10^5$ cells/well). The buffer was supplemented with 25 mM Tris for pH-dependent experiments. Metal-chelate and chromogenic indicator (ferrozine or bathocuproine disulfonate) were added to each well, and the cells were incubated in the dark at 37 °C. The absorbance of the supernatant was measured after 35 min to determine the amount of reduced metal. Iron(II)-ferrozine complexes were assayed at 562 nm and copper(I)-bathocuproine disulfonate complexes at 482 nm. Standard curves for each metal-indicator complex were used to determine picomoles of reduced metal. Activities were calculated as picomoles of reduced metal per min divided by total cellular protein per well. Total cell protein content was determined by the Bradford method (42) (Bio-Rad) using cells lysed by 30 min of incubation

in 1% v/v Triton X-100 at 4 °C. $Fe^{3+}$-NTA was prepared by addition of NTA to an $FeCl_3$ solution dissolved in 0.1 M HCl at a 1:1 Fe/NTA molar ratio. $Fe^{3+}$-citrate was prepared by dissolving $Fe^{3+}$-citrate in $H_2O$. $Cu^{2+}$-NTA was prepared by addition of NTA to a $CuSO_4$ solution (1:4 Cu/NTA ratio). $Cu^{2+}$/histidine solution was prepared by addition of L-histidine to a $CuSO_4$ solution (1:2 $Cu^{2+}$/histidine ratio). All metal solutions were adjusted to pH 7.0. To correct for endogenous ferric or cupric reductase activities, the cell surface activity of empty vector-transfected cells was subtracted in each experiment. Each experiment utilized a common culture of transfected cells to allow direct comparison between the metalloreductase activities. Three activity measurements were made at each substrate concentration, and the rates obtained were fit by nonlinear least squares analysis to the Michaelis-Menten equation (Equation 1) using GraphPad Prism 5.0.

$$v_o = V_{max}[S]/(K_m + [S]) \quad \text{(Eq. 1)}$$

The means ± S.D. for the kinetic parameters in Table 1 were derived from at least three independent transfections.

*Immunofluorescence Microscopy*—HEK-293F cells were maintained in DMEM supplemented with 10% v/v FBS in T-75 flasks at 37 °C and 5% v/v $CO_2$. Twenty four hours prior to transfection, cells were plated onto glass coverslips in a 6-well dish. Transfections were performed with Lipofectamine 2000 (Invitrogen) according to the manufacturer's protocol using the same Steap4 expression constructs detailed above. Twenty four hours post-transfection, cells were washed three times with PBS and fixed in 4% v/v formaldehyde/PBS for 15 min. Cells were then washed three times with PBS and permeabilized by incubation with 0.2% v/v Triton X-100/PBS for 20 min. Cells were washed three times with PBS and subsequently incubated in blocking buffer (1% v/v BSA/PBS) for 30 min. Cells were then incubated with primary antibody diluted in blocking buffer (anti-StrepMAB (IBA LifeSciences) at 1:250 and anti-CD71 (FITC-conjugated; BD Biosciences) at 1:100) for 1 h. Cells were then washed three times with PBS for 5 min and incubated 60 min with 5 μg/ml anti-mouse $IgG_1$, Alexa Fluor 633-conjugated secondary antibody (Invitrogen) in blocking buffer. Cells were subsequently washed three times with PBS, stained with DAPI for 5 min, and mounted on glass cover slides with Vectashield mounting medium (Vector Laboratories). Samples were visualized with a Leica SP5 confocal microscope. Images were processed with Imaris software (Bitplane).

*Expression and Purification of the Steap4 N-terminal Oxidoreductase Domain*—The open reading frame of the rat Steap4 oxidoreductase domain was amplified from cDNA (Open Biosystems) using primers that added an N- or C-terminal $His_6$ tag and attB sites for Gateway cloning into pDEST14 (Invitrogen). Mutants were made using a QuikChange kit (Stratagene). All clones were sequence-verified. The human STEAP3 oxidoreductase fragment (1–215 C-terminal $His_6$) was expressed and purified as described previously (35). Neither the human nor the rat Steap fragments copurified with a flavin. Rat oxidoreductase domain constructs were overexpressed by autoinduction (43) (24 h at 25 °C) in *Escherichia coli* BL21(DE3)RIL (Stratagene), and cells were pelleted and stored at −80 °C. Cells were lysed by microfluidizer (Microfluidics) in lysis buffer (20 mM Tris, 0.5 M NaCl, 5 mM imidazole, 10 mM 2-mercaptoethanol, pH 8.0) plus 100 μM phenylmethylsulfonyl fluoride. Bacterial debris was pelleted (30,000 × *g*, 20 min, 4 °C). The supernatant was bound to 2 ml of Ni-NTA resin at 22 °C and washed with 10 column volumes of lysis buffer before eluting with 20 mM Tris, 0.1 M NaCl, 0.3 M imidazole, 10 mM 2-mercaptoethanol, and 20% v/v glycerol, pH 8.0. The eluant was analyzed by 12% Tris/Tricine SDS-PAGE. If necessary, contaminants were removed with a 5-ml HiTrap Q column (GE Healthcare). Typically, fractions with the oxidoreductase domain were pooled, diluted 1:10 into buffer A (20 mM Tris, 20% v/v glycerol, 1 mM TCEP, pH 8.0), and bound to the Q column at 22 °C. The Q column was washed to base line with buffer A, and then protein was eluted with a linear gradient of 20 mM Tris, 1.0 M NaCl, 10% v/v glycerol, 1 mM TCEP, pH 8.0. The oxidoreductase domain eluted at ~150 mM NaCl. Fractions were analyzed by SDS-PAGE, and those with oxidoreductase domain were pooled and concentrated to ~10 mg/ml by ultrafiltration (Amicon Ultra-4) and applied to a Superdex-75 HR 10/30 column (GE Healthcare) equilibrated with 10 mM Tris, 150 mM NaCl, 10% v/v glycerol, 1 mM TCEP, pH 8.0, at 22 °C. Fractions with oxidoreductase domain were pooled, concentrated to ~10 mg/ml by ultrafiltration, and stored at 4 °C. Protein concentrations were determined by the Bradford assay (42) with BSA standard. For analytical ultracentrifugation, protein was exchanged into 10 mM Tris, 50 mM NaCl, 2% v/v glycerol, 2 mM TCEP, pH 8.0, and sent to the University of Texas Health Sciences Center for Macromolecular Interactions for analysis.

*NADPH Oxidase Assay*—The oxidation of NADPH was monitored spectrophotometrically at 340 nm using the WinUV Kinetics module in a Varian Cary 50 Bio spectrophotometer. Typical reactions (350 μl) were performed in 0.1 M citric acid, 0.15 M NaCl, pH 5.5, at 22 °C. The initial pH optimization was done with 200 μM NADPH and 200 μM FAD using 1-cm cuvettes. Because of the need to work with higher flavin concentrations to measure flavin $K_m$ values, subsequent work utilized 0.2-cm cuvettes with NADPH held constant at 100 μM. Three hundred nanomolar protein was used for the more active 1–203 fragment and 3–10 μM protein for the less active 1–195 construct. Components were mixed, and the reaction was initiated by addition of NADPH. The auto-oxidation of NADPH in reaction buffer with substrates but without protein was subtracted to yield reaction velocity. Within each experiment, three velocity measurements were made at each substrate concentration. The initial rates obtained from these assays were fit by nonlinear least squares analysis to the Michaelis-Menten equation (Equation 1) using GraphPad Prism. A representative experiment for each flavin is shown in Fig. 3. Kinetic parameters in Table 2 are the means ± S.D. from three or more such experiments, each using an independent preparation of protein. Substrate stock solutions were made in water and stored at −20 °C in single-use aliquots. The concentration of stock solutions was determined in 0.1 M sodium phosphate, pH 7.0, using the extinction coefficients NADPH $\epsilon_{340\ nm} = 6{,}220\ M^{-1}\ cm^{-1}$, FAD $\epsilon_{450\ nm} = 11{,}300\ M^{-1}\ cm^{-1}$, FMN $\epsilon_{446\ nm} = 12{,}200\ M^{-1}\ cm^{-1}$, and riboflavin $\epsilon_{445\ nm} = 12{,}500\ M^{-1}\ cm^{-1}$ (44–46).

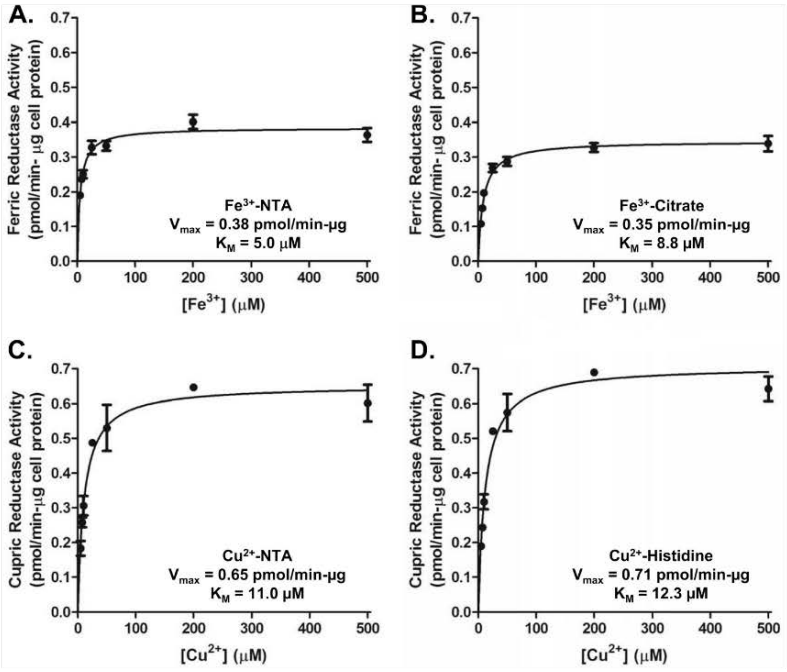


FIGURE 1. **Cell surface metalloreductase activity.** The cell surface metalloreductase activity of various Steap4 constructs was measured using four different substrates. Shown here are representative data for the Steap4(1–470) construct. A typical experiment is shown for each substrate as follows: $Fe^{3+}$-NTA (*A*), $Fe^{3+}$-citrate (*B*), $Cu^{2+}$-NTA (*C*), and $Cu^{2+}$-histidine (*D*). $V_{max}$ and $K_m$ values were derived by fitting the Michaelis-Menten equation to the data with GraphPad Prism 5.0. The kinetic parameters reported in Table 1 represent the mean of at least three such independent experiments.

*Crystallization, Data Collection, and Model Refinement*—Crystals of the rat Steap4 N-terminal domain, residues 1–195 with a C-terminal $His_6$ tag, were grown by hanging drop vapor diffusion. Drops contained 2 $\mu$l of protein at 7 mg/ml, 1 mM NADPH, and 2 $\mu$l of well solution (0.1 M BisTris-HCl, pH 5.5, 1.9–2.2 M $(NH_4)_2SO_4$). Cryoprotectant was introduced by sequential soaks (2–5 min) in well solution supplemented with 1 mM NADPH and 10, 12.5, and 15% v/v glycerol. A dataset to 2.2 Å was collected at 100 K at SSRL beamline 9-2. Data were processed with HKL2000 (Table 3) (47). The structure was solved by molecular replacement with MRBUMP (48) using a search model derived from the human Steap3 structure (Protein Data Bank code 2VQ3 (35)). Model building and refinement using COOT and REFMAC5 (48) yielded a model with $R_{work}$ = 20.3% and $R_{free}$ = 23.8% (Table 3). The model was deposited under Protein Data Bank code 2YJZ. Figures were prepared using PyMOL (49) and LIGPLOT (50).

## RESULTS

*Cell Surface Ferric and Cupric Reductase Activities for Rat Steap4*—Although the initial demonstration of Steap4 metalloreductase activity was done with the mouse protein (3), our efforts to express and crystallize the mouse (and human) Steap4 N-terminal oxidoreductase domain were unsuccessful. In contrast, we found that the *R. norvegicus* (rat) Steap4 oxidoreductase domain was amenable to structural studies (below), and for this reason we chose rat Steap4 for our functional work.

*Does Rat Steap4 Exhibit a Preference for $Fe^{3+}$ or $Cu^{2+}$?*—Steap2–4 have been shown to reduce both $Fe^{3+}$ and $Cu^{2+}$ in cell surface metalloreductase assays when transfected into HEK-293T cells (3). Although it is clear that $Fe^{3+}$ is a physiologically relevant substrate for Steap3 in the transferrin cycle, it is not clear whether $Fe^{3+}$ or $Cu^{2+}$ is a physiologically relevant substrate for Steap4. To address the relative specificity of Steap4 for iron and copper, kinetic parameters were derived from cell surface metalloreductase data fit to the Michaelis-Menten equation for each of four different substrates as follows: $Fe^{3+}$-NTA, $Fe^{3+}$-citrate, $Cu^{2+}$-NTA, and $Cu^{2+}$-histidine. For each independent experiment, cells from the same transfection were used to measure each of these four activities, allowing direct comparison of the iron and copper data within each experiment (Fig. 1). The experiments were repeated three times (different transfections), and the kinetic constants were averaged to give the values in Table 1. For each substrate, the mean $V_{max}$ values were quite similar, ranging from 0.35 to 0.54 pmol $\mu g^{-1}$ $min^{-1}$. More relevant to the question of specificity, the $K_m$ values for $Fe^{3+}$-NTA and $Fe^{3+}$-citrate were 4.8 ± 0.7 and 6.8 ± 1.9 $\mu$M, respectively. Similarly, $K_m$ values for $Cu^{2+}$-NTA and $Cu^{2+}$-histidine were 11.2 ± 4.4 and 9.9 ± 2.2 $\mu$M. Although the $Cu^{2+}$-NTA data were less reproducible between experiments than the other substrates, it was quite reproducible between replicates in any one experiment (Fig. 1).

To place these data within the context of physiologically relevant metalloreductases, first consider Dcytb, a ferric/cupric

**TABLE 1**
**Full-length Steap4 cell surface metalloreductase activity**

| Construct | Fe-NTA | | Fe-Citrate | | Cu-NTA | | Cu-Histidine | |
|---|---|---|---|---|---|---|---|---|
| | $K_m$ (μM) | $V_{max}$ (pmol/μg cell lysate-min) | $K_m$ (μM) | $V_{max}$ (pmol/μg cell lysate-min) | $K_m$ (μM) | $V_{max}$ (pmol/μg cell lysate-min) | $K_m$ (μM) | $V_{max}$ (pmol/μg cell lysate-min) |
| Steap4 (1-470) | 4.8 ± 0.7 | 0.39 ± 0.04 | 6.8 ± 1.9 | 0.35 ± 0.05 | 11.2 ± 4.4 | 0.54 ± 0.17 | 9.9 ± 2.2 | 0.52 ± 0.23 |
| Steap4(20-470) | 4.6 ± 2.9 | 0.30 ± 0.05 | 3.9 ± 0.4 | 0.27 ± 0.03 | 7.3 ± 4.1 | 0.40 ± 0.10 | 8.3 ± 3.5 | 0.47 ± 0.07 |
| Steap4 (1-470)-L194A | 7.9 ± 1.0 | 0.97 ± 0.26 | 8.9 ± 4.8 | 0.93 ± 0.38 | 7.7 ± 6.2 | 0.54 ± 0.30 | 14.0 ± 1.6 | 1.15 ± 0.03 |
| Steap4 (1-470)-L196A | 5.9 ± 1.9 | 0.36 ± 0.12 | 9.4 ± 3.4 | 0.33 ± 0.10 | 9.9 ± 3.2 | 0.52 ± 0.16 | 11.8 ± 1.4 | 0.58 ± 0.16 |
| Steap4 (1-470)-W200A | 1.2 ± 0.5 | 0.32 ± 0.13 | 4.1 ± 1.3 | 0.22 ± 0.22 | 17.0 ± 6.0 | 0.52 ± 0.43 | 8.4 ± 2.1 | 0.44 ± 0.28 |

| | $V_{max}/K_m$ | | | |
|---|---|---|---|---|
| | Fe-NTA | Fe-Citrate | Cu-NTA | Cu-Histidine |
| Steap4 (1-470) | 0.08 | 0.05 | 0.05 | 0.05 |

Data are means ± S.D. from least three completely independent experiments, *i.e.* different transfections.

reductase implicated in intestinal iron absorption. The reported $K_m$ values for Dcytb are 74 and 23 μM for iron and copper NTA chelates, respectively (51). Steap4 thus shows higher affinity than DcytB for each of these metals. In the same vein, Steap4 $K_m$ values for $Fe^{3+}$-NTA are comparable with those for mouse Steap3[4] and thus are consistent with a potential functional overlap with Steap3 (2, 3, 35).

*Potential Steap4 Activity in Acidic Organelles*—Although non-transferrin-bound iron (NTBI) can undergo reduction and transport at the cell surface, plasma iron is generally present in iron-loaded transferrin or ferritin, which is endocytosed and concentrated within endosomal and lysosomal compartments, respectively, where the iron is then unloaded and reduced prior to transport across these organellar membranes (2, 52). Because the lumen of these compartments is mildly acidic, endosomal and lysosomal ferric reductases would be expected to function at acidic pH (pH 5–6.5). Accordingly, we examined the pH dependence of Steap4 metalloreductase activity. We found significant ferric and cupric reductase activity between pH 5.0 and pH 7.0 (Fig. 2). However, at basic pH, the ferric reductase activity quickly declined, although the cupric reductase activity was retained. As for Dcytb, the loss of ferric reductase activity may reflect the relative insolubility of ferric ion at basic pH (51). Regardless, the pH curves clearly demonstrate the potential for Steap4 activity in endosomes, lysosomes, and other organelles with acidic lumenal pH.

*N-terminal NADPH Oxidase Activity*—With the goal of finding soluble fragments suitable for kinetic and structural analysis of the putative Steap4 NADPH oxidase activity, we purified two oxidoreductase domain fragments that lacked the C-terminal transmembrane domain. These two fragments differed by eight residues at the C terminus. The C terminus of the longer construct, residues 1–203, was equivalent to the human Steap3 construct previously utilized for crystallographic studies (35).

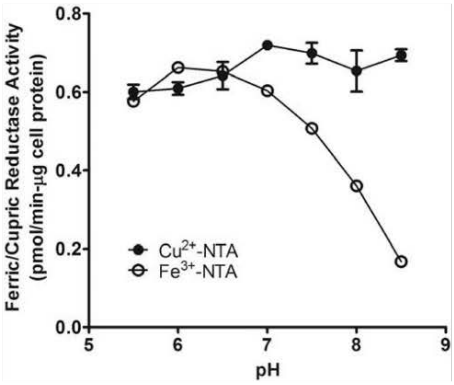


FIGURE 2. **Cell surface metalloreductase activity of full-length rat Steap4 (Steap4(1–470)) was measured as a function of pH in the presence of 50 μM $Fe^{3+}$-NTA or 50 μM $Cu^{2+}$-NTA.** Substantial ferric and cupric reductase activity was seen at acidic pH, suggesting that, in addition to cell surface activity, Steap4 may also function within the acidic lumen of intracellular compartments.

The second, shorter construct spanned residues 1–195. Both constructs had C-terminal $His_6$ tags.

For each construct, the purified protein was colorless, and absorbance spectroscopy suggested these fragments did not copurify with a flavin. Initial work with the shorter construct at pH 7 (approximate cytosolic pH) demonstrated low but measurable NADPH oxidase activity in the presence of exogenous flavin. When the longer construct was utilized, a substantial increase in activity was seen (Fig. 3). We found that both constructs displayed similar pH dependence, with maximal activity at pH 5.5. In addition to FAD, both constructs were also clearly able to utilize FMN and riboflavin.

Using the longer construct and titrating flavin concentrations up 400 μM, it was possible to measure $K_m$ values for each of these flavins (Table 2). The $K_m$ values for FAD (114 ± 22 μM), FMN (128 ± 20 μM), and riboflavin (183 ± 61 μM) were largely similar, differing by less than a factor of 2, as were the $k_{cat}/K_m$

[4] M. D. Kleven and C. M. Lawrence, unpublished data.

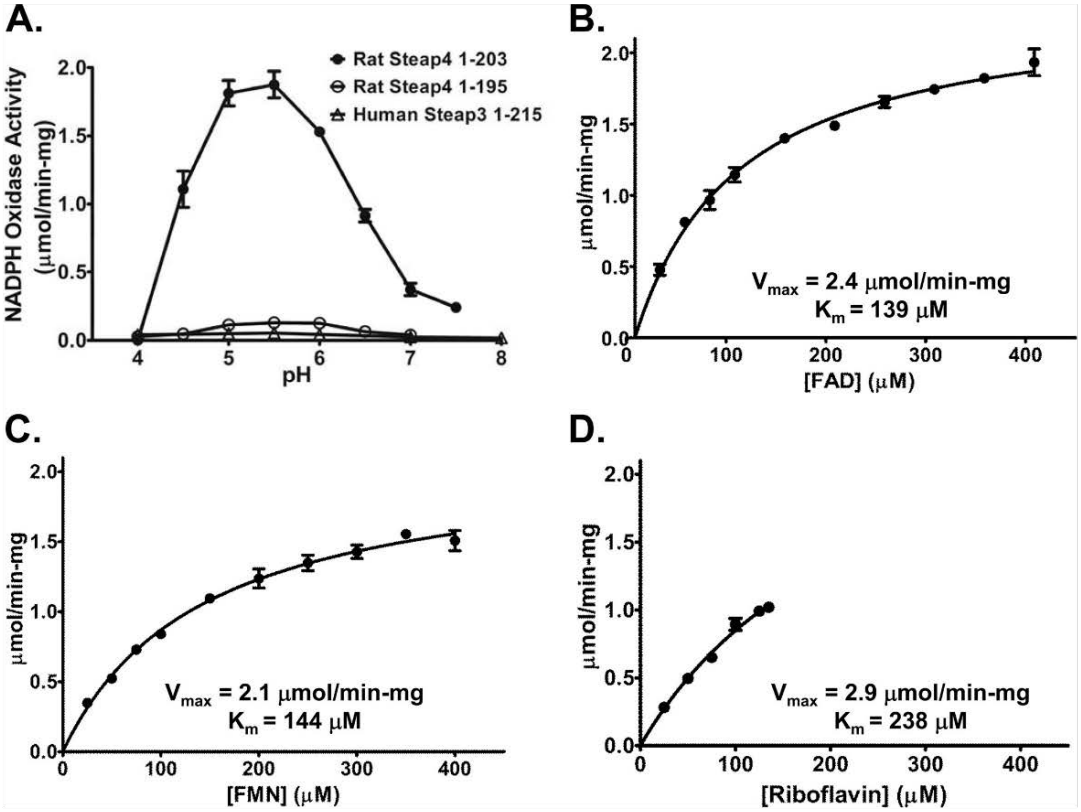


FIGURE 3. **Flavin-dependent NADPH oxidase activity of the purified N-terminal cytoplasmic domain.** *A*, activity as a function of pH. Two constructs of the rat Steap4 N-terminal oxidoreductase domain were compared with the human Steap3(1–215) fragment. The longer Steap4 construct (1–203, *filled circles*) had significantly higher activity than the shorter construct (1–195, *open circles*); both constructs were significantly more active than the human Steap3 fragment (*open triangles*). *B–D*, activity of Steap4(1–203) as function of flavin concentration. A typical experiment is shown for each flavin, along with the $V_{max}$ and $K_m$ values derived by fitting the Michaelis-Menten equation to the data. The maximum riboflavin concentration (*D*) was limited to due to its low solubility in assay buffer. The kinetic parameters reported in Table 2 represent the mean of at least three such independent experiments.

values, demonstrating that the longer Steap4 fragment does not strongly differentiate between these flavins. This, in turn, suggests recognition is primarily through the isoalloxazine and/or ribitol moieties common to these three flavins.

We also tested the activity of the equivalent human Steap3 oxidoreductase domain fragment, residues 1–215. The extra length of the human protein is due to additional N-terminal residues, such that residue 203 in the rat Steap4 corresponds to residue 215 in human Steap3 (supplemental Fig. 1). However, the activity of the Steap3(1–215) construct was only barely detectable, and in contrast to the equivalent rat Steap4 construct, millimolar flavin concentrations were required to observe activity (Fig. 3).

*Oligomeric State of the Oxidoreductase Domain in Solution*—Both the long and short oxidoreductase constructs appeared to be monomeric in solution, as assayed by size exclusion chromatography. At protein concentrations up to 13 mg/ml (570 μM) in 150 mM NaCl at pH 8.0 (standard purification conditions), the apparent molar mass of Steap4(1–203) was 24 kDa, in good agreement with the theoretical mass of a 23-kDa monomer. This was confirmed by analytical ultracentrifugation for the Steap4(1–203) construct (data not shown).

*Structure of the Steap4 Oxidoreductase Domain*—Although we were unable to grow crystals of the long Steap4 oxidoreductase domain suitable for structure determination, single crystals of the short construct grown in the presence of NADPH diffracted to 2.2 Å. With these data (Table 3), we determined the structure of the shorter construct by molecular replacement.

*Structural Similarity to Steap3*—Although there are several critical differences (discussed below), the structure of the Steap4 oxidoreductase domain is largely similar to Steap3, with a root mean square deviation of 1.0 Å over 169 structurally equivalent Cα positions. Like Steap3, it folds into a mixed eight-stranded β-sheet with accompanying α-helices that is formed of two subdomains (Fig. 4*A*). The first six strands (β1–β6) run parallel and form a classic dinucleotide-binding element. The second subdomain is composed of an extended reverse turn containing a short bit of α-helix (α5), followed by a βαβ supersecondary structural element ($\beta_7$-$\alpha_6$-$\beta_8$) that contributes two

**TABLE 2**
**N-terminal oxidoreductase domain NADPH oxidase activity**

| Construct | $V_{max}$ (μmole/min-mg) | NADPH $K_m$ (μM) | FAD $K_m$ (μM) | FMN $K_m$ (μM) | riboflavin $K_m$ (μM) |
|---|---|---|---|---|---|
| Steap4(1-203) | 2.2 ± 0.3 | 6.3 ± 1.5 | 114 ± 22 | 128 ± 20 | 183 ± 61 |
| Steap4(1-195) | 0.6 ± 0.2 | 8.5 ± 0.9 | 825 ± 293 | | |
| Steap4(20-203) | 2.3 ± 0.4 | 8.1 ± 1.8 | 128 ± 31 | | |
| Steap4(1-203)L194A | 1.7 ± 0.5 | 7.2 ± 1.5 | 186 ± 44 | | |
| Steap4(1-203)L196A | 2.3 ± 0.8 | 7.0 ± 3.8 | 253 ± 104 | | |
| Steap4(1-203)W200A | 2.2 ± 0.5 | 7.0 ± 1.4 | 104 ± 28 | | |
| | $k_{cat}/K_m$ ($M^{-1}s^{-1}$) | | | | |
| | FAD | FMN | riboflavin | | |
| Steap4(1-203) | 14 | 14 | 9 | | |

Data are the means ± S.D. from at least three independent experiments, *i.e.* different enzyme preparations. $V_{max}$ was measured at constant NADPH (100 μm) by varying the FAD concentration, typically 25-400 μm, although concentrations up to 1000 μm were used for some constructs. Kinetic data were fit to the Michaelis-Menten equation with GraphPad Prism.

**TABLE 3**
**X-ray data collection and refinement statistics.**

| Space group | $P2_12_12_1$ |
|---|---|
| **Unit cell parameters** | |
| *a*, *b*, *c* | 69.228, 85.111, 128.035 Å |
| $\alpha = \beta = \gamma$ | 90.00° |
| Wavelength | 0.99984 Å |
| Resolution range[a] | 50.00 to 2.20 (2.28 to 2.20) |
| Total reflections observed | 303,911 |
| **Unique reflections** | |
| Observed | 39,044 |
| Total possible | 39,398 |
| Redundancy | 7.8 (6.4) |
| Data coverage | 99.1% (94.8%) |
| Mean $(I)/\sigma(I)$ | 7.9 (2.8) |
| $R_{sym}$[b] | 10.1% (45.9%) |
| Refinement resolution range | 37.00 to 2.20 Å |
| $R_{cryst}/R_{free}$[c] | 20.3%/23.8% |
| Coordinate error[d] | 0.151 Å |
| Real space correlation coefficient[e] | 0.957 |
| Root mean square deviation from ideality, bonds/angles | 0.021 Å/1.861° |
| Ramachandran plot, favored/outliers[f] | 98.2%/0.0 |
| Average residual *B* values | 34.747 Å$^2$ |
| Protein Data Bank code | 2YJZ |

[a] Numbers in parentheses refer to the highest resolution shell.
[b] $R_{sym} = 100 \cdot \Sigma_h \Sigma_i |I_i(h) - \langle I(h) \rangle| / \Sigma_h I(h)$, where $I_i(h)$ is the *i*th measurement of the *h*th reflection, and $\langle I(h) \rangle$ is the average value of the reflection intensity.
[c] $R_{cryst} = \Sigma ||F_o| - |F_c|| / \Sigma |F_o|$, where $F_o$ and $F_c$ are the structure factor amplitudes from the data and the model, respectively. $R_{free}$ is calculated similarly, using 5% of the structure factors held back as a test set.
[d] Data are based on maximum likelihood.
[e] Correlation coefficient is between the model and the $2mF_o - DF_c$ electron density map.
[f] Data were calculated using MOLPROBITY.

C-terminal β-strands. These strands run parallel to each other but anti-parallel to the first six strands. This is followed by a terminal α-helix (α7) that extends back to the edge of the active site cleft. This cleft accommodates the nicotinamide moiety of NADPH and presumably the isoalloxazine ring of a flavin.

In the archaeal FNO structure, the first subdomain functions to bind NADPH. Accordingly, we find that the crystallized Steap4 nucleotide-binding subdomain does indeed bind NADPH, and the conformation is nearly identical to that seen for Steap3 (35). A multiple sequence alignment identifies 20 strictly conserved residues within the oxidoreductase domain (supplemental Fig. 1). Notably, eight of these (40%) make direct contact with the bound NADPH, as illustrated in Fig. 4*B*. Clearly then, the multiple sequence alignment is able to discriminate residues critical to the Steap family metalloreductase activity, many of which are involved in substrate recognition.

We lack a flavin-bound structure for any Steap. Attempts to cocrystallize or soak flavin into the Steap4 crystals were unsuccessful. However, superpositional docking of the FNO ternary complex (with NADPH and $F_{420}$) on Steap4 predicts the binding of NADPH to Steap4 relatively well. This suggests the FNO ternary complex could also serve as a starting point to model potential flavin interactions with Steap4. Thus, when the nicotinamide ring of FNO is positioned on the bound Steap4 nicotinamide ring, and an isoalloxazine ring is substituted for the tricyclic ring of $F_{420}$, we find that the isoalloxazine ring is nicely accommodated by Steap4. Potential hydrogen bond interactions between Asn-106 and O4 of the isoalloxazine ring and between the 2′-OH of the nicotinamide ribose and isoalloxazine O4 are suggested (Fig. 4*C*). So too are hydrophobic interactions with the Thr-136 and Ser-138 side chains. Notably, Asn-106 and Ser-138 are strictly conserved, although Thr-136 tolerates only the isosteric Val substitution (supplemental Fig. 1). Similarly, the H-bond interaction with the ribose ring should also be conserved. Overall, however, much of the docked flavin remains solvent-exposed. This docking exercise thus highlights the uncharacteristically open nature of the flavin-binding site. Importantly, however, the predicted open nature of the site is entirely consistent with the relatively high $K_m$ values for FMN and FAD seen for the soluble Steap4 oxidoreductase domain constructs (Table 2).

*Structural Similarity to the Steap3 Dimer*—Although the rat Steap4 oxidoreductase domain appears monomeric by size exclusion and analytical ultracentrifugation (see above), the

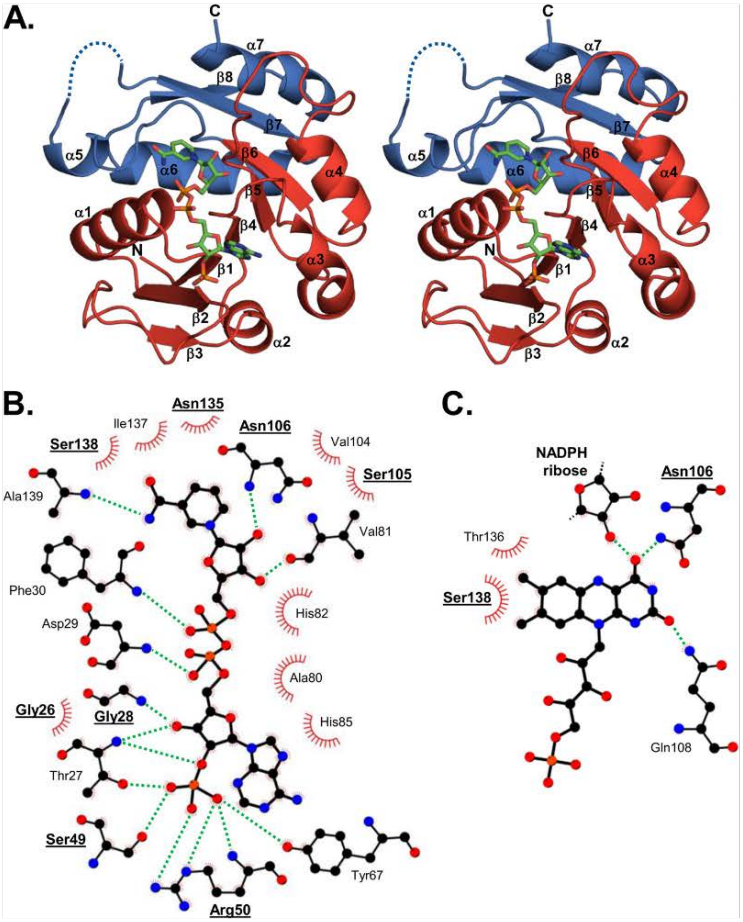


FIGURE 4. **Rat Steap4 structure.** *A*, stereo view of the Steap4 N-terminal domain with bound NADPH. The N-terminal domain (*red*, residues 19–132) is formed by a classic dinucleotide binding fold (six-stranded parallel β-sheet (3–2–1–4-5–6) with β-strands connected by right-handed α-helical crossovers). This is followed by an additional 63-residue subdomain (*blue*, residues 133–195) formed of two additional strands running antiparallel to the first six strands and three connecting α-helices. The C-terminal helix, α7, terminates near the nicotinamide ring of the NADPH (*green*). The disordered residues Leu-147–Asp-148–Ala-149 are indicated by *dashed line* between α5 and β7. N and C termini are denoted by *N* and *C*, respectively. *B*, NADPH recognition. Rat Steap4 residues that make hydrogen bonds (*green dashed lines*) with NADPH are shown in a two-dimensional LigPlot (50) *ball and stick* representation. Residues that make van der Waals interactions with NADPH are shown surrounded by *red arcs*. Strictly conserved residues are *underlined*. Carbon atoms are *black*; nitrogen is *blue*; oxygen is *red*, and phosphorus is *orange*. *C*, putative flavin interactions. Flavin was docked onto the Steap4 protein by superposition of the nicotinamide ring in the Steap4 structure with the nicotinamide ring of the flavin containing FNO structure (Protein Data Bank code 1JAY). Potential FMN interactions were highlighted after substituting an isoalloxazine ring for the tricyclic ring of $F_{420}$ and truncating the tail of $F_{420}$ to replicate the ribitol-phosphate of FMN. Conserved residues are highlighted as in *B*. For clarity, only the nicotinamide ribosyl moiety of NADPH is shown.

four subunits within the crystallographic asymmetric unit are packed as two very similar "dimers." These dimers are not only nearly identical to each other but also to the Steap3 crystal dimer. Importantly, each of these three crystallographically independent dimers utilize the same set of secondary structural elements, which include residues that are highly conserved in the mammalian Steap3 and Steap4 sequences (35). They also bury the same approximate surface area (~700 $Å^2$ per subunit) and orient the truncated C termini on the same side of the dimer. In the context of the full-length protein, the C termini of the N-terminal domain should mark the membrane proximal face of the dimer, as inspection of the multiple sequence alignment (supplemental Fig. 1) suggests a short connecting loop (~7 residues) between the last residue of the oxidoreductase domain and the first transmembrane helix in the C-terminal domain. Thus, in concert with the solution state homodimer observed for the Steap3 oxidoreductase domain, the crystallographic Steap4 dimers reinforce the idea that full-length Steap3 and Steap4 are likely to function as homodimers *in vivo* (35).

*Disordered N-terminal Residues Are Unnecessary for Enzymatic Activity*—Two portions of the Steap4 oxidoreductase domain are not visible in the electron density and are likely disordered in the crystal. These are as follows: first, a short loop between α5 and β7 (residues 147–149), which is also poorly ordered in Steap3 (residues 157–162); second, the N-terminal 18 residues are also disordered, as are the first 28 residues at the

N terminus of the Steap3 oxidoreductase domain (35). Interestingly, these extreme N-terminal residues are the most poorly conserved region among Steap family oxidoreductase domains (supplemental Fig. 1). This suggests these N-terminal residues may be unnecessary for enzymatic activity.

To test this hypothesis, we constructed two variants as follows: (i) a 19-residue N-terminal deletion in the full-length Steap4 protein to give the Steap4(20–470) variant, and (ii) the equivalent N-terminal deletion within the stand-alone oxidoreductase domain to give the Steap4(20–203) variant. We then analyzed the respective cell surface metalloreductase and NADPH oxidase activities of these variants. Within experimental error, the $K_m$ and $V_{max}$ values for the metalloreductase activity of the Steap4(20–470) variant were essentially unchanged (Table 1). Similarly, the N-terminal truncation to the isolated oxidoreductase domain (Steap4(20–203)) showed no significant change in the $V_{max}$ and $K_m$ values for NADPH and FAD relative to the Steap4 oxidoreductase domain (Steap4(1–203), Table 2). It thus appears that these N-terminal residues are not directly involved in the enzymatic activity of the Steap proteins, and instead they function in an alternative role (discussed below).

*Structural Basis for Steap4 Oxidoreductase Activity*—The NADPH oxidase activity of the Steap3 and Steap4 oxidoreductase domains (Fig. 3) revealed a striking difference between the activities of seemingly equivalent constructs. Although Steap4(1–203) shows significant flavin-dependent NADPH oxidase activity, Steap3(1–215) shows only minimal activity (Fig. 3). A structural explanation for the increased activity of Steap4 is of obvious interest.

A closer examination of the Steap3 and Steap4 oxidoreductase crystal structures reveals a number of minor differences, but two seem particularly significant with regard to the enhanced activity of Steap4. The first is the connection between strands β4 and β5, which is present as a short α-helix in Steap3 (α5) but as extended "random coil" in Steap4 (Fig. 5*A*). The second is found at the C-terminal tail. In Steap3, the C-terminal helix (α9) is broken at the edge of the active site pocket by Pro-205, with the Leu-206 side chain dropping into the putative binding site for the isoalloxazine moiety of the flavin (Fig. 5*A*). In contrast, although an equivalent proline in Steap4 (Pro-193) also disrupts the C-terminal helix (α7), the helix is merely kinked, and the corresponding leucine (Leu-194) does not descend into the putative substrate-binding site but instead tucks up against the side chain of Met-110. Notably, Met-110 lies within the extended β4-β5 loop, *i.e.* it is found in the same random coil segment that substitutes for the α-5 helix of Steap3 (described above). Interestingly, structural superposition of Steap3 on Steap4 shows that the Leu-206 side chain of Steap3 is excluded from adopting a similar position due to the presence of the Steap3 α5 helix (Fig. 5*A*). Thus, helix loss in the β4-β5 loop may correlate with the "active" conformation of the C-terminal tail.

The multiple sequence alignment provides additional insight in this regard. First, all mammalian Steap2 and Steap4 sequences contain a hydrophobic residue equivalent to Met-110. In contrast, the mammalian Steap3 sequences contain a hydrophilic side chain at this position along with a two residue hydrophilic insertion that, collectively, appear to support helix formation (supplemental Fig. 1). Helix formation in the β4-β5 connection may thus be conserved in mammalian Steap3 structures but is absent in Steap2 and Steap4.

Although the structural differences between Steap3 and Steap4 correlate nicely with the increased NADPH oxidase activity of Steap4, they do not explain the difference between the short and long Steap4 constructs (Fig. 1). However, further work at higher FAD concentrations using 0.2-cm cuvettes allowed $K_m$ values to be determined for the shorter construct as well, revealing a striking difference. Specifically, truncation of residues 196–203 increased the $K_m$ value for FAD from 114 ± 22 to 825 ± 293 μM (Table 2), suggesting these residues participate in FAD recognition, perhaps by extending over the top of the flavin-binding site, as they do in FNO, to sandwich the isoalloxazine rings between these C-terminal residues and the nicotinamide of NADPH (Fig. 5*B*). Of these residues, Leu-196 and Trp-200 are strictly conserved and might therefore play a particularly significant role in isoalloxazine recognition.

*Steap4 Variants, L194A, L196A, and W200A*—To test this idea, we characterized the L196A and W200A variants, not only in the isolated oxidoreductase domain using the NADPH oxidase assay but also in full-length Steap4 where we measured cell surface metalloreductase activity. At the same time, we also characterized the L194A variants, because this residue is also strictly conserved, and the corresponding leucine in Steap3 (Leu-206) intrudes into the active site (35).

For the full-length variants, significant changes in metal $K_m$ values relative to the wild-type enzyme were not anticipated, as the flavin-binding site is in the cytoplasm, although the metals bind on the cell surface. Indeed, the affinities for the various metal substrates were largely unchanged. In contrast, deleterious substitutions within the flavin-binding site could potentially decrease $V_{max}$. However, within experimental error, the $V_{max}$ values for the L196A and W200A variants were also unchanged, whereas those for the L194A variant, if anything, were slightly enhanced. Because the cell surface $V_{max}$ values are dependent upon the amount of Steap4 present on the cell surface, we also monitored the subcellular localization of wild-type (3) and variant Steap4 proteins by immunofluorescence. The subcellular localization did not appear significantly altered in any of the mutants, with both wild-type and variant Steap4 showing partial colocalization with transferrin receptor in the transfected HEK293 cells (Fig. 6). Overall, within the context of full-length protein and the cell surface metalloreductase assay, we concluded that these variant proteins do not exhibit any significant differences. Thus, if these residues contribute to flavin recognition, they do not significantly alter the flavin $K_m$ value relative to endogenous flavin concentrations within the intact cell.

*Oxidoreductase Domain Variants, L194A, L196A, and W200A*—When we examined the effects of these substitutions on the FAD-dependent NADPH oxidase activity of the isolated oxidoreductase domain, changes in NADPH $K_m$ values were not expected and, indeed, were not seen for any of the three variants (Table 2). Similarly, significant changes in $V_{max}$ were also not observed. With regard to FAD, the $K_m$ value for the W200A mutant was identical to wild type, which suggests

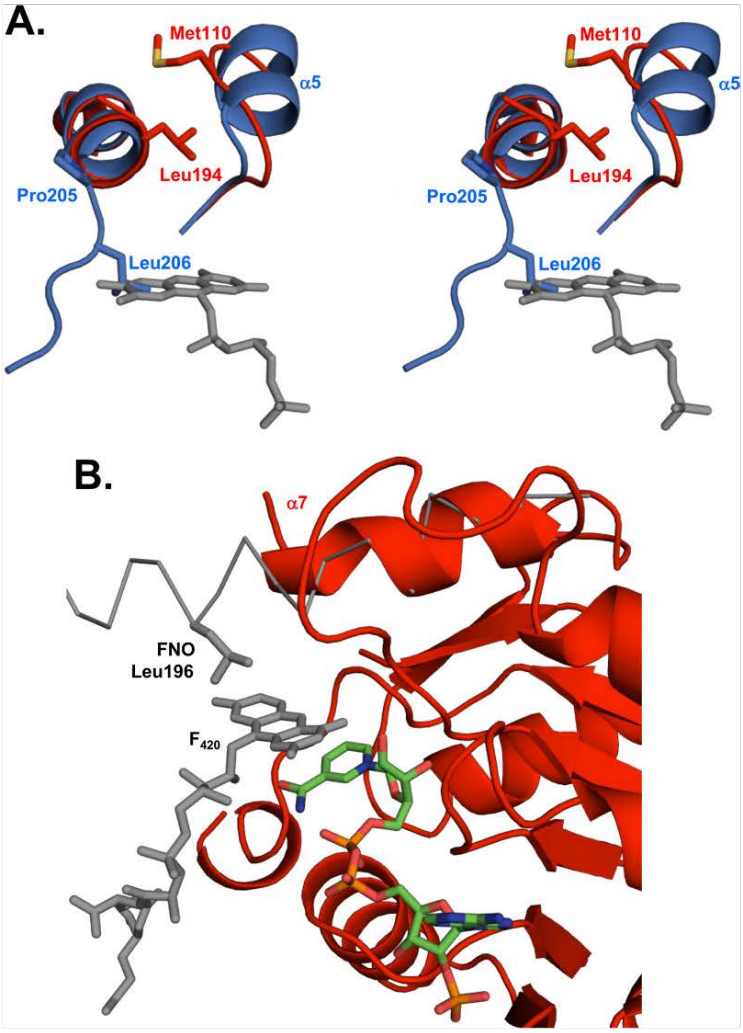


FIGURE 5. **Structural differences between Steap3 and Steap4.** *A*, stereo figure superposition of rat Steap4 (*red*) on human Steap3 (*blue*) highlights structural differences near the putative flavin-binding site. In Steap3, Pro-205 breaks the C-terminal helix allowing Leu-206 to drop into the active site pocket where it clashes with the docked FMN (*gray*). In contrast, the Steap4 C-terminal helix includes an extra turn, repositioning the corresponding Leu-194 against the β5-α4 loop where it makes hydrophobic contact with Met-110. A similar interaction in Steap3 may be prevented by insertion of the hydrophilic α-5 helix at this position (see text for details). *B*, superposition of the archaeal FNO on rat Steap4. In Steap4 (*red*), the C-terminal helix (α7) terminates near the flavin-binding site. In FNO, the corresponding helix (*gray*) extends over the tricyclic ring of $F_{420}$ allowing the FNO Leu-196 side chain to interact with $F_{420}$ (*gray*). For clarity, only the corresponding helix of FNO is shown.

Trp-200 does not participate in flavin recognition. Instead, Trp-200 may function in the linker between the N- and C-terminal domains or within the C-terminal domain itself. The latter possibility is suggested by conservation of Trp-200 in Steap1, which lacks the N-terminal oxidoreductase domain (supplemental Fig. 1). The picture was less clear with the L194A and L196A variants. Although the mean FAD $K_m$ values for L194A (186 ± 44 μM) and L196A (253 ± 104 μM) were higher than wild type, they are arguably within experimental error. Thus, although we were unable to conclude whether the conformation of Steap4 Leu-194 may play a role in positioning Leu-196 over the isoalloxazine, we can certainly conclude that neither variant fully recapitulates the drop in NADPH oxidase activity and increased the $K_m$ value for FAD seen in the shorter construct. Thus, rather than a single conserved residue, it instead appears that the ensemble of C-terminal residues (196–203) is collectively responsible for the increased activity.

## DISCUSSION

*Physiologically Relevant Metalloreductase Activities*—There has been significant work on the potential role of Steap4 in obesity-associated insulin resistance. In contrast, biochemical characterization of its metalloreductase activity is limited, consisting of only an initial but critically important demonstration

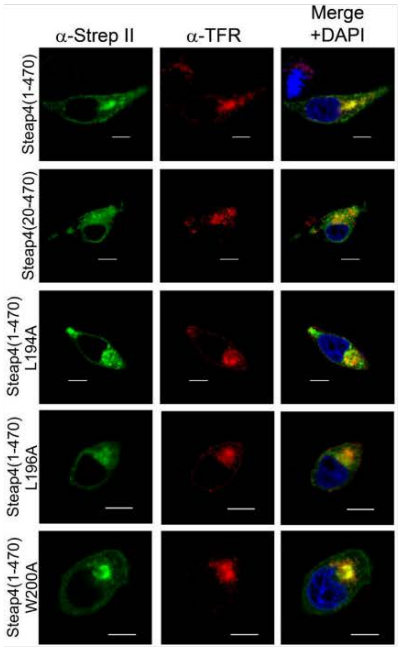


FIGURE 6. **Colocalization of rat Steap4 and transferrin receptor.** HEK-293F cells were transfected with various Steap4 constructs and visualized with immunofluorescence. Steap4 (*green*) and endogenous transferrin receptor-1 (*TFR*; *red*) were visualized by confocal microscopy after staining with anti-Strep-II and anti-transferrin receptor antibodies, respectively. Channels were merged to show colocalization (*yellow*), along with the addition of DAPI to identify nuclei (*blue*). No significant change in expression pattern was observed for any of the mutants. *White bars* indicate 10 μm.

of cell surface ferric and cupric reductase activities (3). Here, we have presented the first in-depth analysis of the Steap4 ferric and cupric reductase activities. We found that the affinity of Steap4 for ferric chelates is equal to or greater than those of other characterized ferric reductases implicated in iron homeostasis, thus demonstrating the potential for physiologically relevant Steap4 ferric reductase activity. Furthermore, Steap4 also shows significant cell surface metalloreductase activity at acidic pH (pH 5.5–6.5), suggesting Steap4 has the capacity to function in endosomal or lysosomal compartments that concentrate iron and other cellular locations that experience acidic pH. Steap4 also shows significant activity at pH 7.5, near the physiological pH of blood plasma. Thus, Steap4 might also participate in reduction of NTBI, enabling iron acquisition during iron overload, perhaps in collaboration with Zip8 or Zip14 (53–55).

The potential for physiologically relevant cupric reductase activity is less clear. Reduction of $Cu^{2+}$ to $Cu^{+}$ is required prior to transport by human CTR1, the primary copper transporter involved in cellular uptake in mammals (56, 57). Although the relevant copper reductase has not yet been identified, several recent reviews consider the Steap family members and/or Dcytb for this role (57, 58). This is, in part, by analogy to yeast where the FRE family of ferric reductases also reduce copper and promote increased copper uptake. In this regard, it is interesting that Steap4 shows greater affinity for $Cu^{2+}$-NTA and $Cu^{2+}$-histidine than Dcytb. Perhaps even more relevant is the $K_m$ value for copper transport by human Ctr1 (2.5 μM), which is also active at acidic pH (5.5–6.5) (59). Although the $K_m$ value for reduction of $Cu^{2+}$-histidine (~10 μM) by Steap4 is somewhat higher than the $K_m$ value for copper transport by Ctr1, these $K_m$ values are at least on the same order of magnitude, suggesting the cupric reductase activity might also be physiologically relevant.

*Oxidoreductase Domain*—Although Steap2–4 have been presumed to be NADPH- and flavin-dependent metalloreductases, our work here with the isolated oxidoreductase domain represents the first demonstration of flavin-dependent NADPH oxidase activity for any member of the Steap family. Experimental confirmation of this predicted activity is germane to the function of Steap2–4 in general. However, it will also greatly facilitate future structure-function studies of Steap4. As opposed to the full-length protein, dissection of the NADPH oxidase activity from the metalloreductase activity allows readout on the initial stages of electron transfer.

*N-terminal Oxidoreductase Residues*—It is noteworthy that truncation of the nonconserved residues at the N terminus of Steap4 had no significant effect on the metalloreductase and NADPH oxidase activities of the full-length protein and the truncated oxidoreductase domain, respectively. At the same time, deletion of the N terminus in the full-length protein did not significantly alter Steap4 colocalization with the transferrin receptor, suggesting that loss of these N-terminal residues does not alter the subcellular localization (Fig. 6). Together, these observations suggest that the disordered N-terminal residues may instead serve a regulatory role or, alternatively, in protein-protein interactions specific to the individual Steap2–4 proteins (60, 61). In this context, it is interesting that phosphoproteomic studies have consistently found the N termini of human and mouse Steap3 to be phosphorylated at Ser-17 and Ser-20 (62–71), and these residues are well conserved in the mammalian Steap3 sequences (supplemental Fig. 1). Proteomic studies have also demonstrated ubiquitylation of mouse Steap4 at Lys-3 and Lys-18 (72), which are similarly well conserved in other mammalian Steap4 proteins (supplemental Fig. 1).

*An Incomplete Flavin-binding Site in the Oxidoreductase Domain*—Several lines of evidence suggest that the N-terminal oxidoreductase domain contains only a portion of the flavin-binding site present in the full-length Steap4 protein. First, the inability of the oxidoreductase domain to discriminate between flavins suggests that the N-terminal domain interacts primarily with the isoalloxazine ring and/or ribitol moieties. However, the full-length protein would presumably display a flavin preference *in vivo*. Thus, portions of the full-length protein not present in our crystal structure would likely be responsible for flavin discrimination and contribute residues important for flavin binding.

Second, unlike the N-terminal fragment studied here, FMN and FAD reductases generally have $K_m$ values for flavins in the high nanomolar to low micromolar range (73). Specific examples with potential relevance to the Steap proteins include archaeal FNO, whose $K_m$ value for $F_{420}$ is 10 μM (74), *E. coli* ferric reductase (Fre) with a $K_m$ value of 0.6–2.5 μM (75, 76), and human NADPH oxidase (Nox) with a $K_m$ value of 60 nm

(77, 78). These values are ~10–1,000-fold lower than the $K_m$ values measured for truncated Steap4. We also note that flavin $K_m$ values of >100 $\mu$M are not physiologically relevant, as cells containing such high flavin concentrations would be intensely yellow ($A_{450}$ >1). In this light, it becomes clear that the isolated N-terminal domain of Steap4 does not contain a high affinity flavin-binding site.

Third, our structural data also support the partial flavin site hypothesis. The crystal structures of the Steap4 oxidoreductase domain reveal a putative flavin-binding site that is distinctly different from the $F_{420}$-binding site in FNO. In FNO, the C-terminal helix is significantly longer and extends over the top of the active site, sandwiching the isoalloxazine ring between the nicotinamide of NADPH on the one side and hydrophobic residues of the C-terminal helix on the other side (Fig. 5). In contrast, the equivalent residues in Steap4 contain two helix breaking proline residues, such that the C-terminal helix is truncated at the edge of the active site, giving rise to an uncharacteristically solvent-exposed active site structure.

Importantly, these structural results are consistent with the kinetic analysis. Specifically, in contrast to Steap3, docking studies show that the Steap4 active site could nicely accommodate the isoalloxazine ring, but in accordance with the observed $K_m$ values, additional interactions that might discriminate between the various flavins are not predicted. Similarly, although the predicted interactions with the isoalloxazine are relatively well conserved, the open solvent-exposed active site would also predict an uncharacteristically high $K_m$ value.

In this context, it is important to remember that the structural and kinetic data on flavin binding and specificity are derived from the truncated oxidoreductase domain, and although FNO is a soluble single domain protein, Steap4 is instead a two domain integral membrane protein in which the flavin is proposed to serve as an intermediate in electron transfer, shuttling electrons between NADPH, bound in the oxidoreductase domain, and the heme group in the transmembrane domain. In addition, access to the enlarged entrance of the Steap oxidoreductase active site (relative to FNO) is primarily from the presumed membrane proximal face of the oxidoreductase domain, which would be expected to abut the transmembrane domain. For these reasons, it seems logical that the transmembrane domain might participate in the construction of the flavin-binding site.

Further support for this idea comes from YedZ, a single domain membrane protein with homology to the Steap transmembrane domain (79, 80). Importantly, YedZ has been observed to copurify with noncovalently bound FMN, demonstrating the ability of a Steap4-like transmembrane domain to participate in flavin recognition (38). This is in contrast to Fre and Nox where the flavin-binding sites are instead found in a cytoplasmic domain. We hypothesize that unlike Fre and Nox, Steap proteins instead utilize the transmembrane domain to complete a high affinity flavin-binding site, with the flavin bound at the interface between the N- and C-terminal domains, giving rise to physiologically relevant affinity ($K_m$ value) for FMN or FAD. Correspondingly, loss of the C-terminal YedZ-like domain in the truncated Steap4 oxidoreductase domain should lead to an aberrantly high, nonphysiological $K_m$ value for flavin, as observed (Table 2).

This hypothesis is also consistent with a recent evolutionary study on the origin of the ferric reductase domain superfamily. This study suggests that Steap proteins are indeed more closely related to the YedZ-like proteins than to Fre and Nox (80). Unlike Fre and Nox, which contain two heme groups (surface-proximal and cytoplasm-proximal), Steap and YedZ are thought to contain only a single surface proximal heme (2, 3, 80). It will be interesting to determine whether loss of the cytoplasm proximal heme in the Steap transmembrane domain is due to substitution of a cytoplasm proximal flavin-binding site.

If the Steap4 transmembrane domain is involved in flavin recognition, the high incidence of strictly conserved residues in the NADPH-binding site of the oxidoreductase domain suggests that residues involved in flavin recognition would be similarly conserved. In this light, strictly conserved residues in the transmembrane domain occur most frequently within the first and second cytoplasmic loops (supplemental Fig. 1). However, kinetic work to assess the potential role of these residues in flavin recognition will require the ability to measure NADPH- and flavin-dependent metalloreductase activity, preferably with purified full-length protein.

Additional work is thus needed to understand the mechanism of Steap4 iron and copper reduction in greater detail, and this includes the need for structural and functional analysis of purified full-length protein. At the same time, however, the biochemical analysis presented here suggests that Steap4 possesses physiologically relevant ferric and cupric reductase activities. For this reason, attention should also turn to specific investigations on the role of Steap4 ferric and cupric reductase activities in obesity-associated insulin resistance and atherosclerosis.

*Acknowledgments—The SSRL Structural Molecular Biology Program is supported by the Department of Energy, Office of Biological and Environmental Research, National Institutes of Health, NCCR Biomedical Technology Program and NIGMS. The Macromolecular Diffraction Laboratory at Montana State University was supported, in part, by a grant from the Murdock Foundation. The Montana State University confocal microscope was purchased with funding from the National Science Foundation-Major Research Instrumentation Program and the M. J. Murdock Charitable Trust.*

## REFERENCES

1. Hubert, R. S., Vivanco, I., Chen, E., Rastegar, S., Leong, K., Mitchell, S. C., Madraswala, R., Zhou, Y., Kuo, J., Raitano, A. B., Jakobovits, A., Saffran, D. C., and Afar, D. E. (1999) STEAP: a prostate-specific cell-surface antigen highly expressed in human prostate tumors. *Proc. Natl. Acad. Sci. U.S.A.* **96,** 14523–14528
2. Ohgami, R. S., Campagna, D. R., Greer, E. L., Antiochos, B., McDonald, A., Chen, J., Sharp, J. J., Fujiwara, Y., Barker, J. E., and Fleming, M. D. (2005) Identification of a ferrireductase required for efficient transferrin-dependent iron uptake in erythroid cells. *Nat. Genet.* **37,** 1264–1269
3. Ohgami, R. S., Campagna, D. R., McDonald, A., and Fleming, M. D. (2006) The Steap proteins are metalloreductases. *Blood* **108,** 1388–1394
4. Korkmaz, C. G., Korkmaz, K. S., Kurys, P., Elbi, C., Wang, L., Klokk, T. I., Hammarstrom, C., Troen, G., Svindland, A., Hager, G. L., and Saatcioglu,

F. (2005) Molecular cloning and characterization of STAMP2, an androgen-regulated six transmembrane protein that is overexpressed in prostate cancer. *Oncogene* **24,** 4934–4945
5. Korkmaz, K. S., Elbi, C., Korkmaz, C. G., Loda, M., Hager, G. L., and Saatcioglu, F. (2002) Molecular cloning and characterization of STAMP1, a highly prostate-specific six transmembrane protein that is overexpressed in prostate cancer. *J. Biol. Chem.* **277,** 36689–36696
6. Grunewald, T. G., Bach, H., Cossarizza, A., and Matsumoto, I. (2012) The STEAP protein family: Versatile oxidoreductases and targets for cancer immunotherapy with overlapping and distinct cellular functions. *Biol. Cell* **104,** 641–657
7. Gomes, I. M., Maia, C. J., and Santos, C. R. (2012) STEAP proteins: from structure to applications in cancer therapy. *Mol. Cancer Res.* **10,** 573–587
8. Gunshin, H., Mackenzie, B., Berger, U. V., Gunshin, Y., Romero, M. F., Boron, W. F., Nussberger, S., Gollan, J. L., and Hediger, M. A. (1997) Cloning and characterization of a mammalian proton-coupled metal-ion transporter. *Nature* **388,** 482–488
9. Fleming, M. D., Romano, M. A., Su, M. A., Garrick, L. M., Garrick, M. D., and Andrews, N. C. (1998) Nramp2 is mutated in the anemic Belgrade (b) rat: evidence of a role for Nramp2 in endosomal iron transport. *Proc. Natl. Acad. Sci. U. S.A.* **95,** 1148–1153
10. Fleming, M. D., Trenor, C. C., 3rd, Su, M. A., Foernzler, D., Beier, D. R., Dietrich, W. F., and Andrews, N. C. (1997) Microcytic anaemia mice have a mutation in Nramp2, a candidate iron transporter gene. *Nat. Genet.* **16,** 383–386
11. Grandchamp, B., Hetet, G., Kannengiesser, C., Oudin, C., Beaumont, C., Rodrigues-Ferreira, S., Amson, R., Telerman, A., Nielsen, P., Kohne, E., Balser, C., and Heimpel, H. (2011) A novel type of congenital hypochromic anemia associated with a nonsense mutation in the STEAP3/TSAP6 gene. *Blood* **118,** 6660–6666
12. ten Freyhaus, H., Calay, E. S., Yalcin, A., Vallerie, S. N., Yang, L., Calay, Z. Z., Saatcioglu, F., and Hotamisligil, G. S. (2012) Stamp2 controls macrophage inflammation through nicotinamide adenine dinucleotide phosphate homeostasis and protects against atherosclerosis. *Cell Metab.* **16,** 81–89
13. Chen, X., Zhu, C., Ji, C., Zhao, Y., Zhang, C., Chen, F., Gao, C., Zhu, J., Qian, L., and Guo, X. (2010) STEAP4, a gene associated with insulin sensitivity, is regulated by several adipokines in human adipocytes. *Int. J. Mol. Med.* **25,** 361–367
14. Qiu, J., Ni, Y. H., Gong, H. X., Fei, L., Pan, X. Q., Guo, M., Chen, R. H., and Guo, X. R. (2007) Identification of differentially expressed genes in omental adipose tissues of obese patients by suppression subtractive hybridization. *Biochem. Biophys. Res. Commun.* **352,** 469–478
15. Zhang, C. M., Chi, X., Wang, B., Zhang, M., Ni, Y. H., Chen, R. H., Li, X. N., and Guo, X. R. (2008) Down-regulation of STEAP4, a highly expressed TNF-$\alpha$-inducible gene in adipose tissue, is associated with obesity in humans. *Acta Pharmacol. Sin.* **29,** 587–592
16. Arner, P., Stenson, B. M., Dungner, E., Näslund, E., Hoffstedt, J., Ryden, M., and Dahlman, I. (2008) Expression of six transmembrane protein of prostate 2 in human adipose tissue associates with adiposity and insulin resistance. *J. Clin. Endocrinol. Metab.* **93,** 2249–2254
17. Wellen, K. E., Fucho, R., Gregor, M. F., Furuhashi, M., Morgan, C., Lindstad, T., Vaillancourt, E., Gorgun, C. Z., Saatcioglu, F., and Hotamisligil, G. S. (2007) Coordinated regulation of nutrient and inflammatory responses by STAMP2 is essential for metabolic homeostasis. *Cell* **129,** 537–548
18. Samuel, V. T., and Shulman, G. I. (2012) Mechanisms for insulin resistance: common threads and missing links. *Cell* **148,** 852–871
19. Elbein, S. C., Kern, P. A., Rasouli, N., Yao-Borengasser, A., Sharma, N. K., and Das, S. K. (2011) Global gene expression profiles of subcutaneous adipose and muscle from glucose-tolerant, insulin-sensitive, and insulin-resistant individuals matched for BMI. *Diabetes* **60,** 1019–1029
20. Konstantopoulos, N., Foletta, V. C., Segal, D. H., Shields, K. A., Sanigorski, A., Windmill, K., Swinton, C., Connor, T., Wanyonyi, S., Dyer, T. D., Fahey, R. P., Watt, R. A., Curran, J. E., Molero, J. C., Krippner, G., Collier, G. R., James, D. E., Blangero, J., Jowett, J. B., and Walder, K. R. (2011) A gene expression signature for insulin resistance. *Physiol. Genomics* **43,** 110–120
21. Moreno-Navarrete, J. M., Ortega, F., Sabater, M., Ricart, W., and Fernández-Real, J. M. (2011) Proadipogenic effects of lactoferrin in human subcutaneous and visceral preadipocytes. *J. Nutr. Biochem.* **22,** 1143–1149
22. Kralisch, S., Sommer, G., Weise, S., Lipfert, J., Lossner, U., Kamprad, M., Schröck, K., Bluher, M., Stumvoll, M., and Fasshauer, M. (2009) Interleukin-1$\beta$ is a positive regulator of TIARP/STAMP2 gene and protein expression in adipocytes *in vitro*. *FEBS Lett.* **583,** 1196–1200
23. Ramadoss, P., Chiappini, F., Bilban, M., and Hollenberg, A. N. (2010) Regulation of hepatic six transmembrane epithelial antigen of prostate 4 (STEAP4) expression by STAT3 and CCAAT/enhancer-binding protein $\alpha$. *J. Biol. Chem.* **285,** 16453–16466
24. Vignozzi, L., Morelli, A., Sarchielli, E., Comeglio, P., Filippi, S., Cellai, I., Maneschi, E., Serni, S., Gacci, M., Carini, M., Piccinni, M. P., Saad, F., Adorini, L., Vannelli, G. B., and Maggi, M. (2012) Testosterone protects from metabolic syndrome-associated prostate inflammation: an experimental study in rabbit. *J. Endocrinol.* **212,** 71–84
25. Sparna, T., Rétey, J., Schmich, K., Albrecht, U., Naumann, K., Gretz, N., Fischer, H. P., Bode, J. G., and Merfort, I. (2010) Genome-wide comparison between IL-17 and combined TNF-$\alpha$/IL-17 induced genes in primary murine hepatocytes. *BMC Genomics* **11,** 226
26. Moldes, M., Lasnier, F., Gauthereau, X., Klein, C., Pairault, J., Fève, B., and Chambaut-Guérin, A. M. (2001) Tumor necrosis factor-$\alpha$-induced adipose-related protein (TIARP), a cell-surface protein that is highly induced by tumor necrosis factor-$\alpha$ and adipose conversion. *J. Biol. Chem.* **276,** 33938–33946
27. Fasshauer, M., Kralisch, S., Klier, M., Lossner, U., Bluher, M., Chambaut-Guérin, A. M., Klein, J., and Paschke, R. (2004) Interleukin-6 is a positive regulator of tumor necrosis factor $\alpha$-induced adipose-related protein in 3T3-L1 adipocytes. *FEBS Lett.* **560,** 153–157
28. Cheng, R., Qiu, J., Zhou, X. Y., Chen, X. H., Zhu, C., Qin, D. N., Wang, J. W., Ni, Y. H., Ji, C. B., and Guo, X. R. (2011) Knockdown of STEAP4 inhibits insulin-stimulated glucose transport and GLUT4 translocation via attenuated phosphorylation of Akt, independent of the effects of EEA1. *Mol. Med. Rep.* **4,** 519–523
29. Guo, Y. Y., Li, N. F., Wang, C. M., Yan, Z. T., Zhang, J. H., Wang, H. M., Zhou, L., and Luo, W. L. (2011) Genetic variation and association of STEAP4 gene with metabolic syndrome in Chinese Uygur patients. *Zhonghua Yi Xue Yi Chuan Xue Za Zhi* **28,** 78–82
30. Miot, A., Maimaitiming, S., Emery, N., Bellili, N., Roussel, R., Tichet, J., Velho, G., Balkau, B., Marre, M., and Fumeron, F. (2010) Genetic variability at the six transmembrane protein of prostate 2 locus and the metabolic syndrome: the data from an epidemiological study on the Insulin Resistance Syndrome (DESIR) study. *J. Clin. Endocrinol. Metab.* **95,** 2942–2947
31. Nanfang, L., Yanying, G., Hongmei, W., Zhitao, Y., Juhong, Z., Ling, Z., and Wenli, L. (2010) Variations of six transmembrane epithelial antigen of prostate 4 (STEAP4) gene are associated with metabolic syndrome in a female Uygur general population. *Arch. Med. Res.* **41,** 449–456
32. Guo, Y. Y., Li, N. F., Zhou, L., Yao, X. G., Wang, H. M., Zhang, J. H., and Luo, W. L. (2011) A common variation within the STEAP4 gene exons is associated with obesity in Uygur general population. *Chin. Med. J.* **124,** 2096–2100
33. Guo, Y. Y., Zhou, L., Yao, X. G., Yan, Z. T., Wang, H. M., Luo, W. L., Shen, Y., and Li, N. F. (2011) Association of STEAP4 genetic polymorphisms with insulin resistance in Uygur Chinese general population. *Zhongguo Yi Xue Ke Xue Yuan Xue Bao* **33,** 299–305
34. Drakesmith, H., and Prentice, A. M. (2012) Hepcidin and the iron-infection axis. *Science* **338,** 768–772
35. Sendamarai, A. K., Ohgami, R. S., Fleming, M. D., and Lawrence, C. M. (2008) Structure of the membrane proximal oxidoreductase domain of human Steap3, the dominant ferrireductase of the erythroid transferrin cycle. *Proc. Natl. Acad. Sci. U.S.A.* **105,** 7410–7415
36. Sanchez-Pulido, L., Rojas, A. M., Valencia, A., Martinez-A, C., and Andrade, M. A. (2004) ACRATA: a novel electron transfer domain associated to apoptosis and cancer. *BMC Cancer* **4,** 98
37. Warkentin, E., Hagemeier, C. H., Shima, S., Thauer, R. K., and Ermler, U. (2005) The structure of F420-dependent methylenetetrahydromethanop-

terin dehydrogenase: a crystallographic "superstructure" of the selenomethionine-labeled protein crystal structure. *Acta Crystallogr. D Biol. Crystallogr.* **61,** 198–202
38. Drew, D., Slotboom, D. J., Friso, G., Reda, T., Genevaux, P., Rapp, M., Meindl-Beinker, N. M., Lambert, W., Lerch, M., Daley, D. O., Van Wijk, K. J., Hirst, J., Kunji, E., and De Gier, J. W. (2005) A scalable, GFP-based pipeline for membrane protein overexpression screening and purification. *Protein Sci.* **14,** 2011–2017
39. Su, D., and Asard, H. (2006) Three mammalian cytochromes $b_{561}$ are ascorbate-dependent ferrireductases. *FEBS J.* **273,** 3722–3734
40. McKie, A. T., Barrow, D., Latunde-Dada, G. O., Rolfs, A., Sager, G., Mudaly, E., Mudaly, M., Richardson, C., Barlow, D., Bomford, A., Peters, T. J., Raja, K. B., Shirali, S., Hediger, M. A., Farzaneh, F., and Simpson, R. J. (2001) An iron-regulated ferric reductase associated with the absorption of dietary iron. *Science* **291,** 1755–1759
41. Raymond, C., Tom, R., Perret, S., Moussouami, P., L'Abbé, D., St-Laurent, G., and Durocher, Y. (2011) A simplified polyethyleneimine-mediated transfection process for large-scale and high-throughput applications. *Methods* **55,** 44–51
42. Bradford, M. M. (1976) Rapid and sensitive method for quantitation of microgram quantities of protein utilizing principle of protein-dye binding. *Anal. Biochem.* **72,** 248–254
43. Studier, F. W. (2005) Protein production by auto-induction in high density shaking cultures. *Protein Expr. Purif.* **41,** 207–234
44. Aliverti, A., Curti, B., and Vanoni, M. A. (1999) Identifying and quantitating FAD and FMN in simple and in iron-sulfur-containing flavoprotein. *Methods Mol. Biol.* **131,** 9–23
45. Fischer, M., Haase, I., Feicht, R., Richter, G., Gerhardt, S., Changeux, J. P., Huber, R., and Bacher, A. (2002) Biosynthesis of riboflavin-6,7-dimethyl-8-ribityllumazine synthase of *Schizosaccharomyces pombe*. *Eur. J. Biochem.* **269,** 519–526
46. Hinkson, J. W. (1968) Azotobacter free-radical flavoprotein. Preparation and properties of the apoprotein. *Biochemistry* **7,** 2666–2672
47. Otwinowski, Z., and Minor, W. (1997) Processing of x-ray diffraction data collected in oscillation mode. *Methods Enzymol.* **276,** 307–326
48. Collaborative Computational Project No. 4 (1994) The CCP4 Suite: Programs for protein crystallography. *Acta Crystallogr. D Biol. Crystallogr.* **50,** 760–763
49. Schrödinger, L. (2011) *The PyMOL Molecular Graphics System*, Version 1.2, Schrödinger, LLC, New York
50. Wallace, A. C., Laskowski, R. A., and Thornton, J. M. (1995) LIGPLOT: a program to generate schematic diagrams of protein-ligand interactions. *Protein Eng.* **8,** 127–134
51. Wyman, S., Simpson, R. J., McKie, A. T., and Sharp, P. A. (2008) Dcytb (Cybrd1) functions as both a ferric and a cupric reductase *in vitro*. *FEBS Lett.* **582,** 1901–1906
52. Li, L., Fang, C. J., Ryan, J. C., Niemi, E. C., Lebrón, J. A., Björkman, P. J., Arase, H., Torti, F. M., Torti, S. V., Nakamura, M. C., and Seaman, W. E. (2010) Binding and uptake of H-ferritin are mediated by human transferrin receptor-1. *Proc. Natl. Acad. Sci. U.S.A.* **107,** 3505–3510
53. Wang, C. Y., Jenkitkasemwong, S., Duarte, S., Sparkman, B. K., Shawki, A., Mackenzie, B., and Knutson, M. D. (2012) ZIP8 is an iron and zinc transporter whose cell-surface expression is up-regulated by cellular iron loading. *J. Biol. Chem.* **287,** 34032–34043
54. Zhao, N., Gao, J., Enns, C. A., and Knutson, M. D. (2010) ZRT/IRT-like protein 14 (ZIP14) promotes the cellular assimilation of iron from transferrin. *J. Biol. Chem.* **285,** 32141–32150
55. Wang, C. Y., and Knutson, M. D. (2013) Hepatocyte divalent metal-ion transporter-1 is dispensable for hepatic iron accumulation and non-transferrin-bound iron uptake in mice. *Hepatology*, in press
56. Kidane, T. Z., Farhad, R., Lee, K. J., Santos, A., Russo, E., and Linder, M. C. (2012) Uptake of copper from plasma proteins in cells where expression of CTR1 has been modulated. *Biometals* **25,** 697–709
57. Kaplan, J. H., and Lutsenko, S. (2009) Copper transport in mammalian cells: special care for a metal with special needs. *J. Biol. Chem.* **284,** 25461–25465
58. Wang, Y., Hodgkinson, V., Zhu, S., Weisman, G. A., and Petris, M. J. (2011) Advances in the understanding of mammalian copper transporters. *Adv. Nutr.* **2,** 129–137
59. Lee, J., Peña, M. M., Nose, Y., and Thiele, D. J. (2002) Biochemical characterization of the human copper transporter Ctr1. *J. Biol. Chem.* **277,** 4380–4387
60. Amzallag, N., Passer, B. J., Allanic, D., Segura, E., Théry, C., Goud, B., Amson, R., and Telerman, A. (2004) TSAP6 facilitates the secretion of translationally controlled tumor protein/histamine-releasing factor via a nonclassical pathway. *J. Biol. Chem.* **279,** 46104–46112
61. Passer, B. J., Nancy-Portebois, V., Amzallag, N., Prieur, S., Cans, C., Roborel de Climens, A., Fiucci, G., Bouvard, V., Tuynder, M., Susini, L., Morchoisne, S., Crible, V., Lespagnol, A., Dausset, J., Oren, M., Amson, R., and Telerman, A. (2003) The p53-inducible TSAP6 gene product regulates apoptosis and the cell cycle and interacts with Nix and the Myt1 kinase. *Proc. Natl. Acad. Sci. U. S.A.* **100,** 2284–2289
62. Hsu, P. P., Kang, S. A., Rameseder, J., Zhang, Y., Ottina, K. A., Lim, D., Peterson, T. R., Choi, Y., Gray, N. S., Yaffe, M. B., Marto, J. A., and Sabatini, D. M. (2011) The mTOR-regulated phosphoproteome reveals a mechanism of mTORC1-mediated inhibition of growth factor signaling. *Science* **332,** 1317–1322
63. Christensen, G. L., Kelstrup, C. D., Lyngsø, C., Sarwar, U., Bøgebo, R., Sheikh, S. P., Gammeltoft, S., Olsen, J. V., and Hansen, J. L. (2010) Quantitative phosphoproteomics dissection of seven-transmembrane receptor signaling using full and biased agonists. *Mol. Cell. Proteomics* **9,** 1540–1553
64. Goswami, T., Li, X., Smith, A. M., Luderowski, E. M., Vincent, J. J., Rush, J., and Ballif, B. A. (2012) Comparative phosphoproteomic analysis of neonatal and adult murine brain. *Proteomics* **12,** 2185–2189
65. Yu, Y., Yoon, S. O., Poulogiannis, G., Yang, Q., Ma, X. M., Villén, J., Kubica, N., Hoffman, G. R., Cantley, L. C., Gygi, S. P., and Blenis, J. (2011) Phosphoproteomic analysis identifies Grb10 as an mTORC1 substrate that negatively regulates insulin signaling. *Science* **332,** 1322–1326
66. Weintz, G., Olsen, J. V., Frühauf, K., Niedzielska, M., Amit, I., Jantsch, J., Mages, J., Frech, C., Dölken, L., Mann, M., and Lang, R. (2010) The phosphoproteome of toll-like receptor-activated macrophages. *Mol. Syst. Biol.* **6,** 371
67. Trost, M., English, L., Lemieux, S., Courcelles, M., Desjardins, M., and Thibault, P. (2009) The phagosomal proteome in interferon-γ-activated macrophages. *Immunity* **30,** 143–154
68. Zanivan, S., Gnad, F., Wickström, S. A., Geiger, T., Macek, B., Cox, J., Fässler, R., and Mann, M. (2008) Solid tumor proteome and phosphoproteome analysis by high resolution mass spectrometry. *J. Proteome Res.* **7,** 5314–5326
69. Pan, C., Gnad, F., Olsen, J. V., and Mann, M. (2008) Quantitative phosphoproteome analysis of a mouse liver cell line reveals specificity of phosphatase inhibitors. *Proteomics* **8,** 4534–4546
70. Villén, J., Beausoleil, S. A., Gerber, S. A., and Gygi, S. P. (2007) Large-scale phosphorylation analysis of mouse liver. *Proc. Natl. Acad. Sci. U.S. A.* **104,** 1488–1493
71. Wiśniewski, J. R., Nagaraj, N., Zougman, A., Gnad, F., and Mann, M. (2010) Brain phosphoproteome obtained by a FASP-based method reveals plasma membrane protein topology. *J. Proteome Res.* **9,** 3280–3289
72. Wagner, S. A., Beli, P., Weinert, B. T., Schölz, C., Kelstrup, C. D., Young, C., Nielsen, M. L., Olsen, J. V., Brakebusch, C., and Choudhary, C. (2012) Proteomic analyses reveal divergent ubiquitylation site patterns in murine tissues. *Mol. Cell. Proteomics* **11,** 1578–1585
73. Tu, S. C. (2001) Reduced flavin: Donor and acceptor enzymes and mechanisms of channeling. *Antioxid. Redox Signal.* **3,** 881–897
74. Kunow, J., Schworer, B., Stetter, K. O., and Thauer, R. K. (1993) A F(420)-dependent NADP reductase in the extremely thermophilic sulfate-reducing archaeoglobus-fulgidus. *Arch. Microbiol.* **160,** 199–205
75. Fieschi, F., Nivière, V., Frier, C., Décout, J. L., and Fontecave, M. (1995) The mechanism and substrate specificity of the NADPH:flavin oxidoreductase from *Escherichia coli*. *J. Biol. Chem.* **270,** 30392–30400
76. Fontecave, M., Eliasson, R., and Reichard, P. (1987) NAD(P)H-flavin oxidoreductase of *Escherichia coli*. A ferric iron reductase participating in the generation of the free-radical of ribonucleotide reductase. *J. Biol. Chem.* **262,** 12325–12331

77. Babior, B. M., and Peters, W. A. (1981) The O2-producing enzyme of human neutrophils. Further properties. *J. Biol. Chem.* **256,** 2321–2323
78. Parkinson, J. F., and Gabig, T. G. (1988) Phagocyte NADPH-oxidase. Studies with flavin analogues as active site probes in Triton X-100-solubilized preparations. *J. Biol. Chem.* **263,** 8859–8863
79. Sanchez-Pulido, L., Rojas, A. M., Valencia, A., Martinez, C., and Andrade, M. A. (2004) ACRATA: a novel electron transfer domain associated to apoptosis and cancer. *BMC Cancer* **4,** doi:10.1186/1471-2407-4-98
80. Zhang, X., Krause, K. H., Xenarios, I., Soldati, T., and Boeckmann, B. (2013) Evolution of the ferric reductase domain (FRD) superfamily: Modularity, functional diversification, and signature motifs. *PLoS One* **8,** e58126

# CHAPTER FOUR

# EXPRESSION AND PARTIAL PURIFICATION OF HUMAN STEAP3 IN SF9 INSECT CELLS

## Introduction

To date, no Steap family member has been purified in the full-length enzymatically active form. Activity studies have been limited to in vitro cell-surface systems or truncated oxidoreductase domain variants [1-3]. A purified, active protein would allow for numerous structure-function studies including, but not limited to, characterizing ferric and cupric reductase kinetics, identifying and characterizing protein-protein interactions, and the three-dimensional protein structure through crystallographic studies.

Expression and purification of recombinant integral membrane proteins is an area of that has received much interest as researchers seek to understand the processes at the membrane interface [4]. Recombinant protein expression is generally performed in *Escherichia coli* strains due to their ubiquity and ease of handling. Mammalian integral membrane proteins are generally poor candidates for overexpression in *E. coli* cells, however, due to issues with folding and that their expression can be toxic to the cell [4]. Additionally, the prokaryotic system is not capable of processing post-translational modifications, which in some cases is a prerequisite for proper folding and function. For these reasons, mammalian integral membrane proteins are normally expressed in

eukaryotic systems like yeast (e. g. *Pichia pastoris*), insect (e.g. Sf9 or Hi-Five), or human (e.g. HEK 293F) cell lines [4].

Baculovirus-mediated gene expression in insect cells is a robust, simple, and inexpensive system for large scale membrane protein overexpression [5]. Importantly, the baculoviruses have a limited host range to invertebrates, thus are noninfectious to humans and are safe to handle. The most common baculovirus used is the *Autographica californica* nuclear polyhedrosis virus (AcNPV). AcNPV has a two-stage life cycle, the early and late phase. In the late phase, a number of genes are abundantly expressed for propagation. In the baculovirus expression vector system (BEVS), a gene of interest is commonly transposed with that of a non-essential late-phase gene, though some systems use replacement of early-phase genes [5]. After isolation of virus carrying the transposition, scaling up to the liter scale of growth, infection and expression is time-efficient and simple. Limitations to the system include both insect-specific composition of membrane lipids and glycosylation.

Since no one has attempted a purification of any Steap family members to date, we chose to investigate the use of the *Spodoptera frugiperda* (Sf9) BEVS system. Can we use this platform to express significant amounts of recombinant Steap3? Furthermore, can a purification scheme be developed that yields pure, active enzyme? To these ends, the first expression of Steap3 in the Spodoptera frugiperda (Sf9) BEVS system is described. Furthermore, detergent solubilization from membranes was optimized and an activity assay developed. Finally, a purification of Steap3 was attempted, analyzing multiple affinity tags and their localizations.

## Materials and Methods

### Cloning and Baculovirus Bacmid Preparation

Homo sapiens Steap3 cDNA was PCR amplified with primers that incorporated attB recombination sites at 5' and 3' ends of the product. Primers also incorporated either Strep-II or hexahistidine affinity tags at the 5' or 3' ends of the gene (Table 1). The PCR product was gel-purified and incorporated into the pDONR201 donor vector using the Gateway BP clonase II system (Invitrogen). The resulting entry clone was sequence-verified and subsequently cloned into the pDEST8 destination vector using the Gateway LR clonase II system (Invitrogen). The resulting pDEST8.Steap3 vector has Steap3 incorporated into the attR recombination sites. The pDEST8.Steap3 vector was transformed into DH10Bac *E. coli* cells (Invitrogen). Transformed cells that transposed Steap3 into the AcNPV bacmid were selected by blue/white screening on Luria Agar plates containing 50 µg/ml kanamycin, 7 µg/ml gentamicin, 10 µg/ml tetracycline, 100 µg/ml Bluo-gal, 40 µg/ml IPTG. Bacmid DNA was purified from candidate colonies by common procedures.

### Sf9 Cell Culture and Baculovirus Generation

*Spodoptera frugiperda* cells were grown in CCM3 media (Thermo) supplemented with 50 units/ml penicillin and 50 µg/ml streptomycin (Gibco). Cells were cultured in spinner flasks at 100-rpm in a 28°C incubator. Sf9 cells were transfected with Steap3-incorporated AcNPV bacmid using Cellfectin-II transfection reagent (Invitrogen)

according to manufacturer's protocols. Briefly, $8x10^5$ Sf9 cells were plated per-well in a 6-well plate and allowed to attach to the surface at room temperature. 3 µg of purified bacmid were mixed with diluted Cellfectin II reagent and incubated for 30 minutes at room temperature. The mixture was then added drop-wise to the plated cells, and was then incubated at room temperature for 3 hours. After incubation, the transfection media was removed and replaced by fresh growth medium. Transfected cells were then grown at 28°C for ~72 hours at which point baculovirus-containing supernatant was collected. Viral titer was determined via plaque assay as follows. Cells were plated in 6-well plates at a density of 1x106 cells per well and allowed to attach to the plate surface. Baculovirus stock was serially diluted to produce dilutions from $10^{-2}$ to $10^{-8}$ and was added to a respective well and incubated at room temperature for 1 hour. The supernatant was then removed and replaced with plaquing medium (1% low-melting temperature agarose in CCM3 medium). Plates were observed for plaques approximately 7 days post-infection. Titer was determined from the following calculation:

Titer (plaque forming units/ml) = (1/dilution factor) x (number of plaques) x 1/(ml of inoculum)

Baculovirus stocks were amplified by infecting cultures at a multiplicity of infection (MOI) of 0.1 and harvesting supernatant ~48 hours post-infection. Virus used for expression studies was amplified at least twice after transfection (third generation).

Expression and Purification of Steap3

On the day of infection, Sf9 cells were diluted to a density of $1x10^6$ cells/ml and Steap3-containing baculovirus was added to the culture at an MOI of 5. After ~20 hours,

the culture was supplemented with 0.3 mM δ-aminolevulinic acid. 72-hours post-infection, cells were harvested by centrifugation of 5,000xG for 10 minutes and the pellet was stored at -80 °C until use in purification.

On the day of purification, cells were resuspended in lysis buffer (20 mM HEPES, pH 7.4, 150 mM NaCl) supplemented with Protease Inhibitor Cocktail III (Roche) at 80 mL/L of culture. All steps were performed at 4 °C. Cells were dounce-homogenized for thirty strokes and sonicated for 5 sessions of 10x1s pulses at 50% output. Debris and unlysed cells were pelleted by centrifugation at 1,000xG for 20 minutes. The supernatant was collected and the crude membranes were pelleted by a Beckman Optima Max ultracentrifuge at 125,000xG for 1 hour. The supernatant was removed and crude membrane fraction was resuspended in lysis buffer with Protease Inhibitor Cocktail III at 8 mL/L of starting culture. The membranes were completely resuspended by 20 strokes with a dounce homogenizer. To solubilize membrane proteins, Triton X-100 was added drop-wise to a final concentration of 1% and rotated for one hour. Insoluble material was pelleted by ultracentrifugation at 125,000xG for 1 hour. The supernatant was collected and applied to either Streptactin of Ni-NTA affinity resins (each in gravity column-mode), according to the incorporated affinity tag of the expressed protein. For Strep-II-tagged proteins, after applying the solubilized protein fraction, the resin was washed with 5 volumes of solubilization buffer (lysis buffer with 1% triton X-100). Bound protein was eluted with 5 volumes of Streptactin elution buffer (solubilization buffer with 2.5 mM desthiobiotin). For hexahistidine-tagged proteins, after applying the solubilized protein fraction to the Ni-NTA resin, the resin was washed with five volumes of wash buffer

(solubilization buffer with 20 mM imidazole). Bound protein was then eluted by five volumes of Ni-NTA elution buffer (solubilization buffer with 300 mM imidazole.

Ferric Reductase Activity Assay

Cell surface assays were performed in reaction buffer (25 mM MES, 25 mM MOPS, 140 mM NaCl, 5.4 mM KCl, 5 mM glucose, 1.8 mM $CaCl_2$, 800 µM $MgCl_2$, pH 7.0) with Fe3+-NTA and chromogenic indicator , ferrozine. Cells were incubated in the dark at 37 ºC. The absorbance of the supernatant was measured after 35 minutes to determine the amount of reduced metal. Iron(II)-ferrozine complexes were assayed at 562 nm. Standard curves for the metal-indicator complex were used to determine picomoles of reduced metal. Activities were calculated as picomoles of reduced iron per minute divided by total cellular protein per well. Total cell protein content was determined by the Bradford method (Bio-Rad) using cells lysed by thirty minute incubation in 1% Triton X-100 at 4 ºC. $Fe^{3+}$-NTA was prepared by addition of NTA to an $FeCl_3$ solution dissolved in 0.1 M HCl at a 1:1 Fe:NTA molar ratio. $Fe^{3+}$-citrate was prepared by dissolving $Fe^{3+}$-citrate in $H_2O$. To correct for endogenous ferric reductase activities, the cell surface activity of uninfected cells was subtracted in each experiment. For assaying fractions from the above purification, the assay was performed identically, except for the addition of 5 µM FAD and 200 µM NADPH.

Western Blotting

Samples were applied to 12 % acrylamide gels and processed by SDS-PAGE according to the Laemmli method at 200 V for 45 minutes. The gel was then incubated in

transfer buffer (25 mM Tris base, 192 mM glycine, 1% SDS, 20% methanol) for five minutes. Proteins were then transferred to a nitrocellulose membrane by electrophoresis at 15 V for 2 hours at 4 °C in transfer buffer. Membranes were blocked overnight with blocking buffer (5% nonfat dry milk in PBS with 0.1% Tween 20). Primary antibodies were bound to the membrane for 1 hour. Primary antibodies used were anti-Strep-II (IBA; operating dilution of 1:5000 in blocking buffer) and anti-Steap3 H-64 (Santa Cruz Biotechnology; operating dilution of 1:200 in blocking buffer). Unbound antibody was washed with three five-minutes washes with PBST. Secondary antibody was then applied to the membrane and incubated for one hour at room temperature. Secondary antibody used were anti-mouse IgG-horseradish peroxidase-conjugate (Thermo; operating dilution of 1:10,000 in blocking buffer) for anti-Strep-II-applied membranes and anti-rabbit IgG-horseradish peroxidase-conjugate (Thermo; operating dilution of 1:500 in blocking buffer) for anti-Steap3-applied membranes. Immunoreactivity was determined through a chemiluminescent product from the SuperSignal West Pico substrate kit (Thermo) according to manufacturer's protocols.

## Results

### Effect of ALA Addition to Baculovirus-Mediated Expression of Steap3 in Sf9 Cells

The functional state of purified Steap3 is of paramount importance. As a result, the heme incorporation of recombinant Steap3 must be taken into account. Previous expression studies of integral membrane hemoproteins have found issues with poor heme incorporation that could be remedied by supplementation with protoporphyrin precursors

[6, 7]. To examine the effect of the precursor δ-aminolevulinic acid (ALA), an infected culture was split in half 20 hours post-infection. To one half, the culture was supplemented with ALA to 0.3 µM and to the other half, the culture was supplemented with an equal volume of PBS. An identically-treated uninfected Sf9 culture was also utilized as negative control. A cell surface reductase assay was performed on cells 48 hours post-infection. Cells supplemented with ALA exhibited an over 5-fold increase in

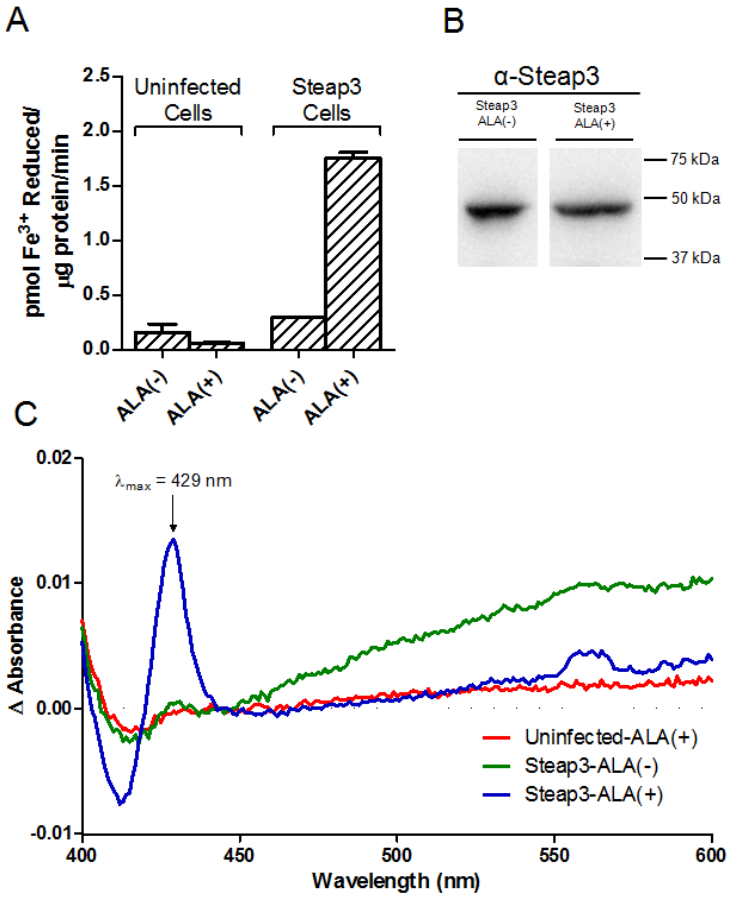


Figure 4.1. Effect of aminolevulinic acid (ALA) supplementation on Steap3 expression. (A) ALA supplementation has no significant impact on cell surface ferric reductase activity of uninfected Sf9 cells, but significantly higher activity is observed in supplemented Steap3-infected cells. (B) The expression level of Steap3 between supplemented and unsupplemented cells is not significantly altered as assessed by an α-Steap3 western blot. (C) The absorbance difference spectrum of ALA-supplemented Steap3-expressing Sf9 cell crude membranes shows spectral peaks indicating significantly elevated heme incorporation.

activity from unsupplemented cells. The uninfected cultures exhibited no significant change in activity. Additionally, when analyzing the reduced-minus-oxidized difference spectra of the crude membranes fraction, there was a significant increase in the ALA-supplemented membranes soret gamma peak (max at 429 nm) from unsupplemented cultures. Western blots of the fractions did show an increase in Steap3 expression from ALA supplementation but only to an estimated two- to three-fold increase. These findings show that ALA supplementation is an important factor in the overexpression of recombinant Steap3 in the BEVS system. All subsequent infections were paired with ALA-supplementation.

### Effect of Affinity-Tag Location on Steap3 Expression

An additional parameter to be resolved in Steap3 expression is the affinity tag location. Proteins may be sensitive to addition of residues on either terminus from an expression standpoint. To examine if such a sensitivity exists with Steap3, baculovirus containing N-terminally-tagged StrepII and C-terminally-tagged StrepII was generated and developed to high titer. Expression levels of each construct were comparable, though slightly higher in C-terminally-tagged Steap3-infected cells (Figure 4.2). There are additional low-molecular weight immunoreactive species that appear, but this is likely a result of unnatural proteolysis. In any case, C-terminally StrepII-tagged Steap3 was further used as a default expression virus.

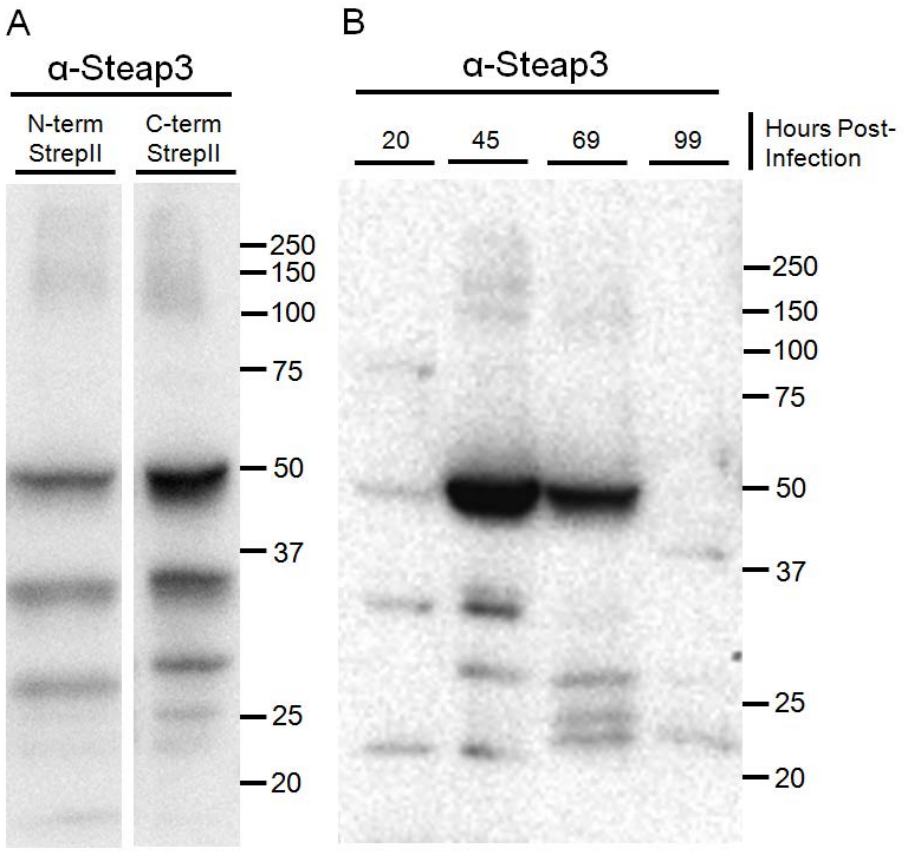


Figure 4.2. Expression analysis of Steap3 in the BEVS system. (A) Western blot of RIPA lysates of Sf9 cells infected with either an N-terminal StrepII-affinity tag fusion or a C-terminal affinity tag fusion. (B) Western blot of a time-course expression analysis of C-terminally StrepII-tagged Steap3. Cells from a master expression culture were removed and RIPA lysates obtained at defined time points. Lanes for each gel were loaded with 20 µg of total protein. Each blot was probed with an anti-Steap3 primary antibody.

Time-Course Expression
Analysis of Steap-Infected Sf9 Cells

Determining the optimal harvest time post-infection is an important factor to be determined as the baculovirus infection cycle has defined points where expression is maximal before eventual lysis of the infected cells reaches near complete levels. C-terminally StrepII-tagged Steap3 baculovirus was added to cells and at times post-

infection, aliquots were removed and for subsequent analysis by western blot (Figure 4.2). Resulting RIPA lysates reveal that expression is very low at the 20-hour time-point when ALA was added to cells. Expression reached a maximal level at the 45-hour time-point, before trailing off at 69-hours and being almost non-existent at 99-hours. From this analysis, future expression cultures were harvested between 45-48 hours.

### Development of Full-Length Steap3 Ferrireductase Assay

While the cell surface ferric reductase assay has been utilized to monitor activity, an altered assay needs to be developed for the fractions during purification. Specifically, in contrast to Steap3 at the plasma membrane of intact cells, post-lysis fractions will likely require additional supplementation such as NADPH and perhaps a flavin for the cytoplasmic oxidoreductase domain as those components would be diluted away. The effect of various cofactors on ferric reductase activity was assessed (Figure 4.3 panel A). It was found that NADPH supplementation increased activity of the Steap3-infected cell cleared lysate fraction from unsupplemented. Activity was increased over three-fold further when FAD was added along with NADPH. The other physiological flavin, FMN actually showed an inhibitory effect when added with NADPH, displaying activity similar to unsupplemented lysate. The temperature-dependence of ferric reductase activity was analyzed to determine the optimal temperature for future assays (Figure 4.3 panel B). Steap3-infected cell lysates showed a clear preference for physiological temperatures, with a nearly three-fold increased activity at 37 °C over 23 °C and even larger affect over activity at 4 °C or 65 °C.

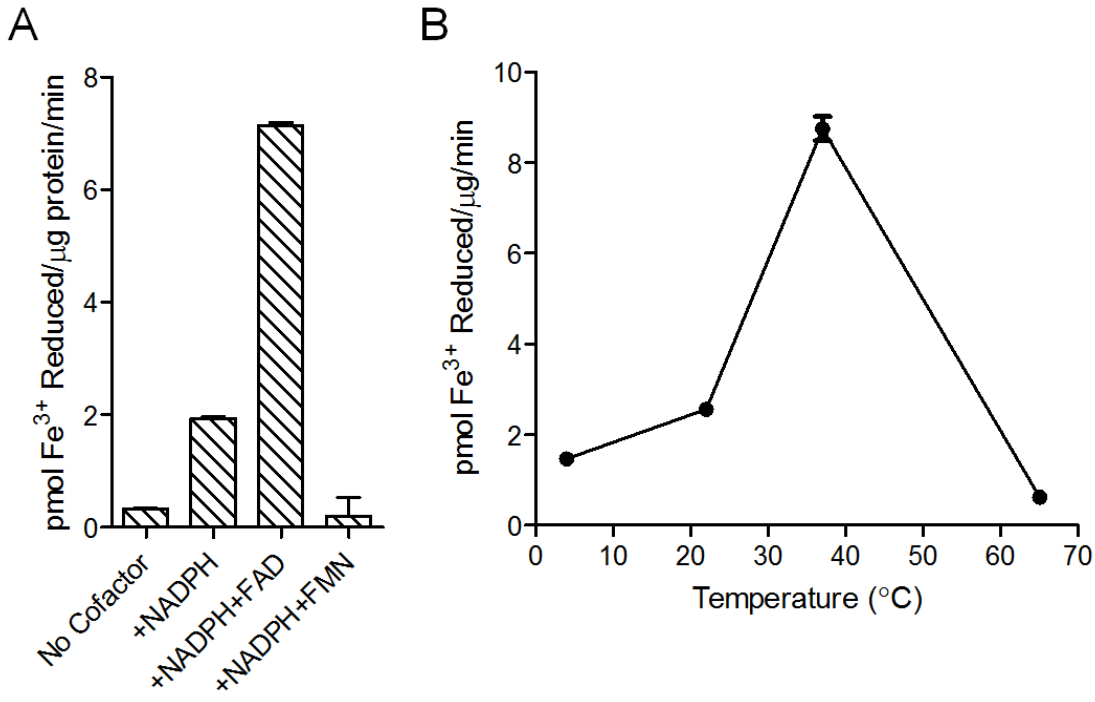


Figure 4.3. Ferric reductase activity assay development for full-length Steap3 expressed in Sf9 cells. Cleared lysate fractions from Steap3-infected Sf9 cells were assayed for ability to reduce $Fe^{3+}$ as detected by the $Fe^{2+}$-ferrozine colorimetric complex. (A) Steap3 requires both NADPH and FAD for maximal activity. (B) Steap3 exhibits maximal NADPH- and FAD-dependent activity around 37 °C. Values represent the mean ± standard deviation.

Purification of Steap3

In an effort to purify active Steap3 from insect cells, expression virus for Steap3 with a Strep-II at the C-terminus was utilized. Cellular membranes were isolated and solubilized with Triton X-100 (See chapter 2 for rationalization of Triton X-100 use). Solubilized membranes were applied to a Streptactin affinity resin and eluted with desthiobiotin. Steap3 could be observed in the elution fractions via SDS-PAGE and absorbance analysis of the heme cofactor (Figure 4.4).

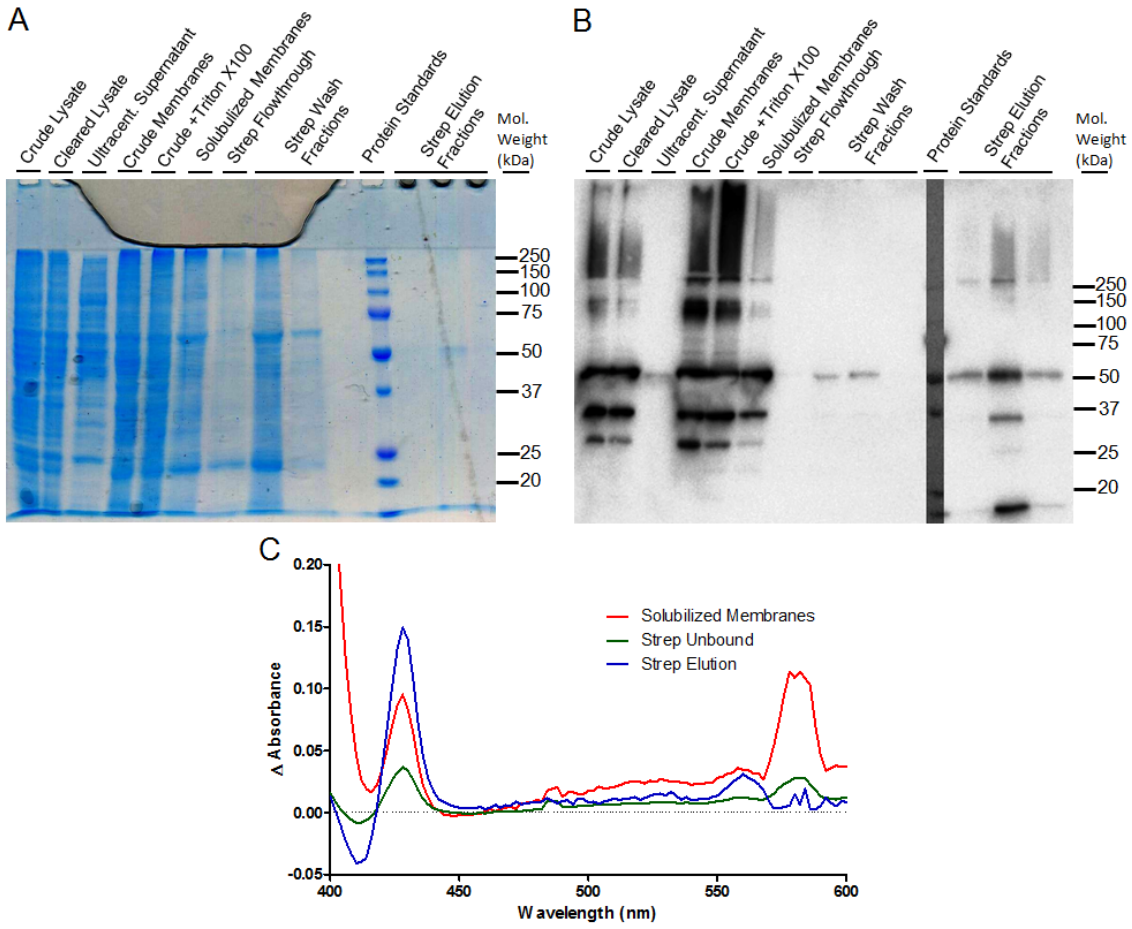


Figure 4.4. Sf9-expressed Steap3 observed in elution fractions from Streptactin affinity chromatography. Triton X-100-solubilized membranes were added to a volume of Streptactin resin, washed, and eluted according to manufacturer's instructions. (A)Coomassie-stained SDS-PAGE gel of Streptactin resin affinity purification of StrepII-tag-fused Steap3 from Sf9 cells. (B) Western blot of purification fractions probing with α-StrepII primary antibody. For both gels, protein standard molecular weights are shown on the right edge of the image. (C) Difference spectra from dithionite-reduced-minus-air-oxidized absorbance spectra of Strep-tactin purification fractions. Samples were normalized to 1 mg/ml total protein concentration.

Ferric reductase activity, however, was almost completely absent in the elution fractions. After applying solubilized membranes to the affinity resin, most activity was lost with only around a third of activity appearing the resin flowthrough or washes.

Furthermore, a recombination of eluent with unbound material was not able to reconstitute activity. The loss of activity in eluted protein was a repeated effect regardless of tag location or identity, with N-terminally-StrepII-tagged Steap3 and C-terminally hexahistidine-tagged Steap3 also being tested.

Table 4.1. Purification table for a representative Streptactin purification of baculovirus-mediated Steap3 expression in Sf9 cells.

| Fraction | Specific Activity (pmol $Fe^{3+}$ Reduced/min-μg) | Total Activity (pmol $Fe^{3+}$ Reduced/min) | Percent Recovery (%) |
|---|---|---|---|
| Cleared Lysate | 7.3 | 388,360 | |
| Crude Membranes | 5.9 | 109,740 | 28.3 |
| Crude Membranes + TX100 | 9 | 198,900 | 51.2 |
| Solubilized Membranes | 6 | 48,000 | 12.4 |
| Insoluble Membranes | 5.2 | 101,400 | 26.1 |
| Streptactin Flowthrough | 3.1 | 12,648 | 3.3 |
| Streptactin Wash | 2.1 | 4,373 | 1.1 |
| Streptactin Elution | 1.8 | 694 | 0.2 |

Liposome Incorporation of Purified Steap3

Purified Steap3 did not exhibit significant levels of ferric reductase activity. One possible cause of the loss of activity is the displacement of structurally essential membrane phospholipids with detergent molecules. To test this hypothesis, a Steap3 liposome incorporation via dialysis was performed. For this purpose, a different detergent must be selected. Triton X-100, the detergent used for normally used solubilization has a very low critical micelle concentration (CMC) of 0.0155% (w/v) which indicates a stable micelle. Detergent molecules in such a micelle will not be displaced by lipid molecules in a dialysis experiment. Instead, Steap3-containing membranes were solubilized with

CHAPS (CMC of ~0.6 %), a dialyzable detergent. CHAPS-solubilized Steap3 was purified via Ni-NTA chromatography and dialyzed in a solution containing soybean phosphatidylcholine. The resulting dialysate showed an improved specific heme spectra from the eluent (Figure 3), indicating a small loss of non-heme containing protein. The ferric reductase activity of the dialysate was not elevated, however. As a result, incorporation of Steap3 into phosphatidylcholine liposomes will not "re-activate" the enzyme.

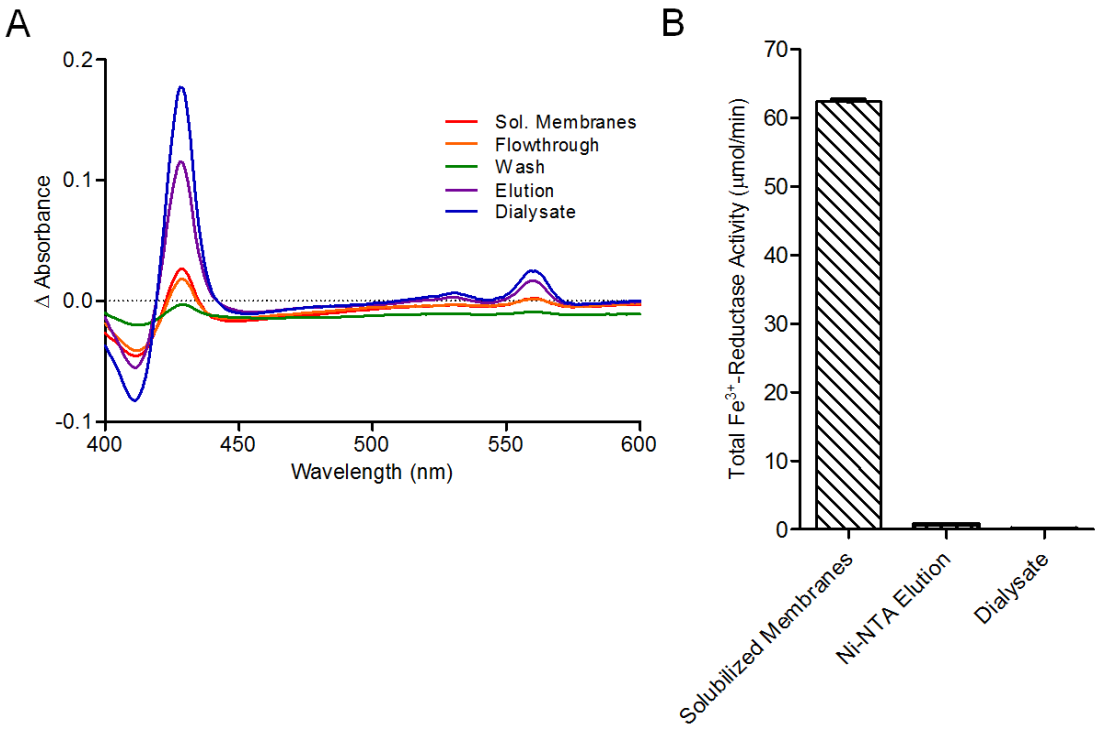


Figure 4.5. Liposome incorporation via dialysis does not activate purified Steap3. His-tagged Steap3 purified via Ni-NTA chromatography was incorporated into L-α-phosphatidylcholine liposomes. The spectral signature of the dialysate has higher specific Soret absorbance than the Ni-NTA elution fraction (A). Fractions were all analyzed at 1 mg/mL concentration. The ferrireductase activity of the dialysate is not improved from the elution fraction, however (B).

## Discussion

While Steap3 plays a central role in a crucial cellular process, the acquisition of iron, there remains many unanswered questions to its biology. Purifying Steap3 would allow for a wide array of fundamental biochemical analyses. Additionally, since they exhibit significant similarity at the amino acid sequence level (>60%) [2], these analyses would have the added benefit of providing insight into the entire Steap family. To date, no study has attempted a purification of any Steap family member. Purification of an integral membrane protein such as Steap3, however, is a challenging process that can require much optimization. The efforts described here represent the first attempt at purifying Steap3 as well as the establishment of the development of a ferric reductase assay for the full-length protein.

While previous and future work (chapter two and five) analyzed the ability of utilizing mammalian HEK-293 cells for Steap3 expression, here the Sf9 baculovirus-mediated expression system was selected for optimizing due to its ease of use and its higher eukaryote processing capabilities that are key for mammalian integral membrane proteins. A first step towards the goal of purifying active Steap3 was to establish expression conditions.

### Expression of Functional Holo-Steap3 Requires ALA Supplementation

Though the BEVS system has many advantages, for hemoproteins, it is not able to keep heme production in line with recombinant protein expression [6]. Delta-aminolevulinic acid supplementation is an established strategy to increase heme

biosynthesis, as ALA is a heme precursor. When Steap3-virus-infected Sf9 cells were treated with ALA or PBS, cell surface ferric reductase activity was over 5-fold higher in ALA-treated Sf9 cells (Figure 4.1). Uninfected cells displayed no significant change in activity upon supplementation, thus the effect was Steap3-specific. The increase in activity could not be attributed to increased expression, thus is due to increased heme-incorporated Steap3. Correspondingly, crude membrane absorbance difference spectra displayed almost no heme spectral signatures in unsupplemented, Steap3-infected cells, producing a spectrum nearly identical to uninfected cells. When supplemented with ALA, a spectral signature indicative of a heme b is observed in crude membranes of Steap3-infected cells. Notably, to my knowledge, this represents the first observance of a Steap family member heme spectra. Together, it can be concluded that ALA supplementation not only improves heme incorporation, but is strictly necessary for the recombinant expression of functional Steap3 in Sf9 cells.

### Steap3 Expression is Unaltered by Affinity Tag Fusion at Either Terminus

Another expression parameter analyzed was affinity tag location. The termini of Steap3 are all predicted to be disordered and relatively long. The first 28 residues do not appear in the Steap3 oxidoreductase domain crystal structure due to high flexibility. After the final transmembrane helix, the final ~40 residues in Steap3 compose the C-terminal tail. There is not a clear functional role for either termini, but as proteins can display an intolerance for fusions, the effect of an affinity tag at each terminus was investigated. The Strep-II affinity was fused to either N- or C-terminus of Steap3 and mature expression

virus was obtained. Western blots of RIPA lysates indicated no significant difference in expression levels between fused termini, though C-terminally-tagged Steap3 appeared to be slightly higher (Figure 4.3, Panel A). Regardless, Steap3 expression in Sf9 cells tolerates fusions at either terminus.

### Steap3 Expression in Sf9 Cells is Optimal at 45 Hours Post-Infection

Due to the viral life cycle and variances in protein maturation time, the optimal time to harvest cells is an important parameter to determine. The proper harvest time was determined through a time-course expression experiment (Figure 4.3, Panel B). The 45 hour time-point was found to have the highest specific Steap3 expression as determined by western blot. Expression was also high at 69 hours, but by 99 hours expression was almost non-existent. This declining expression is likely due to an increasing degree of host-cell lysis by baculovirus, which results in a high concentration of proteases in the culture medium. Subsequent expression studies were performed with a 45-48 hour harvest-point.

### Ferric Reductase Activity of Steap3 Expressed in Sf9 Cells is NADPH-, FAD-, and Temperature-Dependent

As the purification of functional Steap3 was desired, a functional assay for Steap3 in lysed cells was needed. In contrast to the cell-surface ferric reductase assay, in lysed cells and further purified fractions have the cytoplasmic oxidoreductase domain of Steap3 “exposed” to the assay components. Thus, any necessary cofactors that are endogenous in the cytoplasm must be identified and provided in the assay. As the crystal structure of the

Steap3 oxidoreductase domain identified an NADPH binding site and a putative flavin binding site, it was expected that the each cofactor would be necessary for ferric reductase function. NADPH is indeed strictly required for Steap3 ferric reductase activity and, interestingly, there was a clear preference for the flavin FAD over the other common physiological flavin FMN (Figure 4.3, panel A). The activity is increased over three-fold when FAD is added along with NADPH. This suggests that a small fraction is bound to endogenous and that Steap3 will not completely co-purify with a flavin. This represents the first biochemical evidence that Steap3 is an FAD-dependent ferric reductase.

Another important property to consider is the temperature-dependence of the enzyme. As the Steap3 expressed in Sf9 cells is a human gene, an optimal temperature is predicted to be at or near the body temperature for humans. Indeed, Steap3 is a highly temperature-dependent enzyme with a maximal activity at 37 °C (Figure 4.3, panel B). For future enzymatic assays of Steap3, this temperature will be considered an essential parameter.

### Steap3 is Unable to be Purified from Sf9 Cells in its Enzymatically-Active Form

Steap3 was purified from Sf9 membranes utilizing a process including detergent solubilization from membranes and subsequent affinity chromatography purification. Steap3 could be identified in Strep-tactin eluents via both western blotting and absorbance spectrophotometry of the heme cofactor. Though not in substantial amounts (<0.1 mg from 100 mg of crude lysate), the eluent is relatively pure as assessed by coomassie stain (Figure 4.4, panel A).The eluent, however, lacked any considerable ferric

reductase activity (Table 4.1). The flowthrough from the Strep-tactin column contained a portion of the initial activity (~1/3), but the activity of the solubilized membranes fraction is largely lost after application to the resin. Efforts to reconstitute the activity have to date been unsuccessful. This loss of activity suggests that a critical component of ferric reductase activity is lost during affinity chromatography and is not able be successfully re-integrated upon recombination of flowthrough and eluent. Because Steap3 is being expressed in a recombinant manner in cells that do not contain the Steap family, it is unlikely that the lost component is another protein from a complex such as that found in NADPH oxidase. As protein-lipid interactions can be central to function of membrane proteins, it is possible that delipidation during solubilization and purification inactivates the protein.

### Reconstitution of Steap3 into Phosphatidylcholine Liposomes is not Sufficient to Rescue Enzymatic Functionality

To examine the possibility of lipid requirements in Steap3 functionality, a liposome reconstitution experiment was performed. After purification of Steap3 following my established detergent solubilization procedures, Steap3 was integrated into phosphatidylcholine liposomes via dialysis. This dialysate, while still heme-bound, exhibited barely-detectable NADPH- and FAD-dependent ferric reductase activity (Figure 4.5). Future work should examine additional classes of lipids and lipid combinations.

References

1. Ohgami, R.S., et al., *Identification of a ferrireductase required for efficient transferrin-dependent iron uptake in erythroid cells.* Nat. Genet., 2005. **37**(11): p. 1264-9.

2. Ohgami, R.S., et al., *The Steap proteins are metalloreductases.* Blood, 2006. **108**(4): p. 1388-94.

3. Gauss, G.H., et al., *The Crystal Structure of Six-transmembrane Epithelial Antigen of the Prostate 4 (Steap4), a Ferri/Cuprireductase, Suggests a Novel Interdomain Flavin-binding Site.* Journal of Biological Chemistry, 2013. **288**(28): p. 20668-20682.

4. Carpenter, E.P., et al., *Overcoming the challenges of membrane protein crystallography.* Curr Opin Struct Biol, 2008. **18**(5): p. 581-6.

5. Smith, G.E., M.D. Summers, and M.J. Fraser, *Production of human beta interferon in insect cells infected with a baculovirus expression vector.* Mol Cell Biol, 1983. **3**(12): p. 2156-65.

6. Oakhill, J.S., et al., *Functional characterization of human duodenal cytochrome b (Cybrd1): Redox properties in relation to iron and ascorbate metabolism.* Biochim Biophys Acta, 2008. **1777**(3): p. 260-8.

7. Lu, H., et al., *Effects of heme precursors on CYP1A2 and POR expression in the baculovirus/Spodoptera frugiperda system.* J Biomed Res, 2010. **24**(3): p. 242-9.

# CHAPTER FIVE

## CHARACTERIZATION OF A SINGLE B-TYPE HEME, FAD AND METAL BINDING SITES IN THE TRANSMEMBRANE DOMAIN OF SIX TRANS-MEMBRANE EPITHELIAL ANTIGEN OF THE PROSTATE (STEAP) FAMILY PROTEINS

### Contribution of Authors and Co-Authors

Manuscript in Chapter 5

Author: Mark D. Kleven

Contributions: Performed cloning and mutagenesis of Steap3 expression constructs. Developed purification protocol for the purification of Steap3. Developed solubilized ferric reductase activity assay. Performed partial purification of Steap3 constructs for activity analysis. Performed kinetic analysis of Steap3 constructs. Performed confocal microscopy for BiFC assay. Performed amino acid sequence analysis of Steap family members. Generated figures and co-wrote the manuscript in preparation for submission.

Co-author: Mark D. Fleming

Contributions: Provided human Steap3 cDNA clone. Assisted in editing of manuscript.

Co-author: C. Martin Lawrence

Contributions: Researched literature and contributed to method development and interpretation of data. Co-wrote manuscript in preparation for submission.

Manuscript Information Page

Mark D. Kleven, Mark D. Fleming, C. Martin Lawrence
Journal of Biological Chemistry
Status of Manuscript:
_X__ Prepared for submission to a peer-reviewed journal
____ Officially submitted to a peer-review journal
____ Accepted by a peer-reviewed journal
____ Published in a peer-reviewed journal

Published by the American Society of Biochemistry and Molecular Biology

# CHARACTERIZATION OF A SINGLE B-TYPE HEME, FAD AND METAL BINDING SITES IN THE TRANSMEMBRANE DOMAIN OF SIX TRANS-MEMBRANE EPITHELIAL ANTIGEN OF THE PROSTATE (STEAP) FAMILY PROTEINS

Mark D. Kleven[1], Mark D. Fleming[2] and C. Martin Lawrence[1]

[1]Department of Chemistry and Biochemistry, Montana State University Bozeman, MT 59717, USA and [2] Department of Pathology, Children's Hospital and Harvard Medical School, 300 Longwood Avenue, Boston, MA 02115, USA

## Abstract

Six Transmembrane Epithelial Antigen of the Prostate 3, or Steap3, is the major ferric reductase in developing erythrocytes. Steap family proteins are defined by a shared transmembrane domain that in Steap3 has been shown to function as a transmembrane electron shuttle, moving cytoplasmic electrons derived from NADPH across the lipid bilayer to the extracellular face where they are used to reduce $Fe^{3+}$ to $Fe^{2+}$, and potentially $Cu^{2+}$ to $Cu^{1+}$. While the cytoplasmic N-terminal oxidoreductase domain of Steap3 and Steap4 are relatively well characterized, little work has been done to characterize the transmembrane domain of any member of the Steap family. Here we identify and characterize high affinity FAD, iron and single, b-type heme binding sites within the Steap3 transmembrane domain. Further, we show that Steap3 is functional as a homodimer and that it utilizes an intra-subunit electron transfer pathway through a single heme moiety, rather than an intersubunit electron pathway through a potential domain swapped dimer. Importantly, the sequence motifs in the transmembrane domain that are associated with the FAD and metal binding sites are not only present in Steap2

and Steap4, but are also present in Steap1, which lacks the N-terminal oxidoreductase domain. This strongly suggests that Steap1 harbors latent oxidoreductase activity.

## Introduction

The daily production of 200 billion erythrocytes accounts for nearly 80% of the total iron demand in humans [1]. To meet this need, developing erythrocytes utilize the transferrin cycle to import iron into the cell. In this process, iron loaded transferrin is bound at the cell surface by the transferrin receptor. This is followed by endocytosis and acidification of the endosomal compartment, which promotes release of $Fe^{3+}$. The $Fe^{3+}$ is then reduced to $Fe^{2+}$ by Six Transmembrane Epithelial Antigen of the Prostate 3 (Steap3), the major ferric reductase of the erythroid transferrin cycle [2]. Finally, $Fe^{2+}$ is transported across the endosomal membrane by Divalent Metal Transporter 1 (DMT-1), where it supports the synthesis of hemoglobin and other cellular needs, or in iron-replete cells is sequestered within the iron storage protein ferritin.

Among proteins comprising the transferrin cycle, Steap3 was the last to be identified [2, 3]. Seminal work on Steap3 by Ohgami et al. included an amino acid sequence analysis that provided initial clues to its function and mechanism [2]. Steap3 and its homologs Steap2 and Steap4 were predicted to be composed of two distinct domains; an N-terminal cytoplasmic domain and a C-terminal transmembrane domain [2, 4-6]. Surprisingly, the closest homolog for the N-terminal cytoplasmic domain is a prokaryotic enzyme known as $F_{420}$:$NADP^+$ Oxidoreductase, or FNO. FNO utilizes an elaborated Rossmann or dinucleotide binding domain to bind NADPH and the flavin-derivative $F_{420}$ [7]. In methanogens, FNO reduces $F_{420}$ to $F_{420}H_2$, which is subsequently

used to reduce $CO_2$ to methane. Because the flavin analog $F_{420}$ is not known in mammals, the homology suggested that the N-terminal domain of Steap3 would instead bind NAD(P)H and a flavin such as FAD or FMN.

The C-terminal domain was predicted to contain six transmembrane alpha helices with distant homology to the yeast ferric reductases (FRE) and to mammalian NADPH oxidase (NOX), among others [2]. Thus, collectively, the transmembrane domains of the Steap, FRE and NOX protein families place each of these within the "Ferric Reductase Domain" or FRD superfamily [8]. In this light, members of the FRE and NOX families utilize cytosolic domains or subunits to transfer electrons from NADPH to FAD. The reduced FADH2 then transfers its electrons to the transmembrane domain of these proteins, which utilizes two embedded heme cofactors to move the electrons across the membrane to the extracellular or luminal face of the protein for the reduction of iron or O2, respectively. For FRE and NOX, the two heme moieties are coordinated by four histidine residues in their transmembrane segments. Interestingly, in Steap3 and its mammalian homologs, only two of these histidine residues are conserved, thus predicting only a single transmembrane heme [2].

The crystal structures of the truncated cytoplasmic oxidoreductase domains have subsequently been determined for Steap3 and Steap4 [9, 10]. Their structures are quite similar, with a backbone root-mean-square-deviation of 1 Å [10]. Interestingly, in each case these oxidoreductase domains crystallized as two-fold symmetric dimers. Further, the N-terminal Steap3 oxidoreductase domain was found to dimerize at low millimolar concentrations in solution. Collectively, these observations suggests that full-length Steap3 may be present in cellular membranes as a homodimer.

As expected, FNO is indeed a structural homolog to the Steap oxidoreductase domain (Steap3 backbone RMSD of 1.44 Å) [9]. Further, like FNO, both Steap3 and Steap4 were co-crystallized with NADPH. Unlike FNO, however, neither could be co-crystallized with a flavin. And in contrast to FNO, the crystal structures of the isolated oxidoreductase domains of Steap3 and Steap4 show that the nicotinamide ring of NADPH lies in an open, solvent exposed pocket.

Though structural studies of the isolated Steap3 and Steap4 oxidoreductase domains failed to identify a flavin binding site, flavin-dependent NADPH oxidase activity was observed for the truncated Steap4 domain [10]. However, the truncated construct exhibited extremely high $K_m$ values (>100 μM) indicating extremely low, nonphysiological affinity for each of the flavins examined (FAD, FMN and riboflavin). These observations suggest that contrary to initial expectations, the oxidoreductase domain does not contain a high affinity flavin binding site. Further, by process of elimination, it also suggests that structural elements within the C-terminal transmembrane domain could play a major role in flavin recognition.

Thus, while biochemical and structural studies have provided valuable insights into Steap structure-function relationships in the N-terminal oxidoreductase domain, many questions remain regarding the C-terminal transmembrane domain and the full-length protein. For example, while sequence analysis identifies one pair of heme coordinating residues, does the transmembrane domain indeed contain only a single heme cofactor? Or is there a second, cryptic heme present; and if so, how is it bound and what type of heme is utilized (heme a, b or c)? Does the full length protein form a homodimer, and if so, what is the functional impact of dimerization? Does the full length protein bind

a specific flavin with high affinity? If so, does the transmembrane domain play a pivotal role in flavin recogniton, and if so, which elements in the transmembrane domain are responsible for high affinity flavin recognition? Finally, where is the iron binding site? Does the iron bind proximal to the heme, or are electrons transferred from the heme to an iron bound at a more distant binding site?

## Experimental Procedures

### Cloning and Mutagenesis of Steap3 Expression Constructs

Homo sapiens Steap3 cDNA was PCR-amplified with primers that generate a HindIII restriction site on the 5' end of the transcript and a KpnI restriction site on the 3' end (HindIII.Steap3 and Steap3.KpnI, respectively; Table 1). The gene was cloned into the pCDNA3.1 (Invitrogen) expression plasmid utilizing HindIII and KpnI restriction sites in the multiple cloning site. To generate fluorescent protein-tagged gene products the Invitrogen Gateway cloning system was utilized in the following fashion: Homo sapiens Steap3 cDNA was PCR-amplified to add complete attB sites at each termini in two subsequent reactions, the first with attB1.Steap3 and Steap3.attB2 primers and the second with Universal.attB1 and Universal.attB2 primers. The product was cloned into pDONR201 using BP Clonase II (Invitrogen). An expression clone was then generated by LR Clonase II enzyme mix (Invitrogen)-mediated recombination between the Steap3 entry clone and the destination vector pDEST.Venus, kindly provided by Dr. Mensur Dlakic (Montana State University). The resulting expression clone, Steap3.Venus, encodes a Steap3 fusion with an N-terminal FLAG-tag and C-terminal venus fluorescent

protein. Subsequent mutations were introduced into the Steap3 gene using the QuikChange Lightning site directed mutagenesis kit (Stratagene) with primers designed to manufacturer's protocols. All mutations were verified by sequencing prior to use.

For bimolecular fluorescence complementation (BiFC) studies, Steap3.VN173, which encodes a truncation of the venus fluorescent protein containing residues 1-173 at the Steap3 C-terminus, was PCR amplified with primers adding a NheI restriction site and StrepII tag on the 5' end and an EcoRI restriction sites on the 3' end of the Steap3.VN173 product (NheI.StrepII, StrepII.Steap3, and Steap3.EcoRI, respectively). Steap3.VC155, which encodes a truncation of the venus fluorescent protein containing residues 155-238 at the Steap3 C-terminus, was PCR amplified with primers adding a SalI restriction site and hexahistidine tag on the 5' end and NotI restriction site on the 3' end of the Steap3.VC155 product (SalI-His_tag, His_tag-Steap3, and Steap3-NotI, respectively). Each amplified PCR product was cloned into the pIRES bicistronic vector (Clontech) into the first (Steap3.VN173) and second (Steap3.VC155) multiple cloning sites to yield pIRES.Steap3VN.Steap3VC.

Table 1. Primers used in Steap3 cloning.

| **Cloning Primers** | |
|---|---|
| HindIII.StrepII | 5'-AAG CTT GCC GCC ATG TGG AGC CAC CCG CAG |
| Steap3.KpnI | 5'-GGT CTC GGT ACC TCA TAC GTG GCT CGT CTT |
| attB1.hSteap3 | 5′-GTA CAA AAA AGC AGG CTC CAT GCC AGA AGA |
| hSteap3.attB2 | 5′-GTA CAA GAA AGC TGG GTC CTA CGT GGC TCG |
| Universal.attB1 | 5′-GGG GAC AAG TTT GTA CAA AAA AGC AGG CTC |
| Universal.attB2 | 5′-GGG GAC CAC TTT GTA CAA GAA AGC TGG GTC |
| NheI-StrepII | 5'-GGT CTC GCT AGC ATG TGG AGC CAC CCG CAG |
| StrepII-Steap3 | 5'-ACC CGC AGT TCG AAA AAT CGG CGC CAG AAG |
| Steap3-EcoRI | 5'-GCG CAC GAA TTC CTA CTC GAT GTT GTG GCG |
| SalI-His_tag | 5'-GGT CTC GTC GAC ATG CAT CAC CAT CAC CAT |
| His_tag-Steap3 | 5'-CAT CAC CAT CAC CAT CAC ATG CCA GAA GAG |
| Steap3-NotI | 5'-GAG ACC GCG GCC GCT TAC TTG TAC AGC TCG |

Expression and Solubilization of Steap3

HEK-293F cells (Invitrogen) were maintained in Freestyle 293 Expression Medium (Invitrogen) in spinner flasks at 37 ºC and 5% CO2. For transfection, cells were resuspended in fresh media at a density of 2.5 x $10^6$ cells/ml. The expression plasmid was added to cells at a concentration of 3 µg per mL of culture volume and allowed to mix for 5 minutes. Linear polyethyleneimine (MW of 25,000; Polysciences, Inc.) was then added to the cultures at a concentration of 9 µg/mL of culture. After 8 hours, the expression cultures were supplemented with 2.2 mM valproic acid, 0.5 mM 5-aminolevulinic acid and the culture volume was doubled by addition of fresh medium. Cells were harvested 48-hours post-transfection by centrifugation (1,000 xg for 10 minutes) and resuspended in hypotonic buffer (20 mM HEPES, pH 7.5, 4 °C) at a density of 4 mL of buffer per gram of cell pellet. All subsequent steps were performed at 4 °C. Cells were lysed by dounce homogenization followed by passage through a 24-gauge needle three times and sonication for 10 seconds. The lysate was centrifuged for 20 minutes at 1,000 xg to

remove unlysed cells and debris. The supernatant was recovered, followed by isolation of membranes by ultracentrifugation (125,000 xg for 1 hour). The pelleted membranes were resuspended by Dounce homogenization in resuspension buffer (20 mM HEPES, pH 7.5, 150 mM NaCl) at a concentration of 2-3 mg/ml. Detergent activated membranes were then prepared by addition of 1% Triton X-100 followed by rotation for 1 hour.

Steap3 Ferric Reductase Assay

Triton X-100-activated membranes were assayed for ferric reductase activity using the following standard conditions. Membranes were added to reaction buffer (25 mM MES, 25 mM MOPS, 140 mM NaCl, 5.4 mM KCl, 5 mM glucose, 1.8 mM CaCl2, 800 µM MgCl2, pH 7.0, 37 °C) containing 200 µM Fe-NTA, 400 µM ferrozine and 5 µM FAD. The reaction was initiated by addition of 100 µM NADPH. Ferric ion reduction at 37 °C and formation of the $Fe^{2+}$-ferrozine complex was monitored at 562 nm using a thermostated Varian Cary 50 spectrophotometer using an extinction coefficient for the complex of 27,886 $M^{-1}cm^{-1}$ [10]. Titration data was fit to a Michaelis-Menten model with GraphPad Prism 5.0 software to determine the Michaelis constant, $K_m$, and maximum reaction velocity, $V_{max}$.

Fluorescence Microscopy

HEK-293F cells were maintained in DMEM supplemented with 10% FBS in T-75 flasks at 37 °C and 5% $CO_2$. Twenty-four hours prior to transfection, cells were plated onto glass cover slips in a 6-well dish. Transfections were performed with Lipofectamine 2000 (Invitrogen) according to the manufacturer's protocol. Twenty-four hours post-transfection, cells were washed three times with PBS and then fixed in 4% formaldehyde-

PBS for 15 minutes. After washing the cells with PBS, membranes were permeabilized by addition of PBS with 0.1% Triton X-100. Cells were then washed three times with PBS and blocked with 1% BSA in PBS. Samples were then washed three times with PBS and incubated with rabbit anti-transferrin receptor antibody (H-300, Santa Cruz Biotechnology) for one hour at room temperature. Unbound antibody was washed away by three PBS washes before incubation with anti-rabbit IgG-Alexa Fluor 555-conjugate (Invitrogen) for one hour at room temperature. Cells were then washed three times with PBS, stained with DAPI for 5 min, and mounted on glass cover slides with Vectashield mounting medium (Vector Laboratories). Samples were visualized with a Nikon Eclipse E800 fluorescence microscope. Fluorophores were visualized at the following excitation and emission wavelengths: venus fluorescent protein (excitation: 480 nm/emission: 525nm - 560nm); DAPI (excitation: 405 nm/emission: 450 nm – 470 nm); Alexa Fluor-555 (excitation: 540 nm/emission: 605 nm - 660 nm). Images were processed with Metamorph and ImageJ software.

Heme Absorbance Analysis

Triton X-100 activated membranes were analyzed for heme content by absorbance spectroscopy on a Varian Cary 50 spectrophotometer. To obtain oxidized spectra, air-oxidized membranes (1 mg/ml) had their absorbance spectra recorded from 300-700 nm. To obtain reduced spectra, a few grains of sodium dithionite were added to the same sample used for the air-oxidized spectrum, followed by an immediate spectral analysis from 300-700 nm. Finally, difference spectra were obtained by subtracting the oxidized from the reduced spectra.

# Results

## Ferric Reductase Activity of Steap3

Expression of exogenous human Steap3 was performed in the Freestyle 293F system, an HEK-293-derived cell line that is easily-transfectable and can grow to high-densities in suspension cultures. To characterize the enzymatic activity of full-length Steap3, we first developed a ferric reductase activity assay for the intact protein in isolated membranes. Previous enzymatic assays monitored either cell surface ferric reductase activity [2, 3] or flavin dependent NADPH oxidase activity in a truncated protein [10]. This assay follows the formation of the $Fe^{2+}$-ferrozine complex ($\lambda_{max}$=562 nm) and allows the determination of kinetic constants for the full length protein upon the addition of cytoplasmic (NADPH, FAD) and extracellular substrates ($Fe^{3+}$).

We then attempted to purify Steap3 to homogeneity. To this end, we screened a variety of commonly used detergents, from which Triton X-100 was selected for its ability to solubilize Steap3 ferric reductase activity. However, while Steap3 in detergent activated membranes retained activity for an extended period of time (days), all attempts to affinity purify Steap3 activity from the detergent activated membranes, including the use of anti-FLAG, strep-tactin, and Ni-NTA resins, each resulted in near total loss of enzyme activity. It is not clear whether some critical lipid or cofactor is lost during the on-column immobilization, or if the solubilized protein is simply unstable, but add-back experiments, reconstitution of eluted Steap3 into lipid vesicles, and the use of alternative detergents each failed to preserve or restore activity.

Table 2. Fractionation of ferric reductase activity in Steap3-VFP transfected cells.

| Fraction | Specific Activity (pmol $Fe^{3+}$ reduced/ min/fl.unit) | Total Fluorescence | Total Activity (pmol $Fe^{3+}$ reduced/min) |
|---|---|---|---|
| Lysate | 2.8 | 2,463 | 6,896 |
| Ultracentrifugation Supernatant | 0 | 395 | 0 |
| Crude Membranes | 2.3 | 2,080 | 4,784 |
| Crude Membranes + TX-100 | 4.6 | 2,059 | 9,472 |
| Insoluble Membranes | 1.4 | 1,507 | 2,110 |
| Solubilized Membranes | 1.8 | 664 | 2,435 |

However, during the course of this work, it became clear that His6, FLAG and Strep-II fusions at the C-terminus of Steap3 did not adversely impact enzymatic activity in detergent activated membranes. This suggested we could potentially quantitate the amount of Steap3 present in the detergent activated membranes by fusing venus fluorescent protein to the C-terminus of Steap3 (Steap3-VFP). Indeed, the fusion did not impact activity (Fig. 1A) and thus allowed the measurement of specific activity based upon the fluorescent content of the sample (Table 2). For these reasons, the Triton X-100-activated fraction ("Crude Membranes+TX-100") of the Steap3-VFP fusion expressed in the presence of δ-aminolevulinic acid (see below) was used for subsequent enzymatic analysis because it contained the highest level of Steap3 specific activity (Table 2). Further, we found that Steap3 expression was enhanced when valproic acid (VPA) was added to the transfection medium. VPA is a histone deacetylase inhibitor that has previously been shown to enhance transient gene expression in HEK-293 cells [11]. The

presence of VPA in the 293F transfection medium resulted in a ~1.6-fold increase in expression of Steap3-VFP over an unsupplemented expression.

FAD is the Preferred Flavin for Steap3

As described above, Steap3 detergent activated membranes exhibit NADPH and FAD dependent ferric reductase activity. Importantly, however, the addition of other exogenous flavins, specifically FMN and riboflavin, does not contribute to increased ferric reductase activity above that seen for detergent activated membranes in the absence of exogenous flavin (Fig.1C). This strongly suggests that full-length Steap3 does not utilize FMN or riboflavin as a substrate, and that FAD is the physiologically relevant flavin.

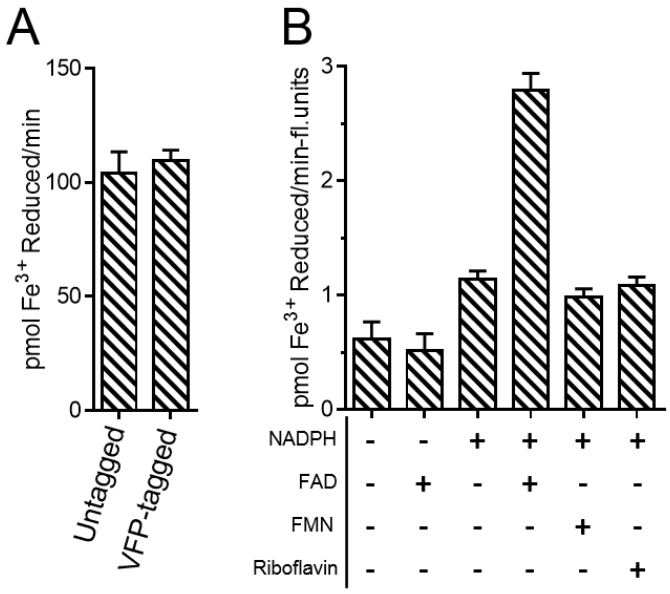


Figure 1. Triton X-100-activated Steap3 is an NADPH- and FAD-dependent ferric reductase. (A) Steap3-containing Triton X-100-activated membranes that exhibit maximal ferric reductase activity in the presence of both NADPH and FAD. The increase in activity observed when NADPH is added alone indicates that some endogenous FAD is present in the membranes. (B) Steap3 is not able to utilize flavins FMN or riboflavin for ferric reductase activity, but is specific to FAD. This is in contrast to the NADPH oxidase activity exhibited by the isolated Steap4 oxidoreductase domain, which was not specific for either of the three flavins [3]. Thus, a full-length Steap protein is able to differentiate flavins to specifically bind FAD. (C) Venus fluorescent protein fusion to Steap3's C-terminus does not alter ferric reductase activity, thus could be utilized for subsequent activity studies. Activities represented are empty vector-subtracted.

Steap3 is a b-Type Cytochrome

δ-aminolevulinic acid (ALA) is a protoporphyrin precursor that is generated in vivo by δ-aminolevulinic acid synthase, the rate-limiting reaction in heme biosynthesis. ALA supplementation has thus been utilized in a variety of expression systems to improve heme incorporation in exogenously-expressed hemoproteins [12, 13]. We found that supplementation with 0.5 μM ALA resulted in greater than 2-fold increase in the difference spectrum Soret band at 429-nm in Steap3-containing membranes and also an

~80% increase in membrane ferric reductase activity. Further, the reduced-minus-oxidized difference spectra obtained for Triton X-100-treated membranes of wild-type Steap3-expressing cells indicates alpha, beta, and gamma Soret peaks at 560 nm, 531 nm, and 428 nm, respectively (Fig. 2A), indicative of the binding of a b-type heme cofactor.

Steap3 Contains a Single B-Type Heme Cofactor

Sequence homology predicted that Steap3 utilizes bis-histidine coordination via His316 and His409 to bind a heme cofactor in the transmembrane domain [2]. However, other model systems for transmembrane ferric reduction, including yeast Fre1, mammalian DcytB and mammalian NADPH oxidase (NOX) all utilize two heme groups to move electrons across the membrane. Thus, it has not been clear whether a second, cryptic, heme binding site is present in Steap family proteins, or if Steap family metalloreductases differ significantly from these other systems in utilizing a single heme cofactor. For this reason, we utilized site directed mutagenesis to reexamine heme incorporation in the His316Ala and His409Ala variant proteins. As expected, and consistent with previous work by Ohgami, et al [2], mutating either conserved histidine to alanine resulted in complete loss of ferric reductase activity (Fig. 2C). More interesting, however, the Steap3-specific heme signal is completely eliminated in each of these histidine variants (Fig. 2B). This strongly suggests that Steap family metalloreductases utilize only a single heme cofactor to shuttle electrons across the transmembrane domain, and that mechanistically, they are fundamentally different from yeast Fre1, and mammalian proteins Dcytb and NOX.

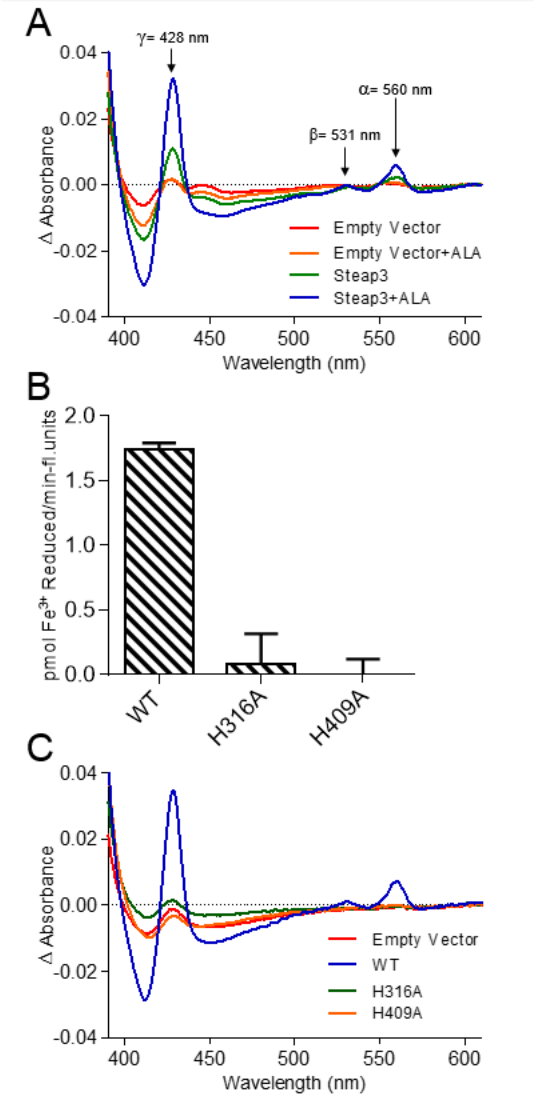


Figure 2. Steap3 transmembrane domain binds a single b-type heme with coordination through His-316 and His-409. (A) The reduced-minus-oxidized difference spectra for Triton X-100-activated membranes of HEK 293 cells transfected with either empty vector or Steap3.Venus. The transfection medium was either unsupplemented or supplemented with 0.5 µM δ-aminolevulinic acid (ALA). Supplementation with ALA results in a significant increase in heme incorporation. Additionally, the resulting alpha, beta and gamma Soret peaks, are indicative of a b-type heme. (B) The strictly-conserved histidine residues, H316 and H409, are also each strictly required for ferric reductase activity, as mutation of either to alanine results in an inactive construct. (C) The reduced-minus-oxidized difference spectra of each histidine mutant reveals a complete deficiency in Steap3-specific heme binding, with only endogenous heme signal present. This strongly suggests that Steap3 binds only a single heme cofactor in the transmembrane domain.

Steap3 Forms an Active Homodimer

The isolated Steap3 N-terminal oxidoreductase domain has been reported to dimerize at low millimolar concentrations in solution and in the crystal, suggesting that full length Steap3 may function as a homodimer in cellular membranes [9]. However, a co-precipitation experiment utilizing FLAG-tagged Steap3 as bait and StrepII-tagged Steap3 as prey with Strep-tactin affinity resin did not produce evidence of an interaction (data not shown). Thus, dimerization may be transient or incompatible with co-precipitation conditions.

To characterize a potential homodimer in vivo, a bimolecular fluorescence complementation assay (BiFC) was performed, which is able to "capture" transiently-interacting protein partners [14]. In the BiFC assay, proteins of interest are tagged with two complimentary fragments of split green fluorescent protein (GFP). If the proteins oligomerize, the complementary GFP fragments are brought together. This facilitates folding and "maturation" of active GFP, resulting in a fluorescent readout. For the Steap3 BiFC assay, HEK 293 cells were co-transfected with Steap3 fused to N- terminal (Steap3.VN173) and C-terminal (Steap3.VC155) fragments of venus fluorescent protein (VFP). Transfected cells visualized at VFP emission wavelengths exhibited a distribution of cellular fluorescence similar to that seen in cells transfected with Steap3 fused to full-length VFP (Fig. 3). This strongly suggests that a Steap3 oligomer does indeed form in vivo.

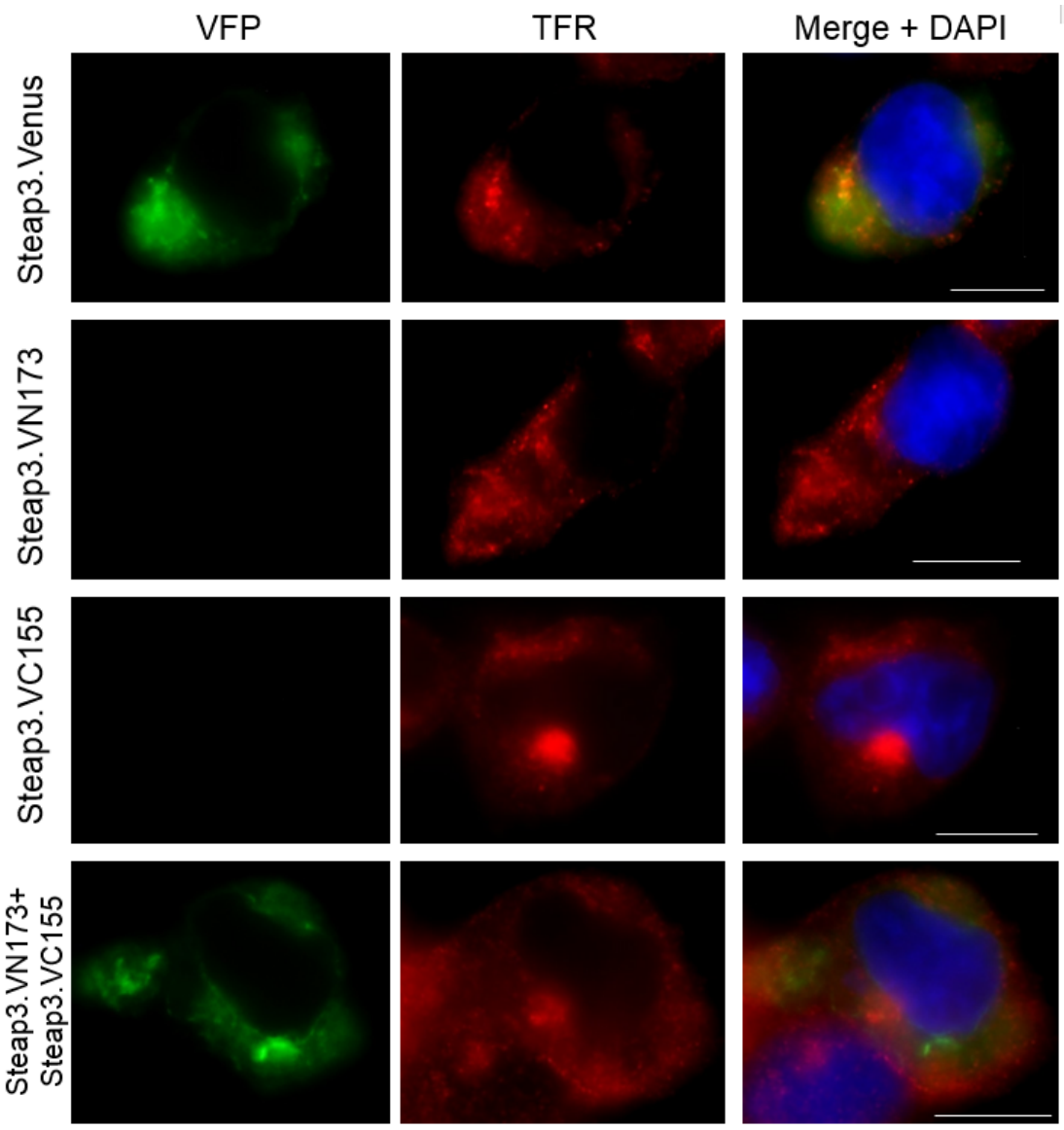


Figure 3. Steap3 is able to form homodimers in a bimolecular fluorescence complementation (BiFC) assay. HEK 293F cells were transfected with one or two of the following expression plasmids: Steap3.Venus (Steap3 C-terminally fused to venus fluorescent protein (VFP; residues 1-238)), Steap3.VN173 (C-terminal fusion of residues 1-173 of VFP), Steap3.VC155 (C-terminal fusion of residues 155-238 of VFP). Plasma membranes were stained with wheat germ agglutinin-Alexa Fluor 633 conjugate (WGA) and nuclei were stained with DAPI. Cellular distribution in the Steap3 BiFC pair (Steap3.VN173+Steap3.VC155) resembled that observed in the non-BiFC construct, Steap3.Venus. The distribution in intracellular membranes is consistent with previous microscopy studies of Steap3 [1, 2]. This indicates that Steap3 is able to form homodimers *in vitro*. White bars indicate 10 µm.

We also wished to analyze the ferric reductase activity of the BiFC dimer, thus the Steap3.VN173 and Steap3.VC155 fusions were cloned into the pIRES dual expression vector (pIRES.Steap3VN.Steap3VC). This ensured the presence of both constructs in each transfected cell. Using this dual expression vector, we found that the specific activity of pIRES.Steap3VN.Steap3VC-transfected cells was 9.9 pmol $Fe^{3+}$ reduced/ min/fluorescent unit, which is actually greater than the specific activity of cells transfected with Steap3.Venus. The increased specific activity was due primarily to decreased fluorescence, which is expected due to the presence of, at most, a single mature VFP per Steap3 dimer. Interestingly, it is believed that once the split GFP has matured, the split protein is stable and the N- and C-terminal fragments do not dissociate, leading to a constitutive oligomer [14]. Thus, not only is Steap3 able to form homodimers in the relevant cellular compartments, it is also enzymatically active in the dimeric state.

## Steap3 Electron Transfer Follows an Intra-Subunit Pathway

Steap3 is composed of two linked domains, the transmembrane and cytoplasmic oxidoreductase domains. Upon dimerization, protomers may thus be capable of performing inter-subunit electron transfer wherein the oxidoreductase domain of one protomer transfers electrons to the transmembrane domain of the other (Fig. 4A). To examine the possibility of such “domain swapping”, cells were again transfected with the BiFC dual expression vector containing two Steap3 genes (pIRES.Steap3VN.Steap3VC). In this case, the two Steap3 constructs were either both wild-type or contained two different Steap3 variants that inactivated either the N- or C-terminal domain, respectively

(Fig. 4B). Specifically, one variant contained an inactivated oxidoreductase domain (S58I; defective NADPH binding [2]) and the other an inactivated transmembrane

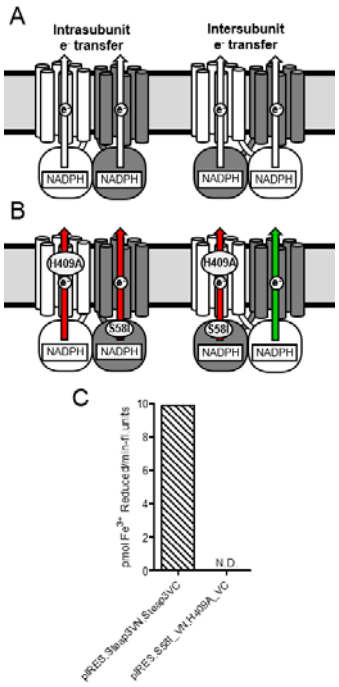


Figure 4. Investigating Steap3 electron transfer pathway. (A) A Steap3 dimer could potentially transfer electrons in an intra- or inter-subunit manner. In intrasubunit electron transfer (left side of Panel A), electrons from the NADPH-binding oxidoreductase domain would be transferred to the subunits own transmembrane domain. In intersubunit electron transfer (right side of Panel A), a domain-swapped dimer would result in the electrons from on oxidoreductase domain transferred to the transmembrane domain of the other subunit. (B) To differentiate between these two alternatives, mutations were introduced to inactivate the cytoplasmic NADPH oxidase domain of one subunit (S58I.VN173) and the transmembrane domain of the other subunit (H409A.VC155). Cells were transfected with a dual expression vector containing the S58I.VN173 and H409A.VC155 constructs (pIRES.S58I_VN. H409A.VC). If the Steap3 dimer undergoes intrasubunit electron transfer, the mutational lesions in the respective subunits would prohibit electron transfer in both subunits (red arrow). In inter-subunit electron transfer, the BiFC heterodimers would complement one another, restoring one of the two electron transfer pathways (green arrow). Thus, the presence of an inter-subunit electron transfer pathway would be indicated by the partial restoration of ferric reductase activity. (C) In contrast to cells expressing the wild-type BiFC pair (pIRES.Steap3VN.Steap3VC), ferric reductase activity of was not detectable (N.D.) in cells expressing the mutant BiFC pair (pIRES.S58I_VN.H409A_VC).

domain (H409A; heme-deficient variant). The ferric-reductase activity in cells expressing the wild-type pair and the mutant pair were then tested. In the case of intra-subunit electron transfer, lesions in the electron transfer pathway in each subunit of the heterodimer should result in the ablation of all activity (Fig. 4B, left). In contrast, for inter-subunit electron transfer, one path is expected to suffer from lesions in both the oxidoreductase and transmembrane domains, while the second pathway would be expected to utilize the "healthy" oxidoreductase domain from one subunit and the "healthy" transmembrane domain of the second, resulting in measurable activity (Fig. 4B, right). However, while activity was observed for the wild type Steap3 pair, the variant pair did not exhibit ferric reductase activity above that of the empty vector controls (Fig. 4C). This suggests that Steap3 does not form a domain swapped dimer, and that Steap3 utilizes an intra-subunit rather than inter-subunit electron transfer pathway.

FAD Binding Site

To our knowledge, the identification and characterization of a flavin-binding site for any full-length Steap family member has not been reported, and the development of the enzymatic assay described above is the first indication that FAD is the preferred flavin for Steap3 (Fig. 1C). To this end, we measured $Fe^{3+}$-reductase activity as a function of FAD concentration. When fit to the Michaelis-Menten model, we find a $K_m$ of 0.9 μM for FAD, indicating the presence of a physiologically relevant FAD binding site. Relative to the isolated N-terminal oxidoreductase domain, the $K_m$ value for full-length Steap3 is lower by more than two orders of magnitude, indicating that the transmembrane domain plays a critical role in the recognition of FAD.

Multiple sequence alignments are frequently used to identify residues critical to protein function. For Steap3, specifically, the utility of this approach can be assessed by mapping strictly conserved residues to the surface of the Steap3 oxidoreductase domain, for which crystal structures have been determined [9]. Towards this goal, the NCBI non-redundant (nr) protein sequence database was utilized to obtain a total of 507 Steap2, Steap3, and Steap4 sequences (Steap1 lacks the oxidoreductase domain), which were then aligned with Clustal Omega [15]. We found that ten residues in the oxidoreductase domain are strictly conserved, 7 of which are surface-exposed. Importantly, 5 of the 7 are found in the NADPH binding pocket of the Steap3 crystal structure (Fig. 5A). We can thus conclude that sequence conservation is a valuable tool for identifying Steap3 residues involved in substrate recognition.

We thus undertook a similar analysis, but with the inclusion of Steap1 sequences, to identify the FAD binding site residues in the transmembrane domain. 652 Steap family sequences were aligned and strictly conserved amino acids were assigned approximate positions within the membrane bilayer as predicted by the membrane topology program Toppred (Fig. 5B) [16]. Of the sixteen strictly conserved residues in the transmembrane domain, nine are predicted to lie on cytoplasmic loops between transmembrane helices 2 and 3 (the α2/α3 loop), or helices 4 and 5 (the α4/α5 loop). As these residues lie in between the N-terminal oxidoreductase domain and histidine residues implicated in heme binding, we considered these as potential residues involved in recognition of FAD.

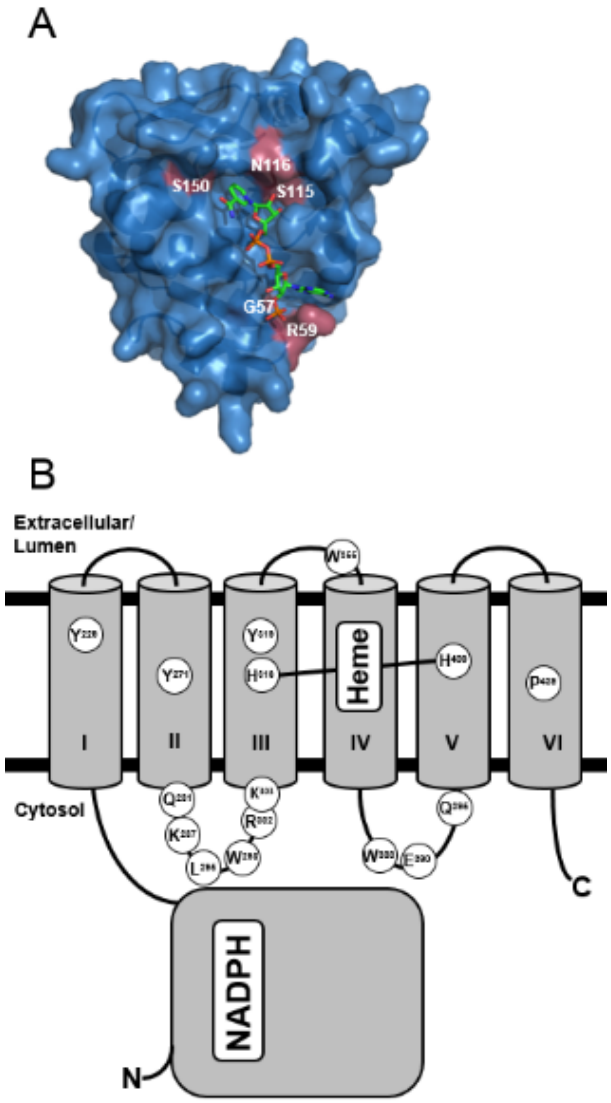


Figure 5. Amino acid conservation of Steap family oxidoreductase and transmembrane domains. Amino acid sequences from Steap family members in the NCBI non-redundant database were aligned with Clustal Omega [15]. (A) Strictly conserved residues(magenta) from all Steap2, Steap3, and Steap4 sequences are mapped on the surface of the crystal structure for the Steap3 oxidoreductase domain (PDB: 2VQ3). The NADPH binding site includes 5 of the 10 strictly conserved residues in the oxidoreductase domain. (B) A second alignment with all Steap1-4 sequences was generated to identify putative ligand binding site residues in the transmembrane domain. The alignment was transposed with the topology prediction program Toppred [16] to determine approximate locations for strictly conserved residues in the Steap3 transmembrane domain. Heme coordination by His-316 and His-409 is represented by a connecting line. Tyr319 is not strictly conserved (>98%), but was targeted for mutagenesis studies due to its proximity to His-316.

Table 3. FAD kinetic characterization of Steap3 $Fe^{3+}$-reductase activity. Values are represented as mean ± the standard deviation. Means from n ≥ 3 independent experiments. N.D. = not determinable. *P<0.05 from one-way ANOVA and Dunnett's multiple comparison test with Wild-Type as control group. The transmembrane topology prediction was generated by the Toppred program [4].

| Variant | Topology Prediction of Mutant | $V_{max}$ (pmoles $Fe^{3+}$ reduced/ min/fluorescent unit) | $K_m$ (μM FAD) | $V_{max}/K_m$ |
|---|---|---|---|---|
| Wild-Type | - | 3.7 ± 1.9 | 0.9 ± 0.4 | 4.4 ± 2.5 |
| Q281A | αII-αIII loop | N.D. | N.D. | - |
| K287A | αII-αIII loop | N.D. | N.D. | - |
| L295A | αII-αIII loop | N.D. | N.D. | - |
| W298A | αII-αIII loop | 2.8 ± 0.3 | 2.2 ± 0.4 | 1.3 ± 0.3* |
| R302A | αII-αIII loop | 1.4 ± 0.8 | 2.8 ± 1.4 | 0.6 ± 0.4* |
| R302E | αII-αIII loop | N.D. | N.D. | - |
| K303A | αII-αIII loop | 2.5 ± 1.2 | 2.8 ± 0.6 | 0.9 ± 0.4* |
| K303E | αII-αIII loop | 2.7 ± 1.7 | 4.6 ± 2.9* | 0.6 ± 0.4* |
| R302A/K303A | αII-αIII loop | 1.4 ± 0.9 | 4.0 ± 2.2* | 0.5 ± 0.5* |
| W388A | αIV-αV loop | 2.3 ± 1.5 | 3.0 ± 0.6 | 0.7 ± 0.4* |
| E390A | αIV-αV loop | 3.0 ± 1.2 | 4.5 ± 1.0* | 0.6 ± 0.1* |
| Q395A | αIV-αV loop | 4.4 ± 1.8 | 17.7 ± 4.4* | 0.3 ± 0.2* |

The nine strictly conserved residues in the α2/α3 and α4/α5 loops of the transmembrane domain were individually mutated to alanine and the kinetic parameters for FAD dependent ferric reductase activity were determined (Table 3). With an increase in the $K_m$ from the wild type value of 0.9 μM to 17.7 μM, the Glu395Ala variant showed the most significant decrease in affinity for FAD, while at the same time, the $V_{max}$ was essentially unchanged. While not as large, we also find a significant increase ($p < 0.05$) in the FAD $K_m$ value for the Glu390Ala variant ($K_m$ = 4.5 μM), which is also in the α4/α5 loop. Because the hallmark of residues involved predominately in substrate recognition

are an increase in $K_m$ with little or no change in $V_{max}$, these data strongly implicate Glu390, Gln395 and the α4/α5 loop in formation of the FAD binding site.

The exact role of residues in the α2/α3 loop was more difficult to assess. Simple alanine substitution for Gln281, Lys287 and Leu295 all resulted in complete loss of activity. We cannot say whether this was because the variants were unable to bind FAD or because these are instead key catalytic or structural residues; dead enzymes tell no tales. However, it does clearly indicate a critical role for the α2/α3 loop. Measurable activity was, however, found for the Trp298Ala, Arg302Ala and Lys303Ala variants. And in each case, we did find increased $K_m$ values for FAD. However, compared to wild type, the differences were not statistically significant ($p > 0.05$). We thus considered the possibility that Arg302 and Lys303 might utilize their positive charge to interact with hydroxyl groups or negative charge on FAD. When we substituted a negatively charged glutamate at each position, the Lys303Glu variant did indeed show a significantly increased $K_m$ (4.6 μM) with a minimally disturbed $V_{max}$. The Arg302Glu mutation however, showed a complete loss of activity, confounding interpretation of the results.

Finally, we also investigated the Arg302Ala/Lys303Ala double mutant and found a slightly increased Km relative to each individual alanine mutant indicative of an additive effect for these residues. More importantly, the double mutant also showed a statistically significant increase in $K_m$ (4.0 μM) over wild type Steap3. Collectively, our mutational analysis thus also implicates Arg302, Lys303 and the α2/α3 loop in general in FAD binding. In conjunction with previous work on the Steap4 oxidoreductase domain demonstrating the lack of a high affinity flavin binding site in the oxidoreductase domain, we conclude that major elements of the high affinity FAD binding site lie in the

transmembrane domain of Steap3, and that conserved residues within the α2/α3 and α4/α5 loops are of particular importance.

$Fe^{3+}$ Binding Site of Steap3

Ferric and cupric reductase activities have been reported for Steap2, Steap3 and Steap4 [2, 3]. More recently, $K_m$ values for both $Fe^{3+}$ and $Cu^{2+}$ have been determined for rat Steap4 using the cell surface metalloreductase assay [10]. Collectively, this work suggested that Steap proteins contain high affinity binding sites for both $Fe^{3+}$ and $Cu^{2+}$, and that Steap family members are likely to be physiologically relevant cupric and ferric reductases involved in homeostasis of these metals. However, to date, metal $K_m$ values have not been reported for Steap3. For this reason, using $Fe^{3+}$-NTA as the substrate we determined that the $K_m$ for $Fe^{3+}$ was 5.0 μM (Table 4), which is nearly identical to that found for Steap4 using the cell surface assay. Unfortunately, $Cu^{2+}$ was spontaneously reduced to $Cu^{1+}$ under these assay conditions due to the presence of NADPH, precluding measurement of a $K_m$ value for $Cu^{2+}$.

Similarly, residues involved in metal recognition have not been reported for any member of the Steap family. However, our success in identifying residues involved in FAD recognition suggested that conserved residues in the luminal or extracellular half of the transmembrane domain, i.e., residues above the heme coordinating histidines in Fig. 5B, might participate in iron recognition. Two strictly conserved residues, Tyr229 and Trp355, are predicted by Toppred to lie on the extracellular/lumenal side of the heme coordinating histidine residues (Fig. 5B). Due to its non-polar side chain, Trp355 was not chosen for mutation. In addition, a third residue, Tyr319, was also selected for mutation

due to its high-degree of conservation (>98%) and proximity to the heme cofactor. Specifically, Tyr319 is predicted to lie approximately one helical turn nearer to the lumenal face than the heme-binding His316 and could thus be well positioned to participate in iron binding and reduction. Indeed, when these tyrosine residues were individually mutated to alanine or phenylalanine, impaired iron reduction was observed. For the conservative Tyr319Phe substitution, the $K_m$ for $Fe^{3+}$ increased by more than three-fold from 5 to 17 μM, while $V_{max}$ was essentially unchanged. Similarly, the Tyr229Phe variant showed an inflated $K_m$ of 15 μM, suggesting that each of these residues play significant roles in recognition of $Fe^{3+}$. The double mutation, Tyr229Phe/Tyr319Phe was also examined, and the $K_m$ increased to 24 μM, with only an insignificantly small decrease in $V_{max}$.

Table 4. $Fe^{3+}$ kinetic characterization of Steap3 $Fe^{3+}$-reductase activity. Values are represented as mean ± the standard deviation. Means from n ≥ 3 independent experiments. N.D. = not determinable. *P<0.05 from one-way ANOVA and Dunnett's multiple comparison test with Wild-Type as control group.

| Variant | $V_{max}$ (pmoles $Fe^{3+}$ reduced/ min/fluorescent unit) | $K_m$ (μM $Fe^{3+}$) | $V_{max}/K_m$ |
|---|---|---|---|
| Wild-Type | 3.0 ± 1.6 | 5.0 ± 1.4 | 0.60 |
| Y229A | 2.7 ± 2.0 | 12.9 ± 3.9* | 0.21 |
| Y229F | 1.9 ± 1.2 | 14.8 ± 2.9* | 0.13* |
| Y271A | N.D. | N.D. | - |
| Y271F | 2.6 ± 0.4 | 5.7 ± 0.2 | 0.45 |
| Y319A | 3.5 ± 1.3 | 9.9 ± 1.6 | 0.35 |
| Y319F | 2.7 ± 0.7 | 17.6 ± 4.5* | 0.15* |
| Y229F/Y319F | 1.7 ± 0.7 | 24.2 ± 2.8* | 0.07* |

While additional residues are likely to participate in iron binding and reduction, the characterization of these conserved tyrosine residues provides significant insight into the nature of the iron binding site. First, the location of Tyr319 approximately one helical turn past heme coordinating His316 suggests the iron biding site lies near the "top" edge of the heme cofactor in the transmembrane domain. Second, that the topological arrangement of the transmembrane helices will bring Tyr229 and Tyr319 in close proximity to each other, allowing them to work in concert to form a recessed iron binding site adjacent to the heme.

## Discussion

### Steap1 Shares the Steap Family FAD and Iron Binding Motifs

Steap1 is highly expressed in multiple cancers and has received interest as an immunotherapeutic target [17, 18]. However, Steap1 lacks the N-terminal oxidoreductase domain found in Steap2, Steap3 and Steap4 and instead substitutes a 70-residue N-terminal tail. Further, attempts to demonstrate Steap1 ferric or cupric reductase activities have been unsuccessful [3]. Thus, it has been unclear whether Steap1 is a functional transmembrane oxidoreductase. However, because the FAD and iron binding motifs that we have identified here in Steap3 are also present in Steap1, it seems that Steap1 might indeed harbor latent transmembrane oxidoreductase activity. If so, this would obviously require a cytosolic source of FAD($H_2$). In addition, it remains possible that Steap1 might oxidize or reduce an alternative extracellular or luminal substrate.

Steap3 Homodimer

In conjunction with the crystallographic structures of the isolated oxidoreductase domains of Steap3 and Steap4, the BiFC study presented here suggest that Steap3 is indeed active as a homodimer. One potential explanation for dimer formation was that Steap3 might utilize an intersubunit electron transfer pathway through a domain swapped dimer. However, the inability of the Ser58Ile and His409Ala mutants to complement each other suggests otherwise. Thus, the functional or regulatory significance of the homodimer remains unclear. However, transferrin receptor is also a dimer [19], and a Steap3 dimer and its cargo of 4 electrons is stoichiometrically matched to the transferrin receptor – transferrin complex that carries 4 iron atoms [9].

Steap3 Transmembrane Domain
Binds a Single, b-Type Heme

Ohgami et al. proposed a model for iron reduction by Steap3 in which a heme cofactor acts as a key intermediary in the transfers of electrons from NADPH and flavin bound in the N-terminal oxidoreductase domain to iron bound at the extracellular or luminal face of the transmembrane domain [2]. Here we confirm their prediction that Steap3 binds a single heme in a bis-histidine fashion (His316 and His409), and show spectroscopically that it is a b-type heme. These histidine residues lie in transmembrane helices 3 and 5 and the topology prediction server Toppred [16] predicts a location slightly above the center of the bilayer towards the extracellular or lumenal space (Fig. 6). These residues are a core feature of the ferric reductase domain (FRD) superfamily, which includes such members as yeast ferric reductase (Fre1) and human NADPH oxidase (NOX) [8]. However, in contrast to a single transmembrane heme in the Steap

proteins, other members of the FRD superfamily contain a second heme cofactor localized near the cytoplasmic face of the membrane [8]. In this context the transmembrane domain of Steap family proteins appears unique. In fact, to our knowledge, there exists no functional evidence for mono-heme cytochromes that perform transmembrane electron transport beyond the Steap family metalloreductases and their bacterial YedZ homologs [20], for which sulfite oxidase activity has been demonstrated [21].

### Steap3 Iron Binding Residues Adjacent to the Heme Cofactor

In our mutational analysis, Tyr229 and Tyr319 were found to participate in iron binding. Tyr229 is predicted to reside in the first transmembrane helix at approximately the same "height" as Tyr319, which is located one α-helical turn above His316, (Fig. 6). The Tyr319 side chain is thus expected to lie near the "top" of the porphyrin ring. This in turn suggests that the iron binding site is also near the top edge of the heme cofactor, as opposed to a more distant site composed of the extracellular loops. This raises the possibility that one or both of the propionate arms of the heme cofactor might serve to coordinate iron in a manner similar to the manganese coordination observed in manganese peroxidase [22]. This would require the heme to be oriented with the propionate arms pointed towards the extracellular space. Such an orientation is indeed observed in structures of integral membrane cytochromes such as the ascorbate dependent ferric reductase DcytB [23] and the cytochrome b subunit of the bc complex [24].

## The Transmembrane Domain Contains a High-Affinity FAD Binding Site

We have shown for the first time that Steap family proteins do indeed utilize a flavin in the reduction of $Fe^{3+}$. In addition, we find that Steap3 exhibits a clear preference for FAD, as the addition of exogenous FMN or riboflavin does not increase activity above the flavin free control. For this reason, we assume that at least some of the activity in the flavin free control is due to low levels of endogenous FAD present in the membrane preparations.

We measure a $K_m$ for FAD in full length Steap3 of approximately 1 μM, greater than two orders of magnitude lower than the non-physiological flavin $K_m$ values (> 100 μM) measured for the isolated N-terminal oxidoreductase domains of Steap3 and Steap4 [10]. Indeed, the structural and kinetic work on these isolated domains previously suggested that the N-terminal oxidoreductase has only a weak interaction with FAD and other flavins, at that this low affinity recognition is primarily via the isoalloxazine ring. We can now conclude that the elements necessary for high-affinity FAD binding reside primarily within the Steap transmembrane domain.

## The αII/αIII and αIV/αV Loops Form the FAD Binding Site

Among the fifteen strictly-conserved residues in the transmembrane domain (Fig. 5B), nine are predicted to lie within loops connecting helix αII to αIII and helix αIV to αV. Our mutational analysis clearly shows these loops are critical for Steap3 activity, where they contribute to FAD binding. Thus, while these loops are distant within the linear sequence, they are expected to lie close to each other in the folded protein

structure, working together to bind FAD (Fig. 6). Interestingly, the αII/αIII loop also contains the endosomal targeting motif for AP-2 [Y288-X-X-Φ (bulky hydrophobic, F291)] [25]. Whether AP-2 might alter the activity of Steap3 during clathrin-mediated endocytosis remains an open question.

### The Transmembrane Domain FAD Binding Site Replaces the Cytoplasm Proximal Heme

As shown above, Steap proteins contain the surface proximal heme common to all members of the FRD superfamily [8], but lack the second, cytoplasm-proximal heme. Interestingly, a bioinformatics analysis of the FRD superfamily shows that YedZ and Steap family proteins are differentiated from other members of the FRD superfamily by replacement of the heme coordinating histidines of the cytoplasm proximal heme with conserved arginine and glutamine residues. Importantly, in Steap3 the arginine and glutamine residues in this superfamily sequence alignment correspond to Arg302 and Gln395. Here we have shown that these residues contribute to the FAD binding pocket in the transmembrane domain. Thus, with regard to the proposed evolutionary pathway of the FRD superfamily [8], we can now conclude that the Steap and YedZ family proteins have lost their cytoplasm proximal heme binding site and replaced it with a cytoplasm proximal FAD binding site.

### Predicted Structure for the Transmembrane Domain

The recently solved crystal structure of DcytB reveals an FRD-like structure in which the cytoplasm and surface proximal hemes are surrounded by six transmembrane helices [23]. Interestingly, the helices follow one another in succession as they work

their way around the heme cofactors. If a similar helical arrangement is considered for the transmembrane domain of Steap3 (Fig. 6), several observations consistent with the biochemical data can be made. First, the arrangement results in placement of the heme coordinating histidine residues on opposite sides of the heme cofactor. Second, it brings the αII/αIII loop in close proximity to the αIV/αV loop so they might collectively work to bind FAD. Third, it could bring the tyrosine residues implicated in iron binding (Tyr229 and Tyr319) into close proximity. For these reasons, we propose the structure shown in Fig. 6 for the Steap3 transmembrane domain, as it is consistent with the structures of integral membrane cytochromes in general, and with the unique structural and biochemical properties of the Steap family elucidated here, namely the location of the iron, single b-type heme and FAD binding sites. Further, it is expected that this structure is shared by all members of the Steap family, including Steap1, as well as the related YedZ family of bacterial transmembrane electron transfer domains.

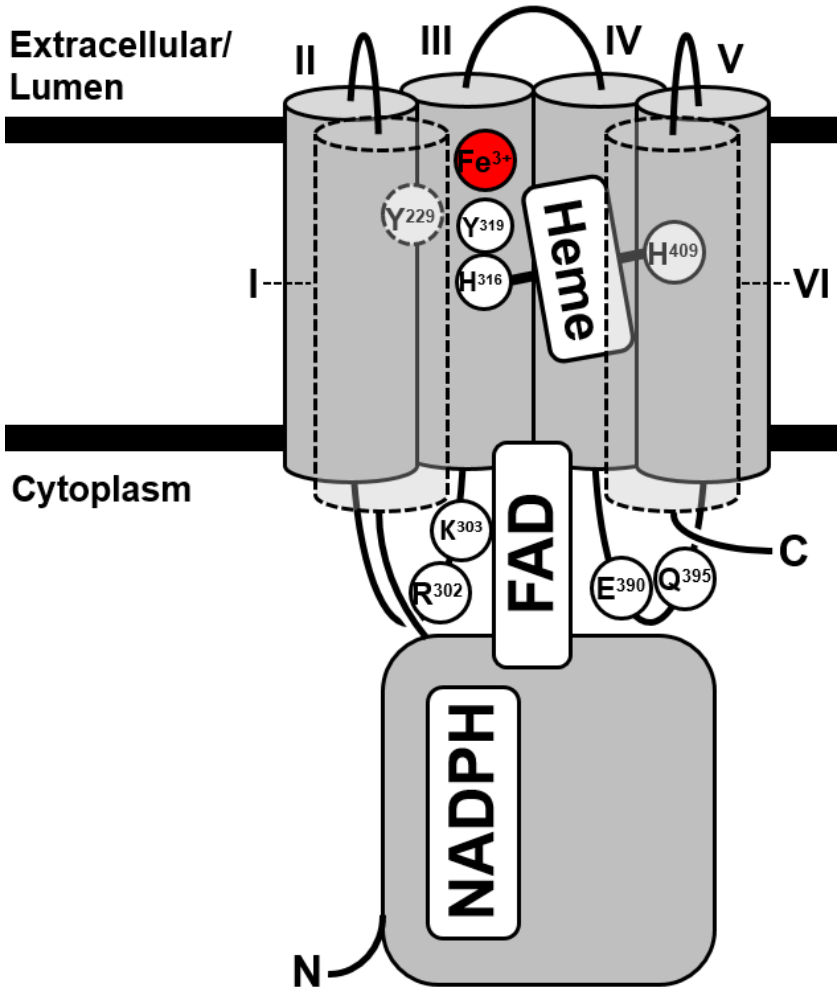


Figure 6. Structural model of the Steap3 transmembrane domain. Strictly-conserved residues key to $Fe^{3+}$, heme, or FAD binding are shown. Residues are oriented based on predictions by the Toppred topology server [16]. The electron source, NADPH, is oriented approximately according to that found in the Steap3 oxidoreductase domain crystal structure, with "H" representing the hydride-containing nicotinamide moiety. The hydride is transferred to FAD, which is bound by transmembrane loops αII/αIII and αIV/αV, including interactions with strictly conserved residues Arg-302, Lys-303, Glu-390, and Gln-395. Single electrons are transferred to a single b-type heme, bound in a bis-histidine fashion via His-316 and His-409. Tyr-229 and Tyr-319 are implicated in binding an $Fe^{3+}$ atom adjacent to the heme cofactor. Foreground segments are represented by dashed boundaries and Tyr-229 is positioned on the backside of helix I in close proximity to Tyr-319 and $Fe^{3+}$. Transmembrane α-helices are numbered by roman numerals. Though the transmembrane helices are represented as partially encircling the heme cofactor, it is expected that the cofactor is completely encircled through analogy of other transmembrane cytochromes.

References


1. Hentze, M.W., M.U. Muckenthaler, and N.C. Andrews, *Balancing acts: molecular control of mammalian iron metabolism.* Cell, 2004. **117**(3): p. 285-97.

2. Ohgami, R.S., et al., *Identification of a ferrireductase required for efficient transferrin-dependent iron uptake in erythroid cells.* Nat. Genet., 2005. **37**(11): p. 1264-9.

3. Ohgami, R.S., et al., *The Steap proteins are metalloreductases.* Blood, 2006. **108**(4): p. 1388-94.

4. Hubert, R.S., et al., *STEAP: a prostate-specific cell-surface antigen highly expressed in human prostate tumors.* Proc. Natl. Acad. Sci. U. S. A., 1999. **96**(25): p. 14523-8.

5. Moldes, M., et al., *Tumor necrosis factor-alpha-induced adipose-related protein (TIARP), a cell-surface protein that is highly induced by tumor necrosis factor-alpha and adipose conversion.* J. Biol. Chem., 2001. **276**(36): p. 33938-46.

6. Porkka, K.P., et al., *Human pHyde is not a classical tumor suppressor gene in prostate cancer.* Int J Cancer, 2003. **106**(5): p. 729-35.

7. Warkentin, E., et al., *The structure of F420-dependent methylenetetrahydromethanopterin dehydrogenase: a crystallographic 'superstructure' of the selenomethionine-labelled protein crystal structure.* Acta Crystallogr. D Biol. Crystallogr., 2005. **61**(Pt 2): p. 198-202.

8. Zhang, X., et al., *Evolution of the Ferric Reductase Domain (FRD) Superfamily: Modularity, Functional Diversification, and Signature Motifs.* PLoS One, 2013. **8**(3): p. e58126.

9. Sendamarai, A.K., et al., *Structure of the membrane proximal oxidoreductase domain of human Steap3, the dominant ferrireductase of the erythroid transferrin cycle.* Proc. Natl. Acad. Sci. U. S .A., 2008. **105**(21): p. 7410-5.

10. Gauss, G.H., et al., *The Crystal Structure of Six-transmembrane Epithelial Antigen of the Prostate 4 (Steap4), a Ferri/Cuprireductase, Suggests a Novel Interdomain Flavin-binding Site.* Journal of Biological Chemistry, 2013. **288**(28): p. 20668-20682.

11. Backliwal, G., et al., *Valproic acid: A viable alternative to sodium butyrate for enhancing protein expression in mammalian cell cultures.* Biotechnology and Bioengineering, 2008. **101**(1): p. 182-189.

12. Kery, V., D. Elleder, and J.P. Kraus, *Delta-Aminolevulinate Increases Heme Saturation and Yield of Human Cystathionine Beta-Synthase Expressed in Escherichia-Coli.* Archives of Biochemistry and Biophysics, 1995. **316**(1): p. 24-29.

13. Jones, F.G., et al., *High-level expression of recombinant immunoreactive thyroid peroxidase in the High Five insect cell line.* Journal of Molecular Endocrinology, 1996. **17**(2): p. 165-174.

14. Hu, C.D., Y. Chinenov, and T.K. Kerppola, *Visualization of interactions among bZip and Rel family proteins in living cells using bimolecular fluorescence complementation.* Molecular Cell, 2002. **9**(4): p. 789-798.

15. Sievers, F., et al., *Fast, scalable generation of high-quality protein multiple sequence alignments using Clustal Omega.* Mol Syst Biol, 2011. **7**: p. 539.

16. Claros, M.G. and G. von Heijne, *TopPred II: an improved software for membrane protein structure predictions.* Comput Appl Biosci, 1994. **10**(6): p. 685-6.

17. Moreaux, J., et al., *STEAP1 is overexpressed in cancers: A promising therapeutic target.* Biochemical and Biophysical Research Communications, 2012. **429**(3-4): p. 148-155.

18. Spratt, D.E., et al., *89Zr-MSTP2109A, A Novel Antibody Based Radiotracer to Evaluate and Guide the Clinical Translation of Antibody-Drug Conjugates Targeting STEAP1.* International Journal of Radiation Oncology Biology Physics, 2014. **90**: p. S791-S791.

19. Lawrence, C.M., et al., *Crystal structure of the ectodomain of human transferrin receptor.* Science, 1999. **286**(5440): p. 779-82.

20. Sanchez-Pulido, L., et al., *ACRATA: a novel electron transfer domain associated to apoptosis and cancer.* Bmc Cancer, 2004. **4**: p. 98.

21. Brokx, S.J., et al., *Characterization of an Escherichia coli sulfite oxidase homologue reveals the role of a conserved active site cysteine in assembly and function.* Biochemistry, 2005. **44**(30): p. 10339-48.

22. Sundaramoorthy, M., et al., *The crystal structure of manganese peroxidase from Phanerochaete chrysosporium at 2.06-A resolution.* J Biol Chem, 1994. **269**(52): p. 32759-67.

23. Lu, P., et al., *Structure and mechanism of a eukaryotic transmembrane ascorbate-dependent oxidoreductase.* Proc Natl Acad Sci U S A, 2014. **111**(5): p. 1813-8.

24. Solmaz, S.R. and C. Hunte, *Structure of complex III with bound cytochrome c in reduced state and definition of a minimal core interface for electron transfer*. J Biol Chem, 2008. **283**(25): p. 17542-9.

25. Lambe, T., et al., *Identification of a Steap3 endosomal targeting motif essential for normal iron metabolism.* Blood, 2009. **113**(8): p. 1805-8.

26. Amzallag, N., et al., *TSAP6 facilitates the secretion of translationally controlled tumor protein/histamine-releasing factor via a nonclassical pathway*. J. Biol. Chem., 2004. **279**(44): p. 46104-12.

# CHAPTER SIX

## CONCLUDING REMARKS

The Steap family has been identified as performing key cellular functions, but the underlying mechanisms of that function had not been well-understood. Here, the biochemical foundations of the Steap family of metalloreductases have been examined. Through the described work, we now can construct a more complete picture of their function, including the identification of cofactors and their binding sites, substrate binding sites, and protein-protein interactions.

Prior to these studies, the roles of Steap enzymes had been examined in a number of platforms (in vivo tissue, mouse knockout, recombinantly-expressed truncations). For functional studies, the cell-surface ferric reductase assay system developed by Ohgami et al. [1] was utilized here, but a system for the in-depth functional analysis of the enzymatic mechanism, particularly the protein regions on the cytoplasmic face of the membrane, had not been developed. Thus, a particular goal of my work has been on developing systems that allow me to address the unanswered questions of Steap family enzymatic function. To that end bacterial, insect, and mammalian expression systems were developed.

While bacterial expression systems are ill-suited for the recombinant expression of mammalian membrane proteins, they are exceedingly useful for soluble proteins. Thus, *E. coli* cells were utilized for the expression and the purification of the oxidoreductase domain of rat Steap4 (Chapter 3). Unlike the same domain of human Steap3, which

exhibits almost no NADPH oxidase activity, the purified Steap4 truncation was able to be kinetically characterized. There, we were able to determine that, while the oxidoreductase domain alone exhibits flavin-dependent NADPH oxidase activity, the flavin-binding capacity is non-physiologically weak ($K_M$ > 100 μM) and it shows no preference for a particular flavin (FMN, FAD, or riboflavin). Thus, in the cytoplasmic oxidoreductase domain the flavin binding site is largely incomplete and likely is only capable of interacting with the isoalloxazine ring of the flavin.

Studying a full-length Steap protein would allow for a comprehensive examination of the flavin binding site as well as additional attributes including the substrate (iron or copper) binding site and the predicted binding of a heme cofactor in the transmembrane region. Baculovirus-mediated gene expression in Sf9 insect cells was utilized in an attempt to purify full-length human Steap3 for structure-function studies (Chapter 4). Though Steap3 was unable to be purified in the functional state, valuable information was obtained in the process. The heme spectra for any Steap family was shown for the first time here, indicating the binding of a b-type heme. The requirement for FAD in Steap3 ferric reductase activity and intolerance of FMN was first shown in the assays developed here. Finally, the work gave evidence for an as-yet unidentified critical factor to activity that is able to lost during purification, such as lipids or interacting protein partners.

Ohgami et al, initially characterized Steap3 as a ferric reductase in transiently-transfected human HEK-293 cells [1], a well-characterized model human cell line that has recently been utilized as a platform of large-scale recombinant protein expression [2,

3]. This system has the advantage of having human protein expression mechanisms for transfected human genes. As Sf9 cells may be improper for functional Steap3 expression and subsequent purification, this system was chosen due to these advantages. However, there are few examples of these cells used for a similar integral membrane protein expression application [4]. Furthermore, to my knowledge, this described work represents the first use of a HEK-293 line for the recombinant expression of an integral membrane hemoprotein for purification (Chapter 2 and 5). As such it was necessary to determine several parameters for optimal expression. The identification of aminolevulinic acid as a necessary supplement in the Sf9 platform was able to be applied to HEK cells to greatly increase the incorporation of heme into Steap3 and may be applied to future HEK expression studies with hemoproteins. As with Sf9 cells, functional Steap3 was unable to be purified from HEK membranes, but the enzymatic mechanism was able to be characterized in the partially-purified state. This characterization included an analysis of the FAD binding site and the specific residues that compose it. In confirmation of the hypothesis produced from the study of the Steap4 oxidoreductase domain, Steap3 binds FAD with high affinity in the transmembrane domain. By mutating strictly-conserved residues of the transmembrane domain, we were able to show that the binding site is primarily composed of the two intracellular loops between transmembrane helices. Similarly, we were able to show that the extracellular metal ion substrate binds adjacent to the heme cofactor via two strictly-conserved tyrosine residues. Though heme-binding was initially identified in the Sf9 studies, we were also able to confirm that Steap3 bind a single b-type heme in a bis-histidine fashion through two strictly-conserved histidines.

Because these residues are not only conserved amongst all Steap3 sequences in the NCBI nr database, but also the three other Steap family members as well. Notably, this includes Steap1, is highly expressed in prostate cancer cells and has an unknown function as it lacks the oxidoreductase domain. As Steap1 contains these crucial mechanistic residues, it may also function in an electron transfer capacity. Lastly, this system allowed us to examine the propensity of Steap3 to form homodimers, a hypothesis generated from the crystal structure of the Steap3 oxidoreductase domain [5]. Through a bimolecular fluorescence complementation assay, we observed an ability for Steap3 to dimerize in a subcellular distribution comparable to that previously observed for wild-type Steap3 [1]. Additionally, by utilizing select cofactor-binding mutants, we were able to show that a Steap3 dimer performs intra-subunit electron transfer. Together this work provides key fundamental details of Steap family function as well as providing platforms for future study of them.

Future work should address several unanswered questions from this work. In the cell, what impact does dimerization have on ferric reductase activity? The NADPH binding site is adjacent to the dimer interface, thus, is dimerization a necessary to stabilize the NADPH binding pocket? Furthermore, can this dimer form a greater complex with other transferrin cycle proteins, such as TFR or DMT1? If Steap3 is able to complex with the transferrin:TFR complex, how do the four transferrin-bound iron atoms process to the binding site on Steap3? Relatedly, due to the stoichiometric symmetry of four reducing equivalents in a Steap3 dimer and the four iron atoms, is there a regulated mechanism that allows both iron transfer between components and their reduction?

The Steap family's copper reduction role remains ill-defined. Do the iron binding site residues also bind copper? As the primary copper transporter Ctr1 requires the reduction of the metal prior to transport, does Steap3 interact in a controlled process? If so, is this process in a conserved coupled reduction-transport mechanism also found with DMT1 or Zip14 for iron transport?

Several proteomic studies have determined that several Steap family members have post-translational modifications, including glycosylation, phosphorylation and ubiquitylation as found at the modification database, Phosphosite [6]. What effect do these modifications have on their function? Do they contribute to the differences in Steap family tissue distribution?

## References


1. Ohgami, R.S., et al., *Identification of a ferrireductase required for efficient transferrin-dependent iron uptake in erythroid cells.* Nat. Genet., 2005. **37**(11): p. 1264-9.

2. Aricescu, A.R., W. Lu, and E.Y. Jones, *A time- and cost-efficient system for high-level protein production in mammalian cells.* Acta Crystallogr D Biol Crystallogr, 2006. **62**(Pt 10): p. 1243-50.

3. Lee, J.E., M.L. Fusco, and E.O. Saphire, *An efficient platform for screening expression and crystallization of glycoproteins produced in human cells.* Nat Protoc, 2009. **4**(4): p. 592-604.

4. Takayama, H., et al., *High-level expression, single-step immunoaffinity purification and characterization of human tetraspanin membrane protein CD81.* PLoS One, 2008. **3**(6): p. e2314.

5. Sendamarai, A.K., et al., *Structure of the membrane proximal oxidoreductase domain of human Steap3, the dominant ferrireductase of the erythroid transferrin cycle.* Proc. Natl. Acad. Sci. U. S .A., 2008. **105**(21): p. 7410-5.

6. Hornbeck, P.V., et al., *PhosphoSitePlus: a comprehensive resource for investigating the structure and function of experimentally determined post-translational modifications in man and mouse.* Nucleic Acids Res, 2012. **40**(Database issue): p. D261-70.

# APPENDIX A

## SUPPORTING INFORMATION FOR CHAPTER 3

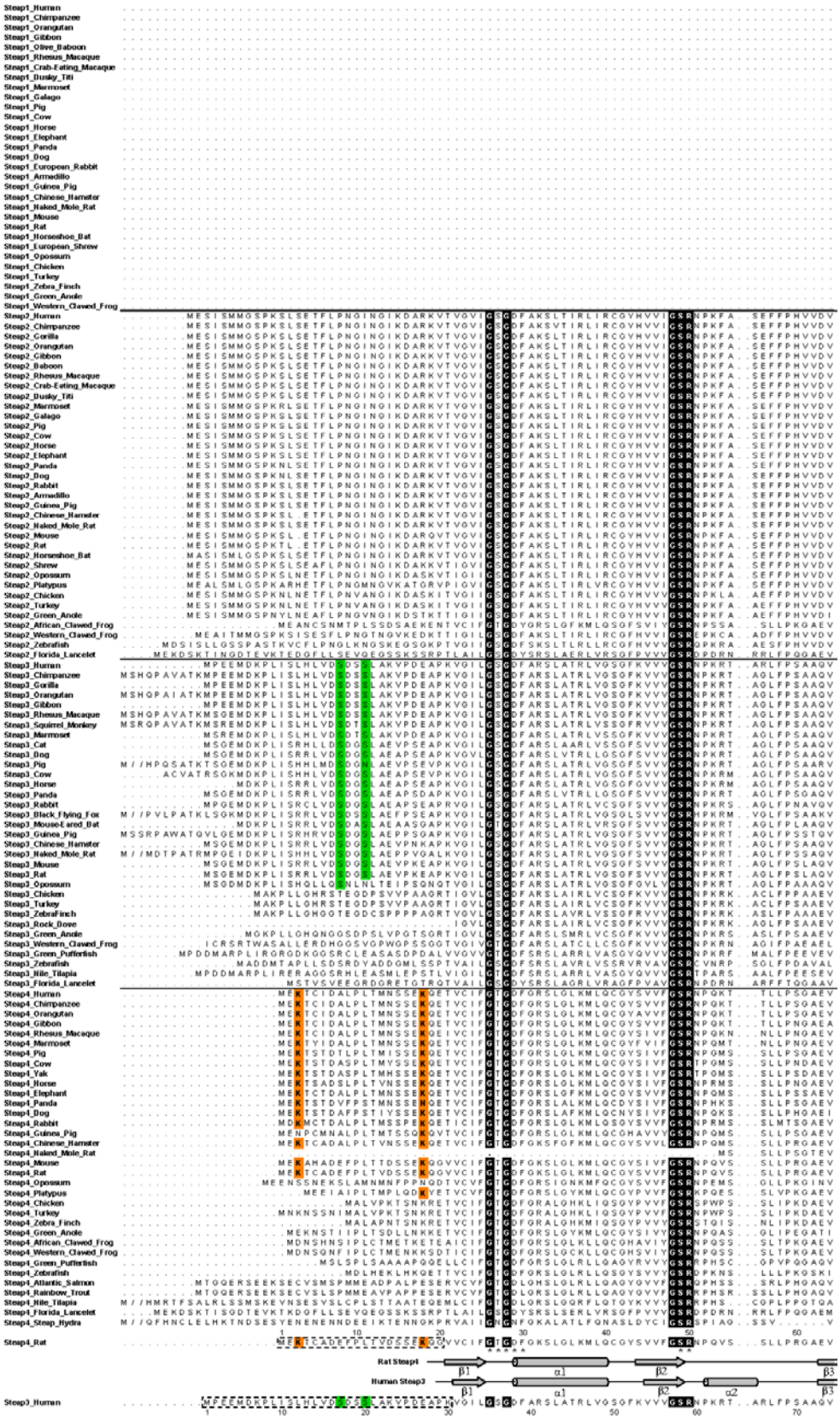
Steap1_Human
Steap1_Chimpanzee
Steap1_Orangutan
Steap1_Gibbon
Steap1_Olive_Baboon
Steap1_Rhesus_Macaque
Steap1_Crab-Eating_Macaque
Steap1_Dusky_Titi
Steap1_Marmoset
Steap1_Galago
Steap1_Pig
Steap1_Cow
Steap1_Horse
Steap1_Elephant
Steap1_Panda
Steap1_Dog
Steap1_European_Rabbit
Steap1_Armadillo
Steap1_Guinea_Pig
Steap1_Chinese_Hamster
Steap1_Naked_Mole_Rat
Steap1_Mouse
Steap1_Rat
Steap1_Horseshoe_Bat
Steap1_European_Shrew
Steap1_Opossum
Steap1_Chicken
Steap1_Turkey
Steap1_Zebra_Finch
Steap1_Green_Anole
Steap1_Western_Clawed_Frog
Steap2_Human
Steap2_Chimpanzee
Steap2_Gorilla
Steap2_Orangutan
Steap2_Gibbon
Steap2_Baboon
Steap2_Rhesus_Macaque
Steap2_Crab-Eating_Macaque
Steap2_Dusky_Titi
Steap2_Marmoset
Steap2_Galago
Steap2_Pig
Steap2_Cow
Steap2_Horse
Steap2_Elephant
Steap2_Panda
Steap2_Dog
Steap2_Rabbit
Steap2_Armadillo
Steap2_Guinea_Pig
Steap2_Chinese_Hamster
Steap2_Naked_Mole_Rat
Steap2_Mouse
Steap2_Rat
Steap2_Horseshoe_Bat
Steap2_Shrew
Steap2_Opossum
Steap2_Platypus
Steap2_Chicken
Steap2_Turkey
Steap2_Green_Anole
Steap2_African_Clawed_Frog
Steap2_Zebrafish
Steap2_Florida_Lancelet
Steap3_Human
Steap3_Chimpanzee
Steap3_Gorilla
Steap3_Orangutan
Steap3_Gibbon
Steap3_Rhesus_Macaque
Steap3_Squirrel_Monkey
Steap3_Marmoset
Steap3_Cat
Steap3_Dog
Steap3_Pig
Steap3_Cow
Steap3_Horse
Steap3_Panda
Steap3_Rabbit
Steap3_Black_Flying_Fox
Steap3_Mouse-Eared_Bat
Steap3_Guinea_Pig
Steap3_Chinese_Hamster
Steap3_Naked_Mole_Rat
Steap3_Mouse
Steap3_Rat
Steap3_Opossum
Steap3_Chicken
Steap3_Turkey
Steap3_ZebraFinch
Steap3_Rock_Dove
Steap3_Green_Anole
Steap3_Western_Clawed_Frog
Steap3_Green_Pufferfish
Steap3_Zebrafish
Steap3_Nile_Tilapia
Steap3_Florida_Lancelet
Steap4_Human
Steap4_Chimpanzee
Steap4_Orangutan
Steap4_Gibbon
Steap4_Rhesus_Macaque
Steap4_Marmoset
Steap4_Pig
Steap4_Cow
Steap4_Yak
Steap4_Horse
Steap4_Elephant
Steap4_Panda
Steap4_Dog
Steap4_Rabbit
Steap4_Guinea_Pig
Steap4_Chinese_Hamster
Steap4_Naked_Mole_Rat
Steap4_Mouse
Steap4_Rat
Steap4_Opossum
Steap4_Platypus
Steap4_Chicken
Steap4_Turkey
Steap4_Zebra_Finch
Steap4_Green_Anole
Steap4_African_Clawed_Frog
Steap4_Western_Clawed_Frog
Steap4_Green_Pufferfish
Steap4_Zebrafish
Steap4_Atlantic_Salmon
Steap4_Rainbow_Trout
Steap4_Nile_Tilapia
Steap4_Florida_Lancelet
Steap4_Steap_Hydra
Steap4_Rat
Rat Steap1
Human Steap2
Steap3_Human

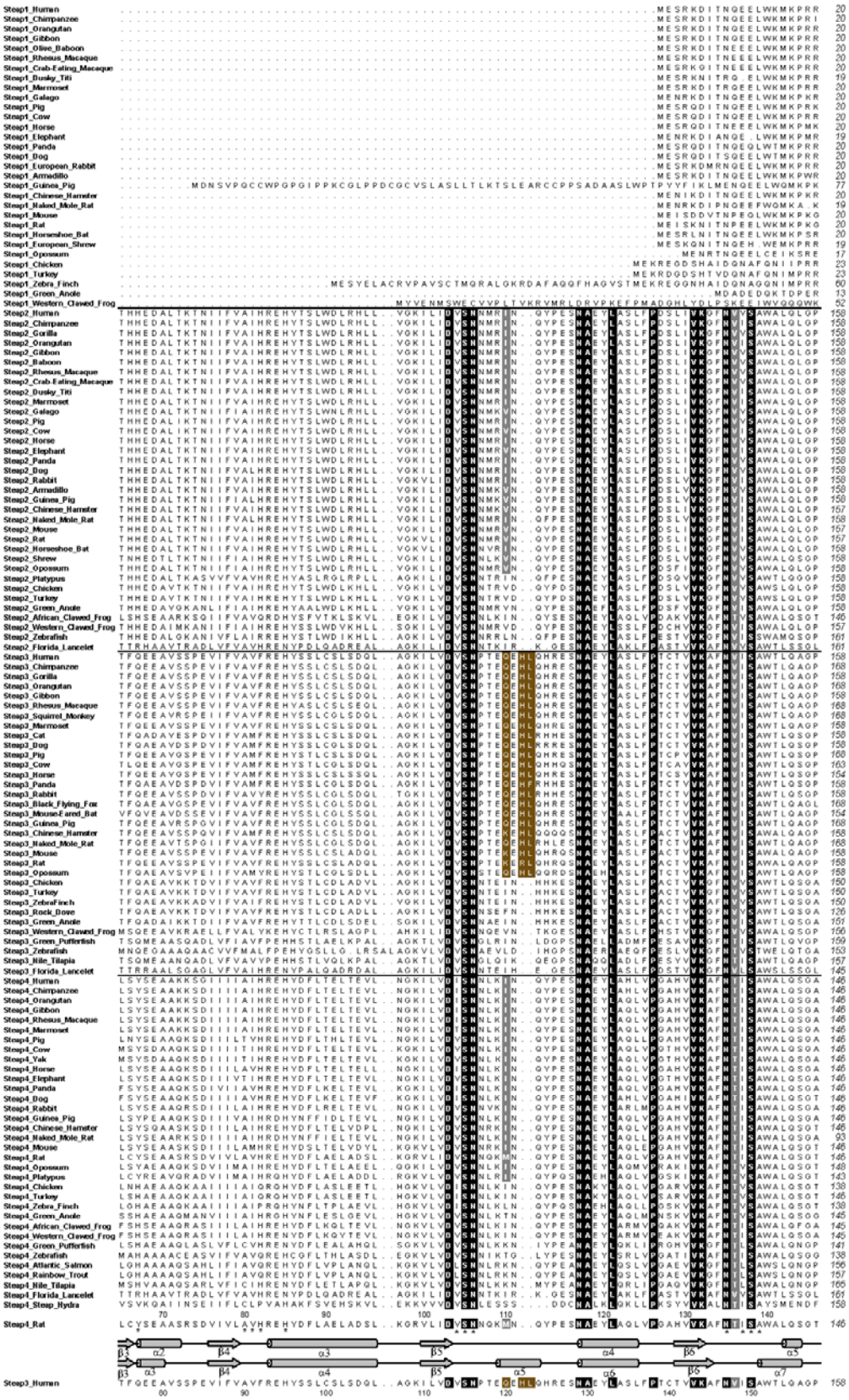

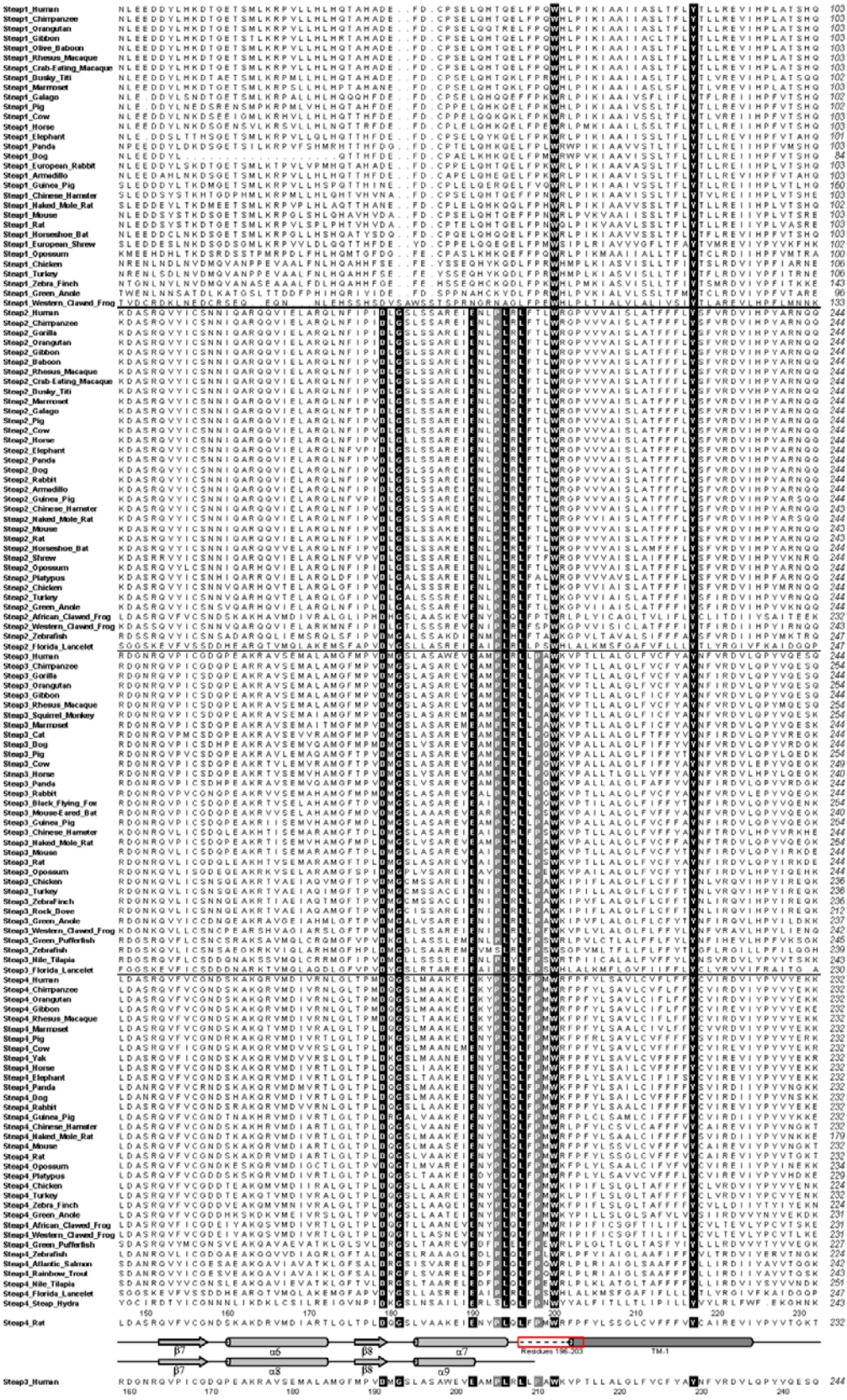
Steap1_Human
Steap1_Chimpanzee
Steap1_Orangutan
Steap1_Gibbon
Steap1_Olive_Baboon
Steap1_Rhesus_Macaque
Steap1_Crab-Eating_Macaque
Steap1_Dusky_Titi
Steap1_Marmoset
Steap1_Galago
Steap1_Pig
Steap1_Cow
Steap1_Horse
Steap1_Elephant
Steap1_Panda
Steap1_Dog
Steap1_European_Rabbit
Steap1_Armadillo
Steap1_Guinea_Pig
Steap1_Chinese_Hamster
Steap1_Naked_Mole_Rat
Steap1_Mouse
Steap1_Rat
Steap1_Horseshoe_Bat
Steap1_European_Shrew
Steap1_Opossum
Steap1_Chicken
Steap1_Turkey
Steap1_Zebra_Finch
Steap1_Green_Anole
Steap1_Western_Clawed_Frog
Steap2_Human
Steap2_Chimpanzee
Steap2_Gorilla
Steap2_Orangutan
Steap2_Gibbon
Steap2_Baboon
Steap2_Rhesus_Macaque
Steap2_Crab-Eating_Macaque
Steap2_Dusky_Titi
Steap2_Marmoset
Steap2_Galago
Steap2_Pig
Steap2_Cow
Steap2_Horse
Steap2_Elephant
Steap2_Panda
Steap2_Dog
Steap2_Rabbit
Steap2_Armadillo
Steap2_Guinea_Pig
Steap2_Chinese_Hamster
Steap2_Naked_Mole_Rat
Steap2_Mouse
Steap2_Rat
Steap2_Horseshoe_Bat
Steap2_Shrew
Steap2_Opossum
Steap2_Platypus
Steap2_Chicken
Steap2_Turkey
Steap2_Green_Anole
Steap2_African_Clawed_Frog
Steap2_Western_Clawed_Frog
Steap2_Zebrafish
Steap2_Florida_Lancelet
Steap3_Human
Steap3_Chimpanzee
Steap3_Gorilla
Steap3_Orangutan
Steap3_Gibbon
Steap3_Rhesus_Macaque
Steap3_Squirrel_Monkey
Steap3_Marmoset
Steap3_Cat
Steap3_Dog
Steap3_Pig
Steap3_Cow
Steap3_Horse
Steap3_Panda
Steap3_Rabbit
Steap3_Black_Flying_Fox
Steap3_Mouse-Eared_Bat
Steap3_Guinea_Pig
Steap3_Chinese_Hamster
Steap3_Naked_Mole_Rat
Steap3_Mouse
Steap3_Rat
Steap3_Opossum
Steap3_Chicken
Steap3_Turkey
Steap3_ZebraFinch
Steap3_Rock_Dove
Steap3_Green_Anole
Steap3_Western_Clawed_Frog
Steap3_Green_Pufferfish
Steap3_Zebrafish
Steap3_Nile_Tilapia
Steap3_Florida_Lancelet
Steap4_Human
Steap4_Chimpanzee
Steap4_Orangutan
Steap4_Gibbon
Steap4_Rhesus_Macaque
Steap4_Marmoset
Steap4_Pig
Steap4_Cow
Steap4_Yak
Steap4_Horse
Steap4_Elephant
Steap4_Panda
Steap4_Dog
Steap4_Rabbit
Steap4_Guinea_Pig
Steap4_Chinese_Hamster
Steap4_Naked_Mole_Rat
Steap4_Mouse
Steap4_Rat
Steap4_Opossum
Steap4_Platypus
Steap4_Chicken
Steap4_Turkey
Steap4_Zebra_Finch
Steap4_Green_Anole
Steap4_African_Clawed_Frog
Steap4_Western_Clawed_Frog
Steap4_Green_Pufferfish
Steap4_Zebrafish
Steap4_Atlantic_Salmon
Steap4_Rainbow_Trout
Steap4_Nile_Tilapia
Steap4_Florida_Lancelet
Steap4_Steap_Hydra
Steap4_Rat
Residues 196-203
TM-1
β7
α5
β8
α7
β7
α8
β8
α9
Steap3_Human

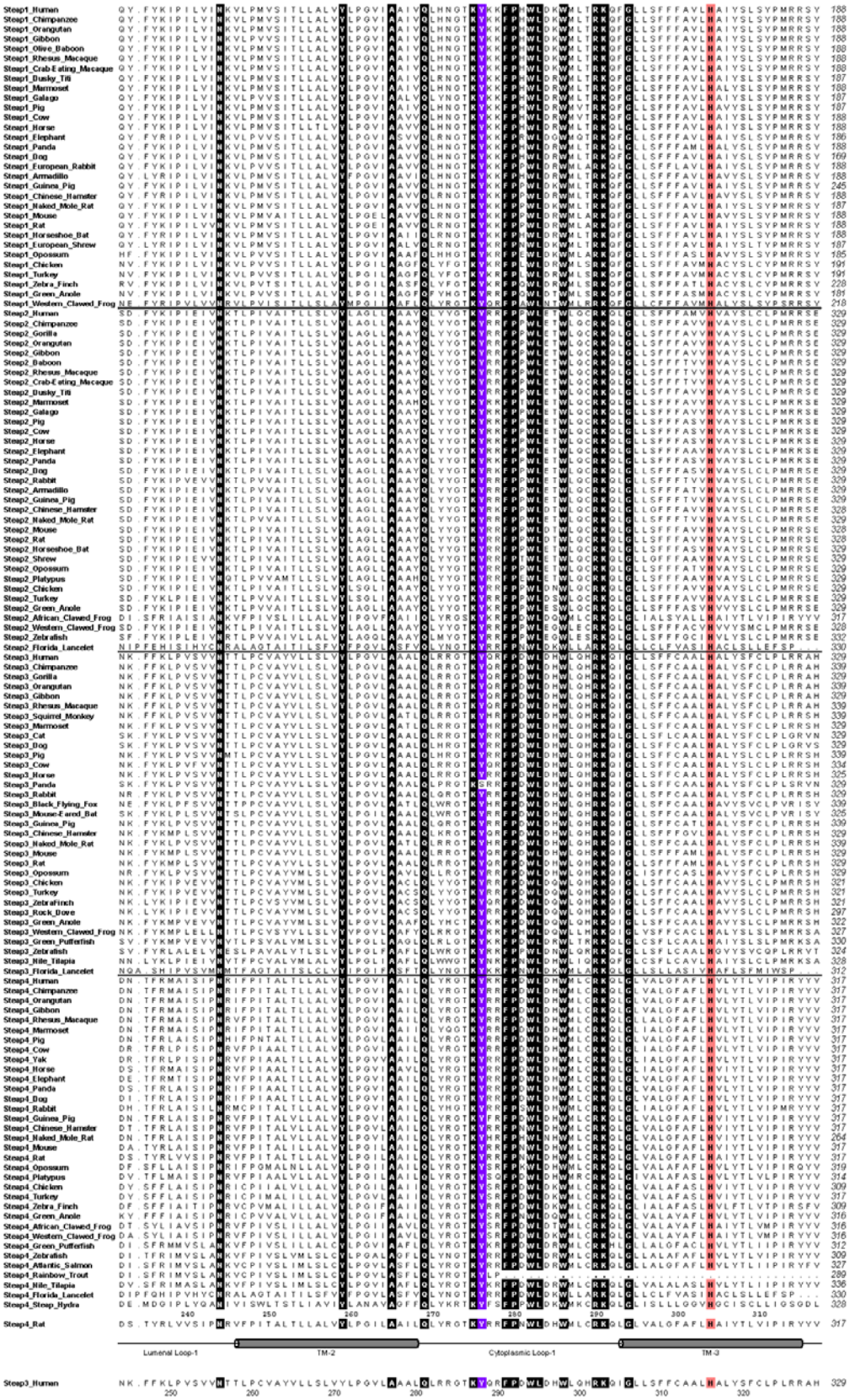
Steap1_Human
Steap1_Chimpanzee
Steap1_Orangutan
Steap1_Gibbon
Steap1_Olive_Baboon
Steap1_Rhesus_Macaque
Steap1_Crab-Eating_Macaque
Steap1_Dusky_Titi
Steap1_Marmoset
Steap1_Galago
Steap1_Pig
Steap1_Cow
Steap1_Horse
Steap1_Elephant
Steap1_Panda
Steap1_Dog
Steap1_European_Rabbit
Steap1_Armadillo
Steap1_Guinea_Pig
Steap1_Chinese_Hamster
Steap1_Naked_Mole_Rat
Steap1_Mouse
Steap1_Rat
Steap1_Horseshoe_Bat
Steap1_European_Shrew
Steap1_Opossum
Steap1_Chicken
Steap1_Turkey
Steap1_Zebra_Finch
Steap1_Green_Anole
Steap1_Western_Clawed_Frog
Steap2_Human
Steap2_Chimpanzee
Steap2_Gorilla
Steap2_Orangutan
Steap2_Gibbon
Steap2_Baboon
Steap2_Rhesus_Macaque
Steap2_Crab-Eating_Macaque
Steap2_Dusky_Titi
Steap2_Marmoset
Steap2_Galago
Steap2_Pig
Steap2_Cow
Steap2_Horse
Steap2_Elephant
Steap2_Panda
Steap2_Dog
Steap2_Rabbit
Steap2_Armadillo
Steap2_Guinea_Pig
Steap2_Chinese_Hamster
Steap2_Naked_Mole_Rat
Steap2_Mouse
Steap2_Rat
Steap2_Horseshoe_Bat
Steap2_Shrew
Steap2_Opossum
Steap2_Platypus
Steap2_Chicken
Steap2_Turkey
Steap2_Green_Anole
Steap2_African_Clawed_Frog
Steap2_Western_Clawed_Frog
Steap2_Zebrafish
Steap2_Florida_Lancelet
Steap3_Human
Steap3_Chimpanzee
Steap3_Gorilla
Steap3_Orangutan
Steap3_Gibbon
Steap3_Rhesus_Macaque
Steap3_Squirrel_Monkey
Steap3_Marmoset
Steap3_Cat
Steap3_Dog
Steap3_Pig
Steap3_Cow
Steap3_Horse
Steap3_Panda
Steap3_Rabbit
Steap3_Black_Flying_Fox
Steap3_Mouse-Eared_Bat
Steap3_Guinea_Pig
Steap3_Chinese_Hamster
Steap3_Naked_Mole_Rat
Steap3_Mouse
Steap3_Rat
Steap3_Opossum
Steap3_Chicken
Steap3_Turkey
Steap3_ZebraFinch
Steap3_Rock_Dove
Steap3_Green_Anole
Steap3_Western_Clawed_Frog
Steap3_Green_Pufferfish
Steap3_Zebrafish
Steap3_Nile_Tilapia
Steap3_Florida_Lancelet
Steap4_Human
Steap4_Chimpanzee
Steap4_Orangutan
Steap4_Gibbon
Steap4_Rhesus_Macaque
Steap4_Marmoset
Steap4_Pig
Steap4_Cow
Steap4_Yak
Steap4_Horse
Steap4_Elephant
Steap4_Panda
Steap4_Dog
Steap4_Rabbit
Steap4_Guinea_Pig
Steap4_Chinese_Hamster
Steap4_Naked_Mole_Rat
Steap4_Mouse
Steap4_Rat
Steap4_Opossum
Steap4_Platypus
Steap4_Chicken
Steap4_Turkey
Steap4_Zebra_Finch
Steap4_Green_Anole
Steap4_African_Clawed_Frog
Steap4_Western_Clawed_Frog
Steap4_Green_Pufferfish
Steap4_Zebrafish
Steap4_Atlantic_Salmon
Steap4_Rainbow_Trout
Steap4_Nile_Tilapia
Steap4_Florida_Lancelet
Steap4_Steap_Hydra
Steap4_Rat
Lumenal Loop-1
TM-2
Cytoplasmic Loop-1
TM-3
Steap3_Human

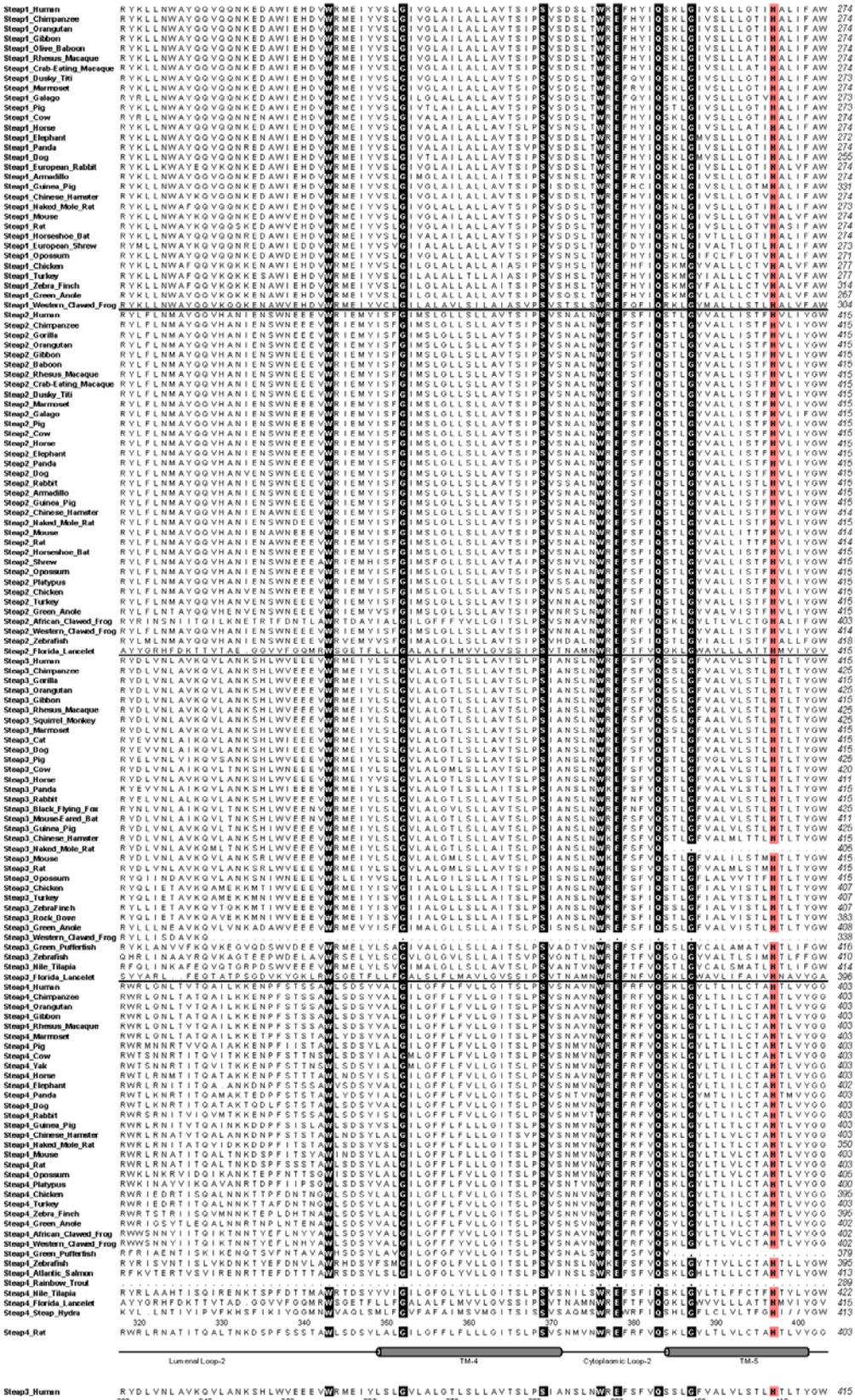
Steap1_Human
Steap1_Chimpanzee
Steap1_Orangutan
Steap1_Gibbon
Steap1_Olive_Baboon
Steap1_Rhesus_Macaque
Steap1_Crab-Eating_Macaque
Steap1_Dusky_Titi
Steap1_Marmoset
Steap1_Galago
Steap1_Pig
Steap1_Cow
Steap1_Horse
Steap1_Elephant
Steap1_Panda
Steap1_Dog
Steap1_European_Rabbit
Steap1_Armadillo
Steap1_Guinea_Pig
Steap1_Chinese_Hamster
Steap1_Naked_Mole_Rat
Steap1_Mouse
Steap1_Rat
Steap1_Horseshoe_Bat
Steap1_European_Shrew
Steap1_Opossum
Steap1_Chicken
Steap1_Turkey
Steap1_Zebra_Finch
Steap1_Green_Anole
Steap1_Western_Clawed_Frog
Steap2_Human
Steap2_Chimpanzee
Steap2_Gorilla
Steap2_Orangutan
Steap2_Gibbon
Steap2_Baboon
Steap2_Rhesus_Macaque
Steap2_Crab-Eating_Macaque
Steap2_Dusky_Titi
Steap2_Marmoset
Steap2_Galago
Steap2_Pig
Steap2_Cow
Steap2_Horse
Steap2_Elephant
Steap2_Panda
Steap2_Dog
Steap2_Rabbit
Steap2_Armadillo
Steap2_Guinea_Pig
Steap2_Chinese_Hamster
Steap2_Naked_Mole_Rat
Steap2_Mouse
Steap2_Rat
Steap2_Horseshoe_Bat
Steap2_Shrew
Steap2_Opossum
Steap2_Platypus
Steap2_Chicken
Steap2_Turkey
Steap2_Green_Anole
Steap2_African_Clawed_Frog
Steap2_Western_Clawed_Frog
Steap2_Zebrafish
Steap2_Florida_Lancelet
Steap3_Human
Steap3_Chimpanzee
Steap3_Gorilla
Steap3_Orangutan
Steap3_Gibbon
Steap3_Rhesus_Macaque
Steap3_Squirrel_Monkey
Steap3_Marmoset
Steap3_Cat
Steap3_Dog
Steap3_Pig
Steap3_Cow
Steap3_Horse
Steap3_Panda
Steap3_Rabbit
Steap3_Black_Flying_Fox
Steap3_Mouse-Eared_Bat
Steap3_Guinea_Pig
Steap3_Chinese_Hamster
Steap3_Naked_Mole_Rat
Steap3_Mouse
Steap3_Rat
Steap3_Opossum
Steap3_Chicken
Steap3_Turkey
Steap3_ZebraFinch
Steap3_Rock_Dove
Steap3_Green_Anole
Steap3_Western_Clawed_Frog
Steap3_Green_Pufferfish
Steap3_Zebrafish
Steap3_Nile_Tilapia
Steap3_Florida_Lancelet
Steap4_Human
Steap4_Chimpanzee
Steap4_Orangutan
Steap4_Gibbon
Steap4_Rhesus_Macaque
Steap4_Marmoset
Steap4_Pig
Steap4_Cow
Steap4_Yak
Steap4_Horse
Steap4_Elephant
Steap4_Panda
Steap4_Dog
Steap4_Rabbit
Steap4_Guinea_Pig
Steap4_Chinese_Hamster
Steap4_Naked_Mole_Rat
Steap4_Mouse
Steap4_Rat
Steap4_Opossum
Steap4_Platypus
Steap4_Chicken
Steap4_Turkey
Steap4_Zebra_Finch
Steap4_Green_Anole
Steap4_African_Clawed_Frog
Steap4_Western_Clawed_Frog
Steap4_Green_Pufferfish
Steap4_Zebrafish
Steap4_Atlantic_Salmon
Steap4_Rainbow_Trout
Steap4_Nile_Tilapia
Steap4_Florida_Lancelet
Steap4_Steap_Hydra
Steap4_Rat
Luminal Loop-2
TM-4
Cytoplasmic Loop-2
TM-5
Steap3_Human

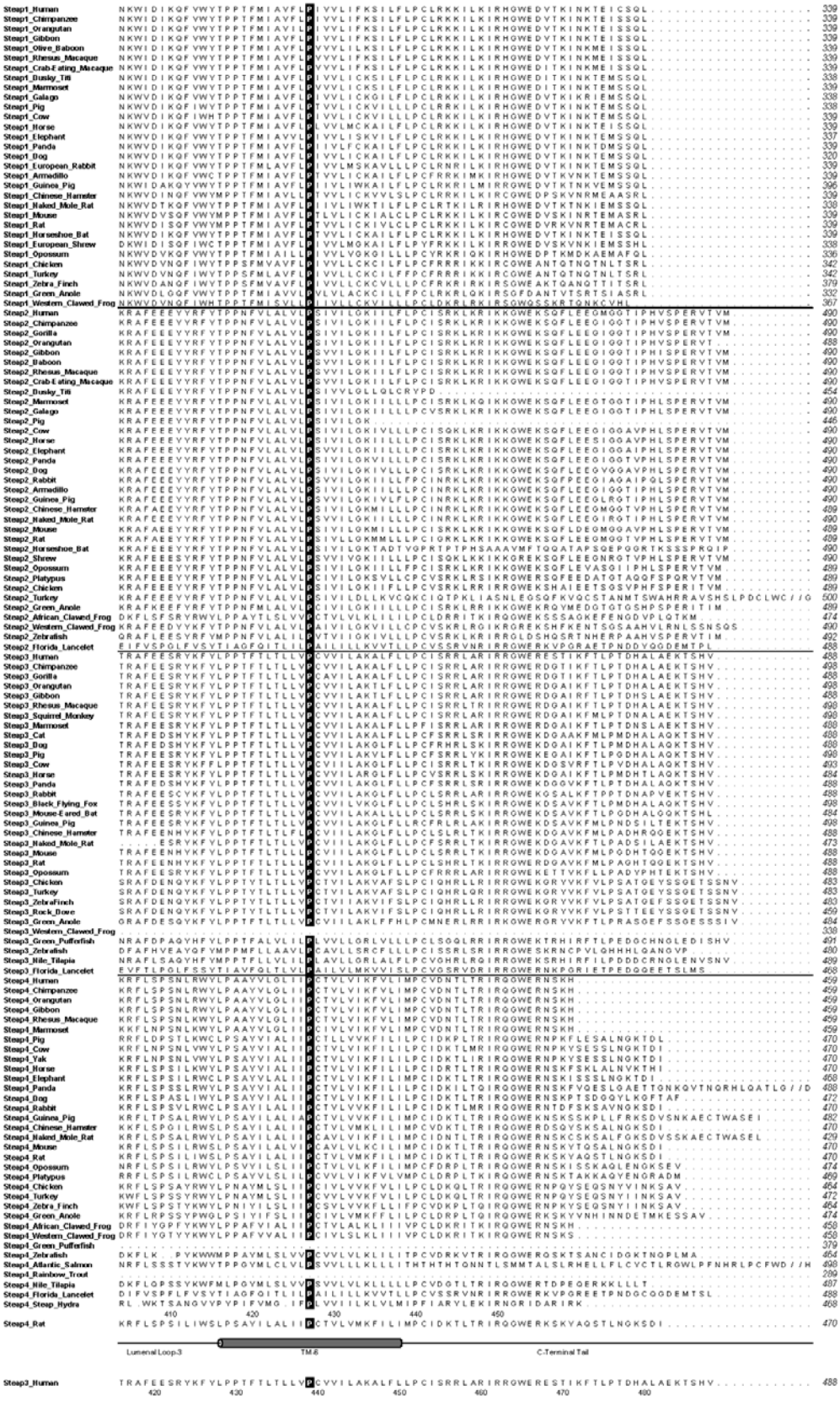
Lumenal Loop 3
TM 8
C-Terminal Tail

Figure A.1. Sequence alignment of metazoan (multi-cellular) Steap proteins. Secondary structure elements of the human Steap3 and rat Steap4 oxidoreductase domain structure are at the bottom of the alignment. Transmembrane-spanning segments for rat Steap4 predicted by TMHMM [1] are also shown. Disordered residues at the N-termini of the Steap3 and Steap4 structures are enclosed in dashed boxes. A red box encloses residues 196-203 of rat Steap4; truncation of these residues reduces the NADPH oxidase activity of the purified oxidoreductase domain. Putative heme-coordinating histidine residues (His304 and His397) are in red. All other strictly conserved residues are highlighted in black. Asterisks below the rat Steap4 sequence denote residues that contact NADPH in the crystal structure, many of these are strictly conserved. The ability of the sequence alignment to discriminate residues involved in substrate recognition suggests that strictly conserved residues in the first (residues 269-292) or second (residues 372-383) cytoplasmic loops of the transmembrane domain might participate in flavin recognition (see text for details). Tyr276 of the endosomal targeting motif [2] is also found in loop1 (violet). Additional Steap oxidoreductase domain residues highlighted in gray include Met110 (hydrophobic interaction with Leu194), Thr136 (putative isoalloxazine ring interaction), Pro193 and Pro198 (C-terminal helix). Potential Steap4 ubiquitination sites at the N-terminus are highlighted in orange (Lys3 and Lys18). In the mammalian Steap3 sequences, residues Gln120 and the His122-Leu123 pair in helix α5 are shown in light brown (human Steap3 numbering), while putative phosphorylation sites are highlighted in green (Ser17 and Ser20). Sequences from the NCBI non-redundant database were aligned with T-Coffee [3] and processed with ALINE [4].

References

1. Krogh, A., et al., *Predicting transmembrane protein topology with a hidden Markov model: application to complete genomes.* J Mol Biol, 2001. **305**(3): p. 567-80.

2. Lambe, T., et al., *Identification of a Steap3 endosomal targeting motif essential for normal iron metabolism.* Blood, 2009. **113**(8): p. 1805-8.

3. Notredame, C., D.G. Higgins, and J. Heringa, *T-Coffee: A novel method for fast and accurate multiple sequence alignment.* J Mol Biol, 2000. **302**(1): p. 205-17.

4. Bond, C.S. and A.W. Schuttelkopf, *ALINE: a WYSIWYG protein-sequence alignment editor for publication-quality alignments.* Acta Crystallogr D Biol Crystallogr, 2009. **65**(Pt 5): p. 510-2.

# REFERENCES CITED

Aisen, P., & Listowsky, I. (1980). Iron transport and storage proteins. *Annu Rev Biochem, 49*, 357-393. doi: 10.1146/annurev.bi.49.070180.002041

Aliverti, A., Curti, B., & Vanoni, M. A. (1999). *Flavoprotein Protocols* (Vol. 131). Totowa, NJ: Humana Press.

Amzallag, N., Passer, B. J., Allanic, D., Segura, E., Thery, C., Goud, B., . . . Telerman, A. (2004a). TSAP6 facilitates the secretion of translationally controlled tumor protein/histamine-releasing factor via a nonclassical pathway. *J Biol Chem, 279*(44), 46104-46112.

Amzallag, N., Passer, B. J., Allanic, D., Segura, E., Thery, C., Goud, B., . . . Telerman, A. (2004b). TSAP6 facilitates the secretion of translationally controlled tumor protein/histamine-releasing factor via a nonclassical pathway. *J. Biol. Chem., 279*(44), 46104-46112.

Andrews, N. C. (2000). Iron homeostasis: insights from genetics and animal models. *Nat Rev Genet, 1*(3), 208-217. doi: 10.1038/35042073

Arner, P., Stenson, B. M., Dungner, E., Naslund, E., Hoffstedt, J., Ryden, M., & Dahlman, I. (2008). Expression of six transmembrane protein of prostate 2 in human adipose tissue associates with adiposity and insulin resistance. *J Clin Endocrinol Metab, 93*(6), 2249-2254.

Backliwal, G., Hildinger, M., Kuettel, I., Delegrange, F., Hacker, D. L., & Wurm, F. M. (2008). Valproic acid: A viable alternative to sodium butyrate for enhancing protein expression in mammalian cell cultures. *Biotechnology and Bioengineering, 101*(1), 182-189.

Bond, C. S., & Schuttelkopf, A. W. (2009). ALINE: a WYSIWYG protein-sequence alignment editor for publication-quality alignments. *Acta Crystallogr D Biol Crystallogr, 65*(Pt 5), 510-512. doi: 10.1107/S0907444909007835

Bradford, M. M. (1976). Rapid and Sensitive Method for Quantitation of Microgram Quantities of Protein Utilizing Principle of Protein-Dye Binding. *Anal Biochem, 72*(1-2), 248-254.

Brokx, S. J., Rothery, R. A., Zhang, G., Ng, D. P., & Weiner, J. H. (2005). Characterization of an Escherichia coli sulfite oxidase homologue reveals the role of a conserved active site cysteine in assembly and function. *Biochemistry, 44*(30), 10339-10348. doi: 10.1021/bi050621a

Cain, C. C., Sipe, D. M., & Murphy, R. F. (1989). Regulation of endocytic pH by the Na+,K+-ATPase in living cells. *Proc Natl Acad Sci U S A, 86*(2), 544-548.

Carpenter, E. P., Beis, K., Cameron, A. D., & Iwata, S. (2008). Overcoming the challenges of membrane protein crystallography. *Curr Opin Struct Biol, 18*(5), 581-586. doi: 10.1016/j.sbi.2008.07.001

CCP4. (1994). The CCP4 Suite: Programs for Protein Crystallography. *Acta Cryst., D50*, 760-763.

Chen, X., Zhu, C., Ji, C., Zhao, Y., Zhang, C., Chen, F., . . . Guo, X. (2010). STEAP4, a gene associated with insulin sensitivity, is regulated by several adipokines in human adipocytes. *Int J Mol Med, 25*(3), 361-367.

Cheng, R., Qiu, J., Zhou, X. Y., Chen, X. H., Zhu, C., Qin, D. N., . . . Guo, X. R. (2011). Knockdown of STEAP4 inhibits insulin-stimulated glucose transport and GLUT4 translocation via attenuated phosphorylation of Akt, independent of the effects of EEA1. *Mol Med Report, 4*(3), 519-523.

Christensen, G. L., Kelstrup, C. D., Lyngso, C., Sarwar, U., Bogebo, R., Sheikh, S. P., . . . Hansen, J. L. Quantitative phosphoproteomics dissection of seven-transmembrane receptor signaling using full and biased agonists. *Mol Cell Proteomics, 9*(7), 1540-1553.

Claros, M. G., & von Heijne, G. (1994). TopPred II: an improved software for membrane protein structure predictions. *Comput Appl Biosci, 10*(6), 685-686.

Cook, J. D., Flowers, C. H., & Skikne, B. S. (2003). The quantitative assessment of body iron. *Blood, 101*(9), 3359-3364. doi: 10.1182/blood-2002-10-3071

Drakesmith, H., & Prentice, A. M. (2012). Hepcidin and the iron-infection axis. *Science, 338*(6108), 768-772.

Drew, D., Slotboom, D. J., Friso, G., Reda, T., Genevaux, P., Rapp, M., . . . De Gier, J. W. (2005). A scalable, GFP-based pipeline for membrane protein overexpression screening and purification. *Protein Sci, 14*(8), 2011-2017.

Elbein, S. C., Kern, P. A., Rasouli, N., Yao-Borengasser, A., Sharma, N. K., & Das, S. K. (2011). Global gene expression profiles of subcutaneous adipose and muscle from glucose-tolerant, insulin-sensitive, and insulin-resistant individuals matched for BMI. *Diabetes, 60*(3), 1019-1029.

Fasshauer, M., Kralisch, S., Klier, M., Lossner, U., Bluher, M., Chambaut-Guerin, A. M., . . . Paschke, R. (2004). Interleukin-6 is a positive regulator of tumor necrosis factor alpha-induced adipose-related protein in 3T3-L1 adipocytes. *FEBS Lett, 560*(1-3), 153-157.

Fieschi, F., Niviere, V., Frier, C., Decout, J. L., & Fontecave, M. (1995). The mechanism and substrate specificity of the NADPH:flavin oxidoreductase from Escherichia coli. *Journal of Biological Chemistry, 270*(51), 30392-30400.

Fischer, M., Haase, I., Feicht, R., Richter, G., Gerhardt, S., Changeux, J. P., . . . Bacher, A. (2002). Biosynthesis of riboflavin - 6,7-dimethyl-8-ribityllumazine synthase of Schizosaccharomyces pombe. *European Journal of Biochemistry, 269*(2), 519-526.

Fleming, M. D., Romano, M. A., Su, M. A., Garrick, L. M., Garrick, M. D., & Andrews, N. C. (1998). Nramp2 is mutated in the anemic Belgrade (b) rat: evidence of a role for Nramp2 in endosomal iron transport. *Proc Natl Acad Sci U S A, 95*(3), 1148-1153.

Fleming, M. D., Trenor, C. C., 3rd, Su, M. A., Foernzler, D., Beier, D. R., Dietrich, W. F., & Andrews, N. C. (1997). Microcytic anaemia mice have a mutation in Nramp2, a candidate iron transporter gene. *Nat Genet, 16*(4), 383-386. doi: 10.1038/ng0897-383

Fontecave, M., Eliasson, R., & Reichard, P. (1987). NAD(P)H-Flavin Oxidoreductase of Escherichia-Coli - a Ferric Iron Reductase Participating in the Generation of the Free-Radical of Ribonucleotide Reductase. *Journal of Biological Chemistry, 262*(25), 12325-12331.

Gauss, G. H., Kleven, M. D., Sendamarai, A. K., Fleming, M. D., & Lawrence, C. M. (2013). The Crystal Structure of Six-transmembrane Epithelial Antigen of the Prostate 4 (Steap4), a Ferri/Cuprireductase, Suggests a Novel Interdomain Flavin-binding Site. *Journal of Biological Chemistry, 288*(28), 20668-20682.

Gomes, I. M., Maia, C. J., & Santos, C. R. (2012). STEAP proteins: from structure to applications in cancer therapy. *Mol Cancer Res, 10*(5), 573-587.

Goswami, T., Li, X., Smith, A. M., Luderowski, E. M., Vincent, J. J., Rush, J., & Ballif, B. A. Comparative phosphoproteomic analysis of neonatal and adult murine brain. *Proteomics, 12*(13), 2185-2189.

Graham, F. L., Smiley, J., Russell, W. C., & Nairn, R. (1977). Characteristics of a human cell line transformed by DNA from human adenovirus type 5. *J Gen Virol, 36*(1), 59-74.

Grandchamp, B., Hetet, G., Kannengiesser, C., Oudin, C., Beaumont, C., Rodrigues-Ferreira, S., . . . Heimpel, H. (2011). A novel type of congenital hypochromic anemia associated with a nonsense mutation in the STEAP3/TSAP6 gene. *Blood, 118*(25), 6660-6666.

Grunewald, T. G., Bach, H., Cossarizza, A., & Matsumoto, I. (2012). The STEAP protein family: Versatile oxidoreductases and targets for cancer immunotherapy with overlapping and distinct cellular functions. *Biol Cell, 104*(11), 641-657.

Gunshin, H., Mackenzie, B., Berger, U. V., Gunshin, Y., Romero, M. F., Boron, W. F., . . . Hediger, M. A. (1997). Cloning and characterization of a mammalian proton-coupled metal-ion transporter. *Nature, 388*(6641), 482-488.

Guo, Y. Y., Li, N. F., Wang, C. M., Yan, Z. T., Zhang, J. H., Wang, H. M., . . . Luo, W. L. (2011). Genetic variation and association of STEAP4 gene with metabolic syndrome in Chinese Uygur patients. *Zhonghua Yi Xue Yi Chuan Xue Za Zhi, 28*(1), 78-82.

Guo, Y. Y., Li, N. F., Zhou, L., Yao, X. G., Wang, H. M., Zhang, J. H., & Luo, W. L. (2011). A common variation within the STEAP4 gene exons is associated with obesity in Uygur general population. *Chin Med J (Engl), 124*(14), 2096-2100.

Guo, Y. Y., Zhou, L., Yao, X. G., Yan, Z. T., Wang, H. M., Luo, W. L., . . . Li, N. F. (2011). Association of STEAP4 genetic polymorphisms with insulin resistance in Uygur Chinese general population. *Zhongguo Yi Xue Ke Xue Yuan Xue Bao, 33*(3), 299-305.

Haider, A. J., Briggs, D., Self, T. J., Chilvers, H. L., Holliday, N. D., & Kerr, I. D. (2011). Dimerization of ABCG2 analysed by bimolecular fluorescence complementation. *Plos One, 6*(10), e25818. doi: 10.1371/journal.pone.0025818

Hasebe, A., Tashima, H., Ide, T., Iijima, M., Yoshimoto, N., Ting, K., . . . Niimi, T. (2012). Efficient production and characterization of recombinant human NELL1 protein in human embryonic kidney 293-F cells. *Mol Biotechnol, 51*(1), 58-66. doi: 10.1007/s12033-011-9440-4

Hentze, M. W., Muckenthaler, M. U., & Andrews, N. C. (2004). Balancing acts: molecular control of mammalian iron metabolism. *Cell, 117*(3), 285-297.

Hinkson, J. W. (1968). Azotobacter free-radical flavoprotein. Preparation and properties of the apoprotein. *Biochemistry, 7*(7), 2666-2672.

Hsu, P. P., Kang, S. A., Rameseder, J., Zhang, Y., Ottina, K. A., Lim, D., . . . Sabatini, D. M. The mTOR-regulated phosphoproteome reveals a mechanism of mTORC1-mediated inhibition of growth factor signaling. *Science, 332*(6035), 1317-1322.

Hu, C. D., Chinenov, Y., & Kerppola, T. K. (2002). Visualization of interactions among bZip and Rel family proteins in living cells using bimolecular fluorescence complementation. *Molecular Cell, 9*(4), 789-798.

Hubert, R. S., Vivanco, I., Chen, E., Rastegar, S., Leong, K., Mitchell, S. C., . . . Afar, D. E. (1999a). STEAP: a prostate-specific cell-surface antigen highly expressed in human prostate tumors. *Proc Natl Acad Sci U S A, 96*(25), 14523-14528.

Hubert, R. S., Vivanco, I., Chen, E., Rastegar, S., Leong, K., Mitchell, S. C., . . . Afar, D. E. (1999b). STEAP: a prostate-specific cell-surface antigen highly expressed in human prostate tumors. *Proc. Natl. Acad. Sci. U. S. A., 96*(25), 14523-14528.

Jones, F. G., Wolstenholme, A., Fowler, S., Smith, S., Ziemnicka, K., Bradbury, J., . . . Smith, B. R. (1996). High-level expression of recombinant immunoreactive thyroid peroxidase in the High Five insect cell line. *Journal of Molecular Endocrinology, 17*(2), 165-174.

Kaplan, J. H., & Lutsenko, S. (2009). Copper transport in mammalian cells: special care for a metal with special needs. *J Biol Chem, 284*(38), 25461-25465.

Kawate, T., & Gouaux, E. (2006). Fluorescence-detection size-exclusion chromatography for precrystallization screening of integral membrane proteins. *Structure, 14*(4), 673-681. doi: 10.1016/j.str.2006.01.013

Kery, V., Elleder, D., & Kraus, J. P. (1995). Delta-Aminolevulinate Increases Heme Saturation and Yield of Human Cystathionine Beta-Synthase Expressed in Escherichia-Coli. *Archives of Biochemistry and Biophysics, 316*(1), 24-29.

Kidane, T. Z., Farhad, R., Lee, K. J., Santos, A., Russo, E., & Linder, M. C. (2012). Uptake of copper from plasma proteins in cells where expression of CTR1 has been modulated. *Biometals, 25*(4), 697-709.

Konstantopoulos, N., Foletta, V. C., Segal, D. H., Shields, K. A., Sanigorski, A., Windmill, K., . . . Walder, K. R. (2011). A gene expression signature for insulin resistance. *Physiol Genomics, 43*(3), 110-120.

Korkmaz, C. G., Korkmaz, K. S., Kurys, P., Elbi, C., Wang, L., Klokk, T. I., . . . Saatcioglu, F. (2005). Molecular cloning and characterization of STAMP2, an androgen-regulated six transmembrane protein that is overexpressed in prostate cancer. *Oncogene, 24*(31), 4934-4945.

Korkmaz, K. S., Elbi, C., Korkmaz, C. G., Loda, M., Hager, G. L., & Saatcioglu, F. (2002a). Molecular cloning and characterization of STAMP1, a highly prostate-specific six transmembrane protein that is overexpressed in prostate cancer. *J Biol Chem, 277*(39), 36689-36696.

Korkmaz, K. S., Elbi, C., Korkmaz, C. G., Loda, M., Hager, G. L., & Saatcioglu, F. (2002b). Molecular cloning and characterization of STAMP1, a highly prostate-specific six transmembrane protein that is overexpressed in prostate cancer. *J. Biol. Chem., 277*(39), 36689-36696.

Kralisch, S., Sommer, G., Weise, S., Lipfert, J., Lossner, U., Kamprad, M., . . . Fasshauer, M. (2009). Interleukin-1beta is a positive regulator of TIARP/STAMP2 gene and protein expression in adipocytes in vitro. *FEBS Lett, 583*(7), 1196-1200.

Krogh, A., Larsson, B., von Heijne, G., & Sonnhammer, E. L. (2001). Predicting transmembrane protein topology with a hidden Markov model: application to complete genomes. *J Mol Biol, 305*(3), 567-580. doi: 10.1006/jmbi.2000.4315

Kunow, J., Schworer, B., Stetter, K. O., & Thauer, R. K. (1993). A F(420)-Dependent NADP Reductase in the Extremely Thermophilic Sulfate-Reducing Archaeoglobus-Fulgidus. *Archives of Microbiology, 160*(3), 199-205.

Laemmli, U. K. (1970). Cleavage of structural proteins during the assembly of the head of bacteriophage T4. *Nature, 227*(5259), 680-685.

Lambe, T., Simpson, R. J., Dawson, S., Bouriez-Jones, T., Crockford, T. L., Lepherd, M., . . . Cornall, R. J. (2009). Identification of a Steap3 endosomal targeting motif essential for normal iron metabolism. *Blood, 113*(8), 1805-1808. doi: 10.1182/blood-2007-11-120402

Latunde-Dada, G. O., Simpson, R. J., & McKie, A. T. (2008). Duodenal cytochrome B expression stimulates iron uptake by human intestinal epithelial cells. *J Nutr, 138*(6), 991-995.

Lawrence, C. M., Ray, S., Babyonyshev, M., Galluser, R., Borhani, D. W., & Harrison, S. C. (1999). Crystal structure of the ectodomain of human transferrin receptor. *Science, 286*(5440), 779-782.

Lee, J., Pena, M. M., Nose, Y., & Thiele, D. J. (2002). Biochemical characterization of the human copper transporter Ctr1. *J Biol Chem, 277*(6), 4380-4387. doi: 10.1074/jbc.M104728200

Li, L., Fang, C. J., Ryan, J. C., Niemi, E. C., Lebron, J. A., Bjorkman, P. J., . . . Seaman, W. E. (2010). Binding and uptake of H-ferritin are mediated by human transferrin receptor-1. *Proc Natl Acad Sci U S A, 107*(8), 3505-3510.

Lu, H., Ma, J., Liu, N., & Wang, S. (2010). Effects of heme precursors on CYP1A2 and POR expression in the baculovirus/Spodoptera frugiperda system. *J Biomed Res, 24*(3), 242-249. doi: 10.1016/S1674-8301(10)60034-6

Lu, P., Ma, D., Yan, C., Gong, X., Du, M., & Shi, Y. (2014). Structure and mechanism of a eukaryotic transmembrane ascorbate-dependent oxidoreductase. *Proc Natl Acad Sci U S A, 111*(5), 1813-1818. doi: 10.1073/pnas.1323931111

McKie, A. T., Barrow, D., Latunde-Dada, G. O., Rolfs, A., Sager, G., Mudaly, E., . . . Simpson, R. J. (2001). An iron-regulated ferric reductase associated with the absorption of dietary iron. *Science, 291*(5509), 1755-1759.

McMillin, G. A., Travis, J. J., & Hunt, J. W. (2009). Direct Measurement of Free Copper in Serum or Plasma Ultrafiltrate. *American Journal of Clinical Pathology, 131*(2), 160-165.

Miot, A., Maimaitiming, S., Emery, N., Bellili, N., Roussel, R., Tichet, J., . . . Fumeron, F. Genetic variability at the six transmembrane protein of prostate 2 locus and the metabolic syndrome: the data from an epidemiological study on the Insulin Resistance Syndrome (DESIR) study. *J Clin Endocrinol Metab, 95*(6), 2942-2947.

Moldes, M., Lasnier, F., Gauthereau, X., Klein, C., Pairault, J., Feve, B., & Chambaut-Guerin, A. M. (2001a). Tumor necrosis factor-alpha-induced adipose-related protein (TIARP), a cell-surface protein that is highly induced by tumor necrosis factor-alpha and adipose conversion. *J. Biol. Chem., 276*(36), 33938-33946.

Moldes, M., Lasnier, F., Gauthereau, X., Klein, C., Pairault, J., Feve, B., & Chambaut-Guerin, A. M. (2001b). Tumor necrosis factor-alpha-induced adipose-related protein (TIARP), a cell-surface protein that is highly induced by tumor necrosis factor-alpha and adipose conversion. *J Biol Chem, 276*(36), 33938-33946.

Moreaux, J., Kassambara, A., Hose, D., & Klein, B. (2012). STEAP1 is overexpressed in cancers: A promising therapeutic target. *Biochemical and Biophysical Research Communications, 429*(3-4), 148-155.

Moreno-Navarrete, J. M., Ortega, F., Sabater, M., Ricart, W., & Fernandez-Real, J. M. (2011). Proadipogenic effects of lactoferrin in human subcutaneous and visceral preadipocytes. *J Nutr Biochem, 22*(12), 1143-1149.

Muir, A., & Hopfer, U. (1985). Regional specificity of iron uptake by small intestinal brush-border membranes from normal and iron-deficient mice. *Am J Physiol, 248*(3 Pt 1), G376-379.

Nanfang, L., Yanying, G., Hongmei, W., Zhitao, Y., Juhong, Z., Ling, Z., & Wenli, L. Variations of six transmembrane epithelial antigen of prostate 4 (STEAP4) gene are associated with metabolic syndrome in a female Uygur general population. *Arch Med Res, 41*(6), 449-456.

Notredame, C., Higgins, D. G., & Heringa, J. (2000). T-Coffee: A novel method for fast and accurate multiple sequence alignment. *J Mol Biol, 302*(1), 205-217. doi: 10.1006/jmbi.2000.4042

Oakhill, J. S., Marritt, S. J., Gareta, E. G., Cammack, R., & McKie, A. T. (2008). Functional characterization of human duodenal cytochrome b (Cybrd1): Redox properties in relation to iron and ascorbate metabolism. *Biochim Biophys Acta, 1777*(3), 260-268. doi: 10.1016/j.bbabio.2007.12.001

Ohgami, R. S., Campagna, D. R., Antiochos, B., Wood, E. B., Sharp, J. J., Barker, J. E., & Fleming, M. D. (2005). nm1054: a spontaneous, recessive, hypochromic, microcytic anemia mutation in the mouse. *Blood, 106*(10), 3625-3631.

Ohgami, R. S., Campagna, D. R., Greer, E. L., Antiochos, B., McDonald, A., Chen, J., . . . Fleming, M. D. (2005a). Identification of a ferrireductase required for efficient transferrin-dependent iron uptake in erythroid cells. *Nat Genet, 37*(11), 1264-1269.

Ohgami, R. S., Campagna, D. R., Greer, E. L., Antiochos, B., McDonald, A., Chen, J., . . . Fleming, M. D. (2005b). Identification of a ferrireductase required for efficient transferrin-dependent iron uptake in erythroid cells. *Nat. Genet., 37*(11), 1264-1269.

Ohgami, R. S., Campagna, D. R., McDonald, A., & Fleming, M. D. (2006). The Steap proteins are metalloreductases. *Blood, 108*(4), 1388-1394.

Otwinowski, Z., & Minor, W. (1997). Processing of X-ray diffraction data collected in oscillation mode. *Methods in Enzymology, 276*, 307-326.

Pan, C., Gnad, F., Olsen, J. V., & Mann, M. (2008). Quantitative phosphoproteome analysis of a mouse liver cell line reveals specificity of phosphatase inhibitors. *Proteomics, 8*(21), 4534-4546.

Passer, B. J., Nancy-Portebois, V., Amzallag, N., Prieur, S., Cans, C., Roborel de Climens, A., . . . Telerman, A. (2003a). The p53-inducible TSAP6 gene product regulates apoptosis and the cell cycle and interacts with Nix and the Myt1 kinase. *Proc. Natl. Acad. Sci. U. S .A., 100*(5), 2284-2289.

Passer, B. J., Nancy-Portebois, V., Amzallag, N., Prieur, S., Cans, C., Roborel de Climens, A., . . . Telerman, A. (2003b). The p53-inducible TSAP6 gene product regulates apoptosis and the cell cycle and interacts with Nix and the Myt1 kinase. *Proc Natl Acad Sci U S A, 100*(5), 2284-2289.

Porkka, K. P., Nupponen, N. N., Tammela, T. L., Vessella, R. L., & Visakorpi, T. (2003). Human pHyde is not a classical tumor suppressor gene in prostate cancer. *Int J Cancer, 106*(5), 729-735.

Qiu, J., Ni, Y. H., Gong, H. X., Fei, L., Pan, X. Q., Guo, M., . . . Guo, X. R. (2007). Identification of differentially expressed genes in omental adipose tissues of obese

patients by suppression subtractive hybridization. *Biochem Biophys Res Commun, 352*(2), 469-478.

Ramadoss, P., Chiappini, F., Bilban, M., & Hollenberg, A. N. (2010a). Regulation of hepatic six transmembrane epithelial antigen of prostate 4 (STEAP4) expression by STAT3 and CCAAT/enhancer-binding protein alpha. *J Biol Chem, 285*(22), 16453-16466.

Ramadoss, P., Chiappini, F., Bilban, M., & Hollenberg, A. N. (2010b). Regulation of hepatic six transmembrane epithelial antigen of prostate 4 (STEAP4) expression by STAT3 and CCAAT/enhancer-binding protein alpha. *J. Biol. Chem., 285*(22), 16453-16466.

Raymond, C., Tom, R., Perret, S., Moussouami, P., L'Abbe, D., St-Laurent, G., & Durocher, Y. (2011). A simplified polyethylenimine-mediated transfection process for large-scale and high-throughput applications. *Methods, 55*(1), 44-51.

Samuel, V. T., & Shulman, G. I. (2012). Mechanisms for insulin resistance: common threads and missing links. *Cell, 148*(5), 852-871.

Sanchez-Pulido, L., Rojas, A. M., Valencia, A., Martinez, A. C., & Andrade, M. A. (2004a). ACRATA: a novel electron transfer domain associated to apoptosis and cancer. *Bmc Cancer, 4*, 98.

Sanchez-Pulido, L., Rojas, A. M., Valencia, A., Martinez, C., & Andrade, M. A. (2004b). ACRATA: a novel electron transfer domain associated to apoptosis and cancer. *Bmc Cancer, 4*.

Schrodinger, L. (2011). The PyMOL Molecular Graphics System. *www.pymol.org*.

Seddon, A. M., Curnow, P., & Booth, P. J. (2004). Membrane proteins, lipids and detergents: not just a soap opera. *Biochim Biophys Acta, 1666*(1-2), 105-117. doi: 10.1016/j.bbamem.2004.04.011

Sendamarai, A. K., Ohgami, R. S., Fleming, M. D., & Lawrence, C. M. (2008a). Structure of the membrane proximal oxidoreductase domain of human Steap3, the dominant ferrireductase of the erythroid transferrin cycle. *Proc. Natl. Acad. Sci. U. S .A., 105*(21), 7410-7415.

Sendamarai, A. K., Ohgami, R. S., Fleming, M. D., & Lawrence, C. M. (2008b). Structure of the membrane proximal oxidoreductase domain of human Steap3, the dominant ferrireductase of the erythroid transferrin cycle. *Proc Natl Acad Sci U S A, 105*(21), 7410-7415.

Shayeghi, M., Latunde-Dada, G. O., Oakhill, J. S., Laftah, A. H., Takeuchi, K., Halliday, N., . . . McKie, A. T. (2005). Identification of an intestinal heme transporter. *Cell, 122*(5), 789-801. doi: 10.1016/j.cell.2005.06.025

Sievers, F., Wilm, A., Dineen, D., Gibson, T. J., Karplus, K., Li, W., . . . Higgins, D. G. (2011). Fast, scalable generation of high-quality protein multiple sequence alignments using Clustal Omega. *Mol Syst Biol, 7*, 539. doi: 10.1038/msb.2011.75

Smith, G. E., Summers, M. D., & Fraser, M. J. (1983). Production of human beta interferon in insect cells infected with a baculovirus expression vector. *Mol Cell Biol, 3*(12), 2156-2165.

Solmaz, S. R., & Hunte, C. (2008). Structure of complex III with bound cytochrome c in reduced state and definition of a minimal core interface for electron transfer. *J Biol Chem, 283*(25), 17542-17549. doi: 10.1074/jbc.M710126200

Sparna, T., Retey, J., Schmich, K., Albrecht, U., Naumann, K., Gretz, N., . . . Merfort, I. (2010). Genome-wide comparison between IL-17 and combined TNF-alpha/IL-17 induced genes in primary murine hepatocytes. *BMC Genomics, 11*, 226.

Spratt, D. E., Doran, M. G., Wongvipat, J., Lewis, J. S., & Evans, M. J. (2014). 89Zr-MSTP2109A, A Novel Antibody Based Radiotracer to Evaluate and Guide the Clinical Translation of Antibody-Drug Conjugates Targeting STEAP1. *International Journal of Radiation Oncology Biology Physics, 90*, S791-S791.

Steiner, M. S., Zhang, X. W., Wang, Y., & Lu, Y. (2000). Growth inhibition of prostate cancer by an adenovirus expressing a novel tumor suppressor gene, pHyde. *Cancer Research, 60*(16), 4419-4425.

Studier, F. W. (2005). Protein production by auto-induction in high density shaking cultures. *Protein Expr Purif, 41*(1), 207-234.

Su, D., & Asard, H. (2006). Three mammalian cytochromes b561 are ascorbate-dependent ferrireductases. *Febs J, 273*(16), 3722-3734.

Sundaramoorthy, M., Kishi, K., Gold, M. H., & Poulos, T. L. (1994). The crystal structure of manganese peroxidase from Phanerochaete chrysosporium at 2.06-A resolution. *J Biol Chem, 269*(52), 32759-32767.

ten Freyhaus, H., Calay, E. S., Yalcin, A., Vallerie, S. N., Yang, L., Calay, Z. Z., . . . Hotamisligil, G. S. (2012). Stamp2 controls macrophage inflammation through nicotinamide adenine dinucleotide phosphate homeostasis and protects against atherosclerosis. *Cell Metab, 16*(1), 81-89.

Trost, M., English, L., Lemieux, S., Courcelles, M., Desjardins, M., & Thibault, P. (2009). The phagosomal proteome in interferon-gamma-activated macrophages. *Immunity, 30*(1), 143-154.

Tu, S. C. (2001). Reduced flavin: Donor and acceptor enzymes and mechanisms of channeling. *Antioxidants & Redox Signaling, 3*(5), 881-897.

Vignozzi, L., Morelli, A., Sarchielli, E., Comeglio, P., Filippi, S., Cellai, I., . . . Maggi, M. (2012). Testosterone protects from metabolic syndrome-associated prostate inflammation: an experimental study in rabbit. *J Endocrinol, 212*(1), 71-84.

Villen, J., Beausoleil, S. A., Gerber, S. A., & Gygi, S. P. (2007). Large-scale phosphorylation analysis of mouse liver. *Proc Natl Acad Sci U S A, 104*(5), 1488-1493.

Vulpe, C. D., Kuo, Y. M., Murphy, T. L., Cowley, L., Askwith, C., Libina, N., . . . Anderson, G. J. (1999). Hephaestin, a ceruloplasmin homologue implicated in intestinal iron transport, is defective in the sla mouse. *Nat Genet, 21*(2), 195-199. doi: 10.1038/5979

Wagner, S. A., Beli, P., Weinert, B. T., Scholz, C., Kelstrup, C. D., Young, C., . . . Choudhary, C. (2012). Proteomic analyses reveal divergent ubiquitylation site patterns in murine tissues. *Mol Cell Proteomics, 11*(12), 1578-1585.

Wallace, A. C., Laskowski, R. A., & Thornton, J. M. (1995). LIGPLOT: a program to generate schematic diagrams of protein-ligand interactions. *Protein Eng, 8*(2), 127-134.

Wang, C. Y., Jenkitkasemwong, S., Duarte, S., Sparkman, B. K., Shawki, A., Mackenzie, B., & Knutson, M. D. (2012). ZIP8 is an iron and zinc transporter whose cell-surface expression is up-regulated by cellular iron loading. *J Biol Chem, 287*(41), 34032-34043.

Wang, L., Jin, Y., Arnoldussen, Y. J., Jonson, I., Qu, S., Maelandsmo, G. M., . . . Saatcioglu, F. (2010). STAMP1 is both a proliferative and an antiapoptotic factor in prostate cancer. *Cancer Res, 70*(14), 5818-5828. doi: 10.1158/0008-5472.CAN-09-4697

Wang, Y., Hodgkinson, V., Zhu, S., Weisman, G. A., & Petris, M. J. Advances in the understanding of mammalian copper transporters. *Adv Nutr, 2*(2), 129-137.

Warkentin, E., Hagemeier, C. H., Shima, S., Thauer, R. K., & Ermler, U. (2005a). The structure of F420-dependent methylenetetrahydromethanopterin dehydrogenase: a crystallographic 'superstructure' of the selenomethionine-labelled protein crystal structure. *Acta Crystallogr. D Biol. Crystallogr., 61*(Pt 2), 198-202.

Warkentin, E., Hagemeier, C. H., Shima, S., Thauer, R. K., & Ermler, U. (2005b). The structure of F420-dependent methylenetetrahydromethanopterin dehydrogenase: a crystallographic 'superstructure' of the selenomethionine-labelled protein crystal structure. *Acta Crystallogr D Biol Crystallogr, 61*(Pt 2), 198-202.

Weintz, G., Olsen, J. V., Fruhauf, K., Niedzielska, M., Amit, I., Jantsch, J., . . . Lang, R. The phosphoproteome of toll-like receptor-activated macrophages. *Mol Syst Biol, 6*, 371.

Wellen, K. E., Fucho, R., Gregor, M. F., Furuhashi, M., Morgan, C., Lindstad, T., . . . Hotamisligil, G. S. (2007). Coordinated regulation of nutrient and inflammatory responses by STAMP2 is essential for metabolic homeostasis. *Cell, 129*(3), 537-548.

Wisniewski, J. R., Nagaraj, N., Zougman, A., Gnad, F., & Mann, M. Brain phosphoproteome obtained by a FASP-based method reveals plasma membrane protein topology. *J Proteome Res, 9*(6), 3280-3289.

Wyman, S., Simpson, R. J., McKie, A. T., & Sharp, P. A. (2008a). Dcytb (Cybrd1) functions as both a ferric and a cupric reductase in vitro. *FEBS Lett., 582*(13), 1901-1906.

Wyman, S., Simpson, R. J., McKie, A. T., & Sharp, P. A. (2008b). Dcytb (Cybrd1) functions as both a ferric and a cupric reductase in vitro. *FEBS Lett, 582*(13), 1901-1906.

Yu, Y., Yoon, S. O., Poulogiannis, G., Yang, Q., Ma, X. M., Villen, J., . . . Blenis, J. Phosphoproteomic analysis identifies Grb10 as an mTORC1 substrate that negatively regulates insulin signaling. *Science, 332*(6035), 1322-1326.

Zanivan, S., Gnad, F., Wickstrom, S. A., Geiger, T., Macek, B., Cox, J., . . . Mann, M. (2008). Solid tumor proteome and phosphoproteome analysis by high resolution mass spectrometry. *J Proteome Res, 7*(12), 5314-5326.

Zhang, C. M., Chi, X., Wang, B., Zhang, M., Ni, Y. H., Chen, R. H., . . . Guo, X. R. (2008). Downregulation of STEAP4, a highly-expressed TNF-alpha-inducible gene in adipose tissue, is associated with obesity in humans. *Acta Pharmacol Sin, 29*(5), 587-592.

Zhang, X., Krause, K. H., Xenarios, I., Soldati, T., & Boeckmann, B. Evolution of the Ferric Reductase Domain (FRD) Superfamily: Modularity, Functional Diversification, and Signature Motifs. *PLoS One, 8*(3), e58126.

Zhang, X., Krause, K. H., Xenarios, I., Soldati, T., & Boeckmann, B. (2013). Evolution of the Ferric Reductase Domain (FRD) Superfamily: Modularity, Functional Diversification, and Signature Motifs. *Plos One, 8*(3), e58126.

Zhao, N., Gao, J., Enns, C. A., & Knutson, M. D. (2010a). ZRT/IRT-like protein 14 (ZIP14) promotes the cellular assimilation of iron from transferrin. *J. Biol. Chem., 285*(42), 32141-32150.

Zhao, N., Gao, J., Enns, C. A., & Knutson, M. D. (2010b). ZRT/IRT-like protein 14 (ZIP14) promotes the cellular assimilation of iron from transferrin. *J Biol Chem, 285*(42), 32141-32150.

Zhou, J., Ye, S. Q., Fujiwara, T., Manolagas, S. C., & Zhao, H. B. (2013). Steap4 Plays a Critical Role in Osteoclastogenesis in Vitro by Regulating Cellular Iron/Reactive Oxygen Species (ROS) Levels and cAMP Response Element-binding Protein (CREB) Activation. *Journal of Biological Chemistry, 288*(42), 30064-30074.